SANDIA REPORT
SAND20XX-XXXX
Printed Click to enter a date

Mixed Integer Nonlinear Programming Approaches to Enhance Resiliency and Response Strategies in Critical Infrastructure

*M. Bynum, A. Castillo, B. Knueven, C. Laird, JP Watson

* listed alphabetically

Prepared by
Sandia National Laboratories
Albuquerque, New Mexico
87185 and Livermore,
California 94550

Issued by Sandia National Laboratories, operated for the United States Department of Energy by National Technology & Engineering Solutions of Sandia, LLC.

NOTICE: This report was prepared as an account of work sponsored by an agency of the United States Government. Neither the United States Government, nor any agency thereof, nor any of their employees, nor any of their contractors, subcontractors, or their employees, make any warranty, express or implied, or assume any legal liability or responsibility for the accuracy, completeness, or usefulness of any information, apparatus, product, or process disclosed, or represent that its use would not infringe privately owned rights. Reference herein to any specific commercial product, process, or service by trade name, trademark, manufacturer, or otherwise, does not necessarily constitute or imply its endorsement, recommendation, or favoring by the United States Government, any agency thereof, or any of their contractors or subcontractors. The views and opinions expressed herein do not necessarily state or reflect those of the United States Government, any agency thereof, or any of their contractors.

Printed in the United States of America. This report has been reproduced directly from the best available copy.

Available to DOE and DOE contractors from
U.S. Department of Energy
Office of Scientific and Technical Information
P.O. Box 62
Oak Ridge, TN 37831

Telephone: (865) 576-8401
Facsimile: (865) 576-5728
E-Mail: reports@osti.gov
Online ordering: http://www.osti.gov/scitech

Available to the public from
U.S. Department of Commerce
National Technical Information Service
5301 Shawnee Rd
Alexandria, VA 22312

Telephone: (800) 553-6847
Facsimile: (703) 605-6900
E-Mail: orders@ntis.gov
Online order: https://classic.ntis.gov/help/order-methods/

ABSTRACT

Motivation

Critical infrastructures are large, complex engineered systems that must be operated robustly under abnormal conditions resulting from natural hazards or intentional acts. For example, electric power systems must be robust to line faults, water utilities must rapidly mitigate contamination incidents, and computing networks must adapt to adversarial intrusions to protect critical information.

Problem

It is difficult for decision-makers within resiliency analysis in critical infrastructure to optimize designs and develop effective response strategies that can account for uncertainties. Facing incomplete information and the sheer scope that a natural hazard or attack vector may incorporate, response can be ineffective without reliable, scalable decision support tools. These problems are intrinsically nonlinear and involve discrete decisions, and unfortunately, existing off-the-shelf mathematical programming methods cannot support optimization-based decision-making of these nonlinear at scale.

Method/Approach and Results

This project emphasized development of fundamental optimization strategies that supported real-time mitigation and response for critical infrastructures. In particular, the project developed multi-tree approaches based on piecewise outer-approximations for solution of mixed-integer nonlinear programming (MINLP) problems. These techniques alternate between an MILP or MISOCP relaxation to obtain a lower bound and candidate discrete solutions and an NLP subproblem to obtain upper bounds. Using tailored relaxations based on problem structure, these methods were used to solve several key applications in resilience and response of critical infrastructure. This work resulted in two open-source, copyrighted software packages:

- CORAMIN (https://github.com/Coramin/Coramin) – an object-oriented mathematical programming framework that supports tailored multi-tree algorithms for solution of large-scale mixed-integer nonlinear programming; and
- EGRET (Electrical Grid Research and Engineering Toolkit) (https://github.com/grid-parity-exchange/Egret) – a declarative mathematical programming framework built upon CORAMIN and Pyomo for formulation and solution of resilience and operations problems in power grid systems.

Furthermore, these tools resulted in several important published results, including the following:

- The first known global optimization approach that could solve the unit-commitment problem with nonlinear power flow constraints on medium-sized test problems.
- Improved parallel optimization-based bounds tightening and strengthening of relaxations of AC power flow constraints.
- Optimization-based approaches for improved grid resilience and use of demand response to improve grid resilience with reduction in capital requirements.

Result Implications

This project developed first-of-a-kind algorithms for decision-making in critical infrastructure resilience operations and planning, as well as a next-generation toolkit for MINLP researchers. These approaches leveraged high-performance computing architectures to solve some of the largest, most challenging nonlinear discrete optimization problems to global optimality, and these successes were captured in open-source software to enable optimization-based decision-making, and efficient solution of MINLP formulations for electric power transmission grids.

CONTENTS

1. Publications resulting from Research 7
   1.1. Evaluating demand response opportunities for power systems resilience using MILP and MINLP Formulations 8
   1.2. Strengthened SOCP relaxations for ACOPF with McCormick envelopes and bounds tightening 47
   1.3. Tightening McCormick relaxations toward global solution of the ACOPF problem 54
   1.4. A multitree approach for global solution of ACOPF problems using piecewise outer approximations 58
   1.5. A global stochastic programming approach for the optimal placement of gas detectors with nonuniform unavailabilities 94
   1.6. Global solution Strategies for Network Constrained Unit Commitment Problem with Nonlinear AC Transmission Models 109
2. Distribution 125

ACRONYMS AND DEFINITIONS

Abbreviation	Definition
ACOPF	alternating current optimal power flow
AIChE	American Institute of Chemical Engineers
EGRET	Electrical Grid Research and Engineering Toolkit
IEEE	Institute of Electrical and Electronics Engineers
MILP	mixed-integer linear programming
MINLP	mixed-integer nonlinear programming
SOCP	second order cone program

1. PUBLICATIONS RESULTING FROM RESEARCH

The following six articles were written by project members and published during the project's three-year research period:

1. Bynum, M., Castillo, A., Watson, J. P., & Laird, C. D. (2019). Evaluating demand response opportunities for power systems resilience using MILP and MINLP Formulations. AIChE Journal.
2. Bynum, M., Castillo, A., Watson, J. P., & Laird, C. D. (2018). Strengthened SOCP relaxations for ACOPF with McCormick envelopes and bounds tightening. Computer Aided Chemical Engineering, Vol. 44, pp. 1555-1560.
3. Bynum, M., Castillo, A., Watson, J. P., & Laird, C. D. (2018). Tightening McCormick relaxations toward global solution of the ACOPF problem. IEEE Transactions on Power Systems, 34(1), 814-817.
4. Liu, J., Bynum, M., Castillo, A., Watson, J. P., & Laird, C. D. (2018). A multitree approach for global solution of ACOPF problems using piecewise outer approximations. Computers & Chemical Engineering, 114, 145-157.
5. Liu, J., & Laird, C. D. (2018). A global stochastic programming approach for the optimal placement of gas detectors with nonuniform unavailabilities. Journal of Loss Prevention in the Process Industries, 51, 29-35.
6. Liu, J., Laird, C. D., Scott, J. K., Watson, J. P., & Castillo, A. (2018). Global Solution Strategies for the Network-Constrained Unit Commitment Problem with AC Transmission Constraints. IEEE Transactions on Power Systems, 34(2), 1139-1150.

The papers resulting from this research project are included in the following sections.

1.1. Evaluating demand response opportunities for power systems resilience using MILP and MINLP Formulations

Evaluating Demand Response Opportunities for Power Systems Resilience Using MILP and MINLP Formulations

Michael Bynum [*],

Anya Castillo [†], Jean-Paul Watson [‡], and Carl D. Laird [§]

Abstract

While peak shaving is commonly used to reduce power costs, chemical process facilities that can reduce power consumption on demand during emergencies (e.g., extreme weather events) bring additional value through improved resilience. For process facilities to effectively negotiate demand response (DR) contracts and make investment decisions regarding flexibility, they need to quantify their additional value to the grid. We present a grid-centric mixed-integer stochastic programming framework to determine the value of DR for improving grid resilience in place of capital investments that can be cost prohibitive for system operators. We formulate problems using both a linear approximation and a nonlinear alternating current power flow model. Our numerical results with both models demonstrate that DR can be used to reduce the

[*]M. Bynum is with the Davidson School of Chemical Engineering, Purdue University, West Lafayette, IN, 47907 USA e-mail: bynumm@purdue.edu and with Sandia National Laboratories, Albuquerque, NM, 87185 USA email: mlbynum@sandia.gov

[†]A. Castillo is with Sandia National Laboratories, Albuquerque, NM, 87185 USA email: arcasti@sandia.gov

[‡]J.P. Watson is with Sandia National Laboratories, Albuquerque, NM, 87185 USA e-mail: jwatson@sandia.gov.

[§]C. Laird with the Davidson School of Chemical Engineering, Purdue University, West Lafayette, IN, 47907 USA and with Sandia National Laboratories, Albuquerque, NM, 87185 USA e-mail: cdlaird@sandia.gov.

capital investment necessary for resilience, increasing the value that chemical process facilities bring through DR. However, the linearized model often underestimates the amount of DR needed in our case studies.

Introduction

Despite ongoing investments in grid modernization, the U.S. electric grid remains vulnerable to a range of events.[1] More recently, disruptions to the U.S. electric grid have resulted in an estimated annual cost of $18-70 billion in security, health and safety, and economic consequences.[2] Natural disasters, although infrequent, can have major impacts on the electric grid through direct damage of infrastructure, or indirectly through interdependent infrastructures such as gas and water. Also, the increasing reliance on renewable generation contributes to the increasing uncertainty on the "threats to, vulnerabilities of, and potential consequences from all hazards on critical infrastructures".[3] Depending on the geographical location, such natural disasters include tornadoes, wildfires, hurricanes, and earthquakes, and can result in significant infrastructure damage. The impact of such disasters has demonstrated the need for resiliency, which is the ability to harden the system against – and quickly recover from – low-frequency, high-consequence events.

Resilience integrates risk management requirements before, during, and after an event.[4] Several papers have investigated various investment and recovery strategies for improving electric grid resilience.[5–10] However, these actions alone may be insufficient or prohibitively expensive. More recently, utilities have leveraged demand response (DR) resources to address many electric grid needs including improved system reliability, economic dispatch, wholesale price mitigation, and ancillary services.[11] Therefore, DR can be utilized to defer or offset the need for generation, transmission, and distribution infrastructure investments to improve resilience. In emergency events, system operators can offer pricing benefits to industrial-scale customers if they can absorb loss or reduction of power. Such interruptible load management can improve the reliability of the electric grid by not treating load at each bus as a fixed

quantity but a decision variable in the system operator's optimization routine.

Chemical process facilities, as large industrial electricity consumers, have an opportunity to serve as active participants to improve system resilience through DR. This can reduce the likelihood of system blackout (which could significantly impact the process facility). Furthermore, DR can bring additional value since it may allow the grid operator to forgo significant capital investment in the grid to meet resilience targets. This presents an economic opportunity for process facilities if they can overcome the operational challenges associated with increased flexibility. The additional value they bring needs to be understood and quantified by the process facility operator so they can effectively negotiate DR constracts and make investment decisions regarding potential retrofit and operational changes to support the required flexibility.

Numerous studies have investigated the opportunity for interruptible load during peak operations and for congestion management.[12,13] Aalami et al.[14] focus on economic incentives for interruptible and curtailable DR programs that incorporate penalty mechanisms for non-compliant participants. Other studies[15–18] have formulated detailed industrial customer facility models without the electric grid physics. These studies generally apply either model-based[19] or data-driven[20] approaches to define the feasible region for each operating mode as a union of convex subregions in the facility's production space. For example, Zhang et al.[21] propose a mode-based plant model formulation for the scheduling of continuous industrial processes to provide interruptible load as operating reserve and solve the problem as a mixed-integer linear program (MILP). Vujanic et al.[22] use robust optimization to operate a batch plant as a DR resource, assuming a fixed capacity of interruptible load. It is clear that there can be financial benefits in operating process facilities to reduce electricity consumption during peak usage periods. However, DR programs also present an opportunity to simultaneously improve grid resilience and provide economic benefit to process facilities that have (or can be retrofitted to provide) the ability to rapidly change electricity consumption in response to requests from power system operators.

In this work we extend the stochastic programming approach proposed by Bynum et al.[23] Specifically we consider the tradeoff of DR versus transmission line hardening investments. We apply a linear approximation of the alternating current power flow (ACPF) model (the linear approximation is typically referred to as DCPF) to demonstrate the opportunity for DR in emergency response. We demonstrate this framework on several test cases. Our numerical results indicate, for these test cases, that a modest amount of DR can significantly reduce the capital investment required to make the electric grid resilient. This suggests that there may be opportunities for flexible process systems and system operators — i.e., Independent System Operators (ISOs) and Regional Transmission Operators (RTOs) — or electric utilities to work together toward both improving electric grid resilience and mutual financial benefit.

In order to evaluate the solution obtained with the DC approximation on the alternating current (AC) power system, we formulate the same DR problem with the nonlinear ACPF equations. This results in a stochastic, nonconvex mixed-integer nonlinear program (MINLP) which can be challenging to solve. Deterministic global optimization of nonconvex MINLPs is typically addressed with Branch and Bound techniques.[24,25] However, multi-tree methods, traditionally used to solve convex MINLPs, have recently been extended and successfully applied to nonconvex problems.[26–29]

In this paper, we use a tailored multi-tree approach involving the solution of a sequence of mixed-integer second order cone programming (MISOCP) relaxations and nonlinear programs (NLPs). Although our algorithm is not guaranteed to find the globally optimal solution, we found that 83 of the 87 problems solved with pglib_opf_case14_ieee[30] were indeed provably solved to global optimality. Our results on both the AC and DC models show similar trends regarding the impact of DR on resilience and the locational value, i.e., at which buses DR should be considered. However, we demonstrate that the DC approximation often underestimates the amount of DR needed.

The rest of this paper is organized as follows. First, we present our stochastic MILP

and MINLP programming formulations for evaluating the tradeoff of line hardening and demand response. We then present a MISOCP relaxation of the MINLP and describe the tools and algorithms used to solve our demand response formulations. Finally, we illustrate the effectiveness of the framework on several standard test cases, followed by a summary and conclusions.

Problem Formulation and Solution Approach

Previous work has focused on operational changes in process facilities to provide peak shaving or interruptible load for the the purposes of cost reduction.[31] However, to assess the value of interruptable load for resilience (and hence reasonable investment targets for required process facility design and retrofit), there is a need to integrate these analyses with grid models.

In this section, we present a framework to quantify the value of DR for improving system resilience due to weather-related events. Specifically, we formulate two stochastic programming problems to investigate the tradeoff between infrastructure investment (i.e., hardening a line to prevent damage in a weather-related event) and mitigation benefits provided by DR. In these stochastic programming formulations, weather events are modeled using a set of discrete scenarios with random transmission line outages. The formulations include parameters for the number of allowed demand response buses (selected from a subset of the overall network buses) and the maximum percentage of load reduction. The goal of the optimization problems is to determine the minimum number and selection of hardened lines along with the selection of demand response nodes required to ensure system feasibility over the line-outage scenarios.

Since the system constraints for ACPF in the transmission network are nonconvex and nonlinear, the resulting MINLP would be too large for efficient solution of realistic grid networks with current off-the-shelf tools. Fortunately, a linearized form, also known as the

DCPF-based model, enables representation of the problem as an MILP and solutions on large networks with this approximation are tractable. We perform the tradeoff analysis on larger cases using the MILP formulation, and compare results from the MILP formulation and the full MINLP formulation on two smaller test cases to assess the impact of the approximation on the conclusions of the analysis. In the next three subsections, we provide background on modeling power systems and describe the DCPF-based and the ACPF-based resilience demand response formulations.

A Review of Power Systems Modeling

An electric grid may be modeled as a graph of nodes and edges where the nodes represent buses (e.g., generating stations, substations) and edges represent transmission elements (e.g., lines, transformers). Generators, which may be found at one or more buses, induce sinusoidal voltage waveforms in the network (i.e., the voltage is not constant). The voltages induced by generators produce current waveforms so that power may be transmissted by transmission lines from the generators to energy consumers. At steady state, these waveforms become phasors (i.e., the amplitude and frequency are constant). Thus, the voltage, current, and power phasors may be modeled with complex numbers with either real and imaginary components or magnitudes and angles.

Power flow through a grid is governed by Ohm's Law for AC circuits, Joule's First Law, and Kirchhoff's circuit laws. Kirchhoff's Current Law (KCL) states that the total current entering a bus must equal the total current leaving the bus. Kirchhoff's Voltage Law (KVL) states that the voltage differences around any cycle in the network must sum to zero. Joule's First Law relates the power flow on a transmission line to the current and voltage. The extension of Ohm's Law to AC systems relates the current on a transmission line to the voltage difference along the line and the admittance of the line. The admittance of a transmission line is a complex physical property of the line with real and imaginary

components, referred to as the conductance and susceptance, respectively. The conductance represents the ease at which electric current passes and is determined as:

$$G_l = R_l/(R_l^2 + X_l^2) \tag{1}$$

where R_l is the line resistance and X_l is the line reactance. The susceptance represents the ease at which electric current changes and is determined as:

$$B_l = -X_l/(R_l^2 + X_l^2). \tag{2}$$

The physical properties of the line may also be expressed in terms of the impedance, which is the inverse of the admittance. Impedance has real and imaginary components resistance and reactance.

With these definitions, the ACPF equations describing power flows on transmission line l from bus b toward bus n are given by,

$$p_{l,b,n} = C_{l,b,n}^{\alpha,p} v_b^2 + C_{l,b,n}^{\beta,p} v_b v_n \cos(\theta_b - \theta_n) + C_{l,b,n}^{\gamma,p} v_b v_n \sin(\theta_b - \theta_n) \tag{3}$$

$$q_{l,b,n} = C_{l,b,n}^{\alpha,q} v_b^2 + C_{l,b,n}^{\beta,q} v_b v_n \cos(\theta_b - \theta_n) + C_{l,b,n}^{\gamma,q} v_b v_n \sin(\theta_b - \theta_n) \tag{4}$$

where the coefficients C are given in the Appendix in terms of transmission line properties resistance and reactance, p is the real component of power flow, q is the imaginary (or reactive) component of power flow, v is the voltage magnitude, and θ is the voltage angle. Note that these equations could also be written in terms of the real and imaginary components of the voltages. More detailed reviews of power flow formulations may be found in the literature.[32,33]

The DCPF-based Formulation

To form the linearized DC model from the ACPF equations, the following assumptions are made:

- the resistance of transmission lines is much less than the reactance, i.e., $R \ll X$, and
- for the voltage phasor: (1) the voltage magnitude is assumed to be nominal, i.e., $v \approx 1$ per-unit, for every bus in the system and
- (2) the voltage phase angle differences between interconnected buses is assumed to be small, i.e., $\sin(\theta_b - \theta_n) \approx \theta_b - \theta_n$.

This results in a representation that includes real power flow only and a linear relationship between power flow on the transmission lines and voltage angles at the buses.

The stochastic programming formulation based on the linearized DCPF model is shown below in disjunctive form.

$$\min \quad |Y|_{true} \tag{5.1}$$

s.t.

$$\sum_{g \in \mathcal{G}_b} p^G_{s,g} - \sum_{\{(l,i,j) \in \mathcal{K} \mid i=b\}} p_{s,l,i,j} = p^L_{s,b} + G^{Sh}_b \qquad \forall\, b \in \mathcal{B}, \forall\, s \in \mathcal{S} \tag{5.2}$$

$$\begin{bmatrix} X^H_{s,l,b,n} \\ p_{s,l,b,n} = \frac{1}{X_l T^m_l}\left(\theta_b, s - \theta_n, s + C^T_{l,b,n}\right) \\ -\Theta^{\max}_{b,n} \leq \theta_{s,b} - \theta_{s,n} \leq \Theta^{\max}_{b,n} \end{bmatrix} \bigvee \begin{bmatrix} \neg X^H_{s,l,b,n} \\ p_{s,l,b,n} = 0 \end{bmatrix} \qquad \forall\, (l,b,n) \in \mathcal{K}, \forall\, s \in \mathcal{S} \tag{5.3}$$

$$X^H_{s,l,b,n} \text{ is } true \qquad \forall\, \{(l,b,n) \in \mathcal{K} \mid l \notin \mathcal{L}^D_s\}, \forall\, s \in \mathcal{S} \tag{5.4}$$

$$Y_l \Leftrightarrow X^H_{s,l,b,n} \qquad \forall\, \{(l,b,n) \in \mathcal{K} \mid l \in \mathcal{L}^D_s\}, \forall\, s \in \mathcal{S} \tag{5.5}$$

$$\begin{bmatrix} X^D_{s,b} \\ (1-\Delta_b)P^L_b \leq p^L_{s,b} \leq P^L_b \end{bmatrix} \bigvee \begin{bmatrix} \neg X^D_{s,b} \\ p^L_{s,b} = P^L_b \end{bmatrix} \qquad \forall\, b \in \mathcal{B}, \forall\, s \in \mathcal{S} \tag{5.6}$$

$$X^D_{s,b} \text{ is } false, \qquad \forall\, \{b \in \mathcal{B} \mid b \notin B^{DR}\} \tag{5.7}$$

$$Z_b \Leftrightarrow X^D_{s,b} \qquad \forall\, b \in \mathcal{B}^{\mathcal{DR}}, \forall\, s \in \mathcal{S} \tag{5.8}$$

$$|Z|_{true} \leq N_z \tag{5.9}$$

$$P^{G,\min}_g \leq p^G_{s,g} \leq P^{G,\max}_g \qquad \forall\, g \in \mathcal{G}, \forall\, s \in \mathcal{S} \tag{5.10}$$

$$-S_l^{\max} \leq p_{s,l,b,n} \leq S_l^{\max} \qquad \forall\, (l,b,n) \in \mathcal{K}, \forall\, s \in \mathcal{S} \tag{5.11}$$

$$\theta_{s,ref} = 0 \qquad \forall\, s \in \mathcal{S} \tag{5.12}$$

$$X^H_{s,l,b,n} \in \{true, false\} \qquad \forall\, (l,b,n) \in \mathcal{K}, \forall\, s \in \mathcal{S} \tag{5.13}$$

$$X^D_{s,b} \in \{true, false\} \qquad \forall\, b \in \mathcal{B}, \forall\, s \in \mathcal{S} \tag{5.14}$$

$$Z_b \in \{true, false\} \qquad \forall\, b \in \mathcal{B}^{DR} \tag{5.15}$$

$$Y_l \in \{true, false\} \qquad \forall\, l \in \mathcal{L} \tag{5.16}$$

The coefficients in the constraints are available from the network data for the particular case study being considered, or computed from equations in the Appendix. The sets $\mathcal{B}$, $\mathcal{B}^{DR}$, $\mathcal{G}$, $\mathcal{G}_b$, $\mathcal{L}$, $\mathcal{L}_b$, and $\mathcal{S}$ are the sets of buses, buses that are candidates for demand response, generators, generators at bus b, branches, branches connected to bus b, and scenarios, respectively. The set $\mathcal{K}$ is a set of 3-tuples. For each branch, there are two 3-tuples in the set: (branch index, "from" bus index, "to" bus index) and (branch index, "to" bus index, "from" bus index).

Here, Y_l is *true* if line l is selected for hardening. The objective function (5.1) seeks to minimize the number of lines selected for hardening, represented by $|Y|_{true}$, which is defined as the count of the number of Y_l variables that are true (i.e., $|\{l \in \mathcal{L} \mid Y_l \text{ is } true\}|$). Equation (5.2) is the power balance at the bus nodes, including any connected generators or transmission lines, as well as demand loads and bus shunts.

The set $\mathcal{L}^D_s$ is the set of lines that are damaged in scenario s. Unless these lines are selected for hardening, these lines will be removed for scenario s in the model. Following this, the equations in (5.3) represent the disjunctions to account for line hardening. The boolean variable $X^H_{s,l,b,n}$ is *true* if line l either was not damaged in scenario s as indicated in (5.4), or was damaged in scenario s but selected for hardening, as enforced in (5.5). If the line is present in scenario s, then the power flow $p_{s,l,b,n}$ is computed and the phase angle constraints are enforced across the line. Otherwise if the line is not present, then the power flow in the line is forced to be zero (i.e., $p_{s,l,b,n} = 0$) and there is no restriction on phase angle difference bounds between the (unconnected) buses.

The disjunction (5.6) along with equations (5.7) and (5.8) encapsulate the selection of

nodes where DR is allowed. Here, Z_b is $false$ (no DR) if bus b is not a candidate for DR or not selected for DR, and $true$ if bus b is a candidate for DR that is then selected as an interruptible load. The set $\mathcal{B}^{DR} \subseteq \mathcal{B}$ is the set of candidate buses that can be selected for DR. If the node is selected for DR, then $X^D_{s,b}$ is $true$ for the corresponding bus and all scenarios (by equation (5.8)), and the system operator is allowed (by disjunction (5.6)) to request a load reduction up to a value of $\Delta_b P^L_b$ with $0 \leq \Delta_b \leq 1$. Otherwise, the requested load, P^L_b, must be satisfied. Equation (5.9) limits the number of DR nodes selected to be no more than N_z using the same definition for the count as that used in the objective function.

Then equations (5.10) and (5.11) represent the generator limits and line thermal limits respectively. The line thermal limits can be included for all branches since the power flow is forced to be zero if a line is damaged (and not selected for hardening). Equation (5.12) fixes the angle of the reference bus to be zero; the selection of reference bus is arbitrary, but necessary to ensure uniqueness of voltage angles.

This optimization problem is converted from disjunctive form to a large-scale MILP using the big-M method for the disjunctions.[34] It can then be used to compute the minimum number of hardened lines required to ensure feasible operation across all weather-event scenarios. By adjusting the values for Δ_b, the allowable fractional reduction in load, and N_z, the allowable number of demand response nodes selected, we can determine the reduction in required hardened lines as a function of these parameters. This enables a tradeoff assessment of the impact of different demand response contracts on the infrastructure investment required to maintain reliability under the scenario set.

The ACPF-based Formulation

The above problem formulation in (5) utilizes the extensively used linear DC approximation of the ACPF equations, resulting in a large-scale MILP problem. The formulation below includes the full nonlinear form of the ACPF equations, resulting in a stochastic MINLP. In this formulation, both real and reactive power are represented, power losses are accounted for,

and the voltage magnitude is not assumed to be uniform across the network. The following variable transformation[35] facilitates both the MINLP formulation and its relaxation.

$$\alpha_{s,b} \equiv v_{s,b}^2 \tag{6.1}$$
$$\beta_{s,b,n} \equiv v_{s,b} v_{s,n} \cos(\theta_{s,b} - \theta_{s,n}) \tag{6.2}$$
$$\gamma_{s,b,n} \equiv v_{s,b} v_{s,n} \sin(\theta_{s,b} - \theta_{s,n}). \tag{6.3}$$

With this variable transformation, an MINLP representation of the resilience DR formulation is,

$$\min \quad |Y|_{true} \tag{7.1}$$

s.t.

$$\sum_{g \in \mathcal{G}_b} p_{s,g}^G - \sum_{\{(l,i,j) \in \mathcal{K} | i=b\}} p_{s,l,i,j} = p_{s,b}^L + G_b^{Sh} \alpha_{s,b} \qquad \forall\, b \in \mathcal{B}, \forall\, s \in \mathcal{S} \tag{7.2}$$

$$\sum_{g \in \mathcal{G}_b} q_{s,g}^G - \sum_{\{(l,i,j) \in \mathcal{K} | i=b\}} q_{s,l,i,j} = q_{s,b}^L - B_b^{Sh} \alpha_{s,b} \qquad \forall\, b \in \mathcal{B}, \forall\, s \in \mathcal{S} \tag{7.3}$$

$$\begin{bmatrix} X_{s,l,b,n}^H \\ p_{s,l,b,n} = C_{l,b,n}^{\alpha,p} \alpha_{s,b} + C_{l,b,n}^{\beta,p} \beta_{s,b,n} + C_{l,b,n}^{\gamma,p} \gamma_{s,b,n} \\ q_{s,l,b,n} = C_{l,b,n}^{\alpha,q} \alpha_{s,b} + C_{l,b,n}^{\beta,q} \beta_{s,b,n} + C_{l,b,n}^{\gamma,q} \gamma_{s,b,n} \\ -\tan(\Theta_{b,n}^{\max}) \beta_{s,b,n} \le \gamma_{s,b,n} \le \tan(\Theta_{b,n}^{\max}) \beta_{s,b,n} \end{bmatrix} \bigvee \begin{bmatrix} \neg X_{s,l,b,n}^H \\ p_{s,l,b,n} = 0 \\ q_{s,l,b,n} = 0 \end{bmatrix} \qquad \forall\, (l,b,n) \in \mathcal{K}, \forall\, s \in \mathcal{S} \tag{7.4}$$

$$X_{s,l,b,n}^H \text{ is } true \qquad \forall\, \{(l,b,n) \in \mathcal{K} \mid l \notin \mathcal{L}_s^D\}, \forall\, s \in \mathcal{S} \tag{7.5}$$

$$Y_l \Leftrightarrow X_{s,l,b,n}^H \qquad \forall\, \{(l,b,n) \in \mathcal{K} \mid l \in \mathcal{L}_s^D\}, \forall\, s \in \mathcal{S} \tag{7.6}$$

$$\beta_{s,b,n} = \beta_{s,n,b} \qquad \forall\, (b,n) \in \mathcal{A}, \forall\, s \in \mathcal{S} \tag{7.7}$$

$$\gamma_{s,b,n} = -\gamma_{s,n,b} \qquad \forall\, (b,n) \in \mathcal{A}, \forall\, s \in \mathcal{S} \tag{7.8}$$

$$\beta_{s,b,n}^2 + \gamma_{s,b,n}^2 = \alpha_{s,b} \alpha_{s,n} \qquad \forall\, (b,n) \in \mathcal{A}, \forall\, s \in \mathcal{S} \tag{7.9}$$

$$\theta_{s,b} - \theta_{s,n} = \arctan\left(\frac{\gamma_{s,b,n}}{\beta_{s,b,n}}\right) \qquad \forall\, (b,n) \in \mathcal{A}, \forall\, s \in \mathcal{S} \tag{7.10}$$

$$\theta_{s,ref} = 0 \qquad \forall\, s \in \mathcal{S} \tag{7.11}$$

$$p_{s,l,b,n}^2 + q_{s,l,b,n}^2 \le (S_l^{\max})^2 \qquad \forall\, (l,b,n) \in \mathcal{K}, \forall\, s \in \mathcal{S} \tag{7.12}$$

$$(V_b^{\min})^2 \le \alpha_{s,b} \le (V_b^{\max})^2 \qquad \forall\, b \in \mathcal{B}, \forall\, s \in \mathcal{S} \tag{7.13}$$

$$P_g^{G,\min} \le p_{s,g}^G \le P_g^{G,\max} \qquad \forall\, g \in \mathcal{G}, \forall\, s \in \mathcal{S} \tag{7.14}$$

$$Q_g^{G,\min} \le q_{s,g}^G \le Q_g^{G,\max} \qquad \forall\, g \in \mathcal{G}, \forall\, s \in \mathcal{S} \tag{7.15}$$

$$\begin{bmatrix} X_{s,b}^D \\ (1-\Delta_b) P_b^L \le p_{s,b}^L \le P_b^L \\ (1-\Delta_b) Q_b^L \le q_{s,b}^L \le Q_b^L \end{bmatrix} \bigvee \begin{bmatrix} \neg X_{s,b}^D \\ p_{s,b}^L = P_b^L \\ q_{s,b}^L = Q_b^L \end{bmatrix} \qquad \forall\, b \in \mathcal{B}, \forall\, s \in \mathcal{S} \tag{7.16}$$

$$X_{s,b}^D \text{ is } false, \qquad \forall\, \{b \in \mathcal{B} \mid b \notin B^{DR}\} \tag{7.17}$$

$$Z_b \Leftrightarrow X^D_{s,b} \qquad \forall\, b \in \mathcal{B}^{\mathcal{DR}}, \forall\, s \in \mathcal{S} \tag{7.18}$$

$$|Z|_{true} \leq N_z \tag{7.19}$$

$$X^H_{s,l,b,n} \in \{true, false\} \qquad \forall\, (l,b,n) \in \mathcal{K}, \forall\, s \in \mathcal{S} \tag{7.20}$$

$$X^D_{s,b} \in \{true, false\} \qquad \forall\, b \in \mathcal{B}, \forall\, s \in \mathcal{S} \tag{7.21}$$

$$Z_b \in \{true, false\} \qquad \forall\, b \in \mathcal{B}^{DR} \tag{7.22}$$

$$Y_l \in \{true, false\} \qquad \forall\, l \in \mathcal{L} \tag{7.23}$$

Again the objective function (7.1) seeks to minimize the number of lines selected for hardening. Constraints (7.2) and (7.3) are the real and reactive power balances. If a branch is out of service and not hardened, the real and reactive power flows are forced to zero on the branch by constraints in disjunction (7.4). If the branch is hardened or not damaged, then constraint (7.4) relates the real and reactive power flows to the new variables $\alpha_{s,b}$, $\beta_{s,b,n}$, and $\gamma_{s,b,n}$ and enforces the angle difference limits through these variables. Equations (7.5) and (7.6) ensure that the boolean variables $X^H_{s,l,b,n}$ are $true$ for all branches without an outage, $true$ for all hardened branches, and $false$ otherwise. The definitions in (6) could be substituted directly into the power flow equations to obtain the standard polar form. However, equations (7.7) - (7.10) provide an alternate form in the transformed variables.[36] The set $\mathcal{A}$ is a set of 2-tuples containing all adjacent (connected) buses. Constraints (7.12) - (7.15) enforce thermal, voltage, and generator limits, respectively. The disjunction in (7.16) is identical to that used in the DC formulation except that it applies to the reactive power load as well. Constraints (7.17) - (7.23) are also identical to those used in the DCPF-based formulation.

The following section presents an MISOCP relaxation of the MINLP formulation (7) which can be used to obtain a valid lower bound on the problem and candidate integer solutions.

MISOCP Relaxation

The resilience formulation proposed in the previous section is a large-scale stochastic MINLP which is very difficult to solve. We will discuss the algorithm used to solve it in detail in the

following section. However, a key component is a convex relaxation of (7). There have been a number of relaxations applied to the alternating current optimal power flow (ACOPF) problem, including the second-order cone (SOC) relaxation,[35,36] the quadratic convex (QC) relaxation,[37] and McCormick relaxations of the rectangular form.[38,39] These relaxations have been used in algorithms for global solution of ACOPF[40–42] and problems including discrete decisions like optimal transmission switching[43] and unit commitment.[29] The algorithm we use to solve this problem is based on the SOC relaxation, which may be obtained from (7) by dropping (7.10) - (7.11), relaxing (7.9) with a convex SOC inequality, and converting the disjunctions to Big-M constraints.[34] The resulting MISOCP relaxation is,

$$\min \sum_{l \in \mathcal{L}} y_l \tag{8.1}$$

s.t.

$$\sum_{g \in \mathcal{G}_b} p^G_{s,g} - \sum_{\{(l,i,j) \in \mathcal{K} \mid i=b\}} p_{s,l,b,n} = p^L_{s,b} + G^{Sh}_b \alpha_{s,b} \qquad \forall\, b \in \mathcal{B}, \forall\, s \in \mathcal{S} \tag{8.2}$$

$$\sum_{g \in \mathcal{G}_b} q^G_{s,g} - \sum_{\{(l,i,j) \in \mathcal{K} \mid i=b\}} q_{s,l,b,n} = q^L_{s,b} - B^{Sh}_b \alpha_{s,b} \qquad \forall\, b \in \mathcal{B}, \forall\, s \in \mathcal{S} \tag{8.3}$$

$$p_{s,l,b,n} = C^{\alpha,p}_{l,b,n} \zeta_{s,l,b} + C^{\beta,p}_{l,b,n} \eta_{s,l,b,n} + C^{\gamma,p}_{l,b,n} \phi_{s,l,b,n} \qquad \forall\, \{(l,b,n) \in \mathcal{K} \mid l \in \mathcal{L}^D_s\}, \forall\, s \in \mathcal{S} \tag{8.4}$$

$$q_{s,l,b,n} = C^{\alpha,q}_{l,b,n} \zeta_{s,l,b} + C^{\beta,q}_{l,b,n} \eta_{s,l,b,n} + C^{\gamma,q}_{l,b,n} \phi_{s,l,b,n} \qquad \forall\, \{(l,b,n) \in \mathcal{K} \mid l \in \mathcal{L}^D_s\}, \forall\, s \in \mathcal{S} \tag{8.5}$$

$$p_{s,l,b,n} = C^{\alpha,p}_{l,b,n} \alpha_{s,b} + C^{\beta,p}_{l,b,n} \beta_{s,b,n} + C^{\gamma,p}_{l,b,n} \gamma_{s,b,n} \qquad \forall\, \{(l,b,n) \in \mathcal{K} \mid l \notin \mathcal{L}^D_s\}, \forall\, s \in \mathcal{S} \tag{8.6}$$

$$q_{s,l,b,n} = C^{\alpha,q}_{l,b,n} \alpha_{s,b} + C^{\beta,q}_{l,b,n} \beta_{s,b,n} + C^{\gamma,q}_{l,b,n} \gamma_{s,b,n} \qquad \forall\, \{(l,b,n) \in \mathcal{K} \mid l \notin \mathcal{L}^D_s\}, \forall\, s \in \mathcal{S} \tag{8.7}$$

$$\underline{\alpha_{s,b}} y_l \leq \zeta_{s,l,b} \leq \overline{\alpha_{s,b}} y_l \qquad \forall\, l \in \mathcal{L}_b \cap \mathcal{L}^D_s, \forall\, b \in \mathcal{B}, \forall\, s \in \mathcal{S} \tag{8.8}$$

$$\overline{\alpha_{s,b}}(y_l - 1) + \alpha_{s,b} \leq \zeta_{s,l,b} \leq \underline{\alpha_{s,b}}(y_l - 1) + \alpha_{s,b} \qquad \forall\, l \in \mathcal{L}_b \cap \mathcal{L}^D_s, \forall\, b \in \mathcal{B}, \forall\, s \in \mathcal{S} \tag{8.9}$$

$$\underline{\beta_{s,b,n}} y_l \leq \eta_{s,l,b,n} \leq \overline{\beta_{s,b,n}} y_l \qquad \forall\, \{(l,b,n) \in \mathcal{K} \mid l \in \mathcal{L}^D_s\}, (b,n) \in \mathcal{A}, \forall\, s \in \mathcal{S} \tag{8.10}$$

$$\overline{\beta_{s,b,n}}(y_l - 1) + \beta_{s,b,n} \leq \eta_{s,l,b,n} \leq \underline{\beta_{s,b,n}}(y_l - 1) + \beta_{s,b,n} \qquad \forall\, \{(l,b,n) \in \mathcal{K} \mid l \in \mathcal{L}^D_s\}, (b,n) \in \mathcal{A}, \forall\, s \in \mathcal{S} \tag{8.11}$$

$$\underline{\gamma_{s,b,n}} y_l \leq \phi_{s,l,b,n} \leq \overline{\gamma_{s,b,n}} y_l \qquad \forall\, \{(l,b,n) \in \mathcal{K} \mid l \in \mathcal{L}^D_s\}, (b,n) \in \mathcal{A}, \forall\, s \in \mathcal{S} \tag{8.12}$$

$$\overline{\gamma_{s,b,n}}(y_l - 1) + \gamma_{s,b,n} \leq \phi_{s,l,b,n} \leq \underline{\gamma_{s,b,n}}(y_l - 1) + \gamma_{s,b,n} \qquad \forall\, \{(l,b,n) \in \mathcal{K} \mid l \in \mathcal{L}^D_s\}, (b,n) \in \mathcal{A}, \forall\, s \in \mathcal{S} \tag{8.13}$$

$$\eta_{s,l,b,n} = \eta_{s,l,n,b} \qquad \forall\, \{(l,b,n) \in \mathcal{K} \mid l \in \mathcal{L}^D_s\}, (b,n) \in \mathcal{A}, \forall\, s \in \mathcal{S} \tag{8.14}$$

$$\phi_{s,l,b,n} = -\phi_{s,l,n,b} \qquad \forall \{(l,b,n) \in \mathcal{K} \mid l \in \mathcal{L}_s^D\}, (b,n) \in \mathcal{A}, \forall\, s \in \mathcal{S} \tag{8.15}$$

$$\eta_{s,l,b,n}^2 + \phi_{s,l,n,b}^2 \leq \zeta_{s,l,b}\zeta_{s,l,n} \qquad \forall \{(l,b,n) \in \mathcal{K} \mid l \in \mathcal{L}_s^D\}, (b,n) \in \mathcal{A}, \forall\, s \in \mathcal{S} \tag{8.16}$$

$$\beta_{s,b,n} = \beta_{s,n,b} \qquad \forall \{(l,b,n) \in \mathcal{K} \mid l \notin \mathcal{L}_s^D\}, (b,n) \in \mathcal{A}, \forall\, s \in \mathcal{S} \tag{8.17}$$

$$\gamma_{s,b,n} = -\gamma_{s,n,b} \qquad \forall \{(l,b,n) \in \mathcal{K} \mid l \notin \mathcal{L}_s^D\}, (b,n) \in \mathcal{A}, \forall\, s \in \mathcal{S} \tag{8.18}$$

$$\beta_{s,b,n}^2 + \gamma_{s,b,n}^2 \leq \alpha_{s,b}\alpha_{s,n} \qquad \forall \{(l,b,n) \in \mathcal{K} \mid l \notin \mathcal{L}_s^D\}, (b,n) \in \mathcal{A}, \forall\, s \in \mathcal{S} \tag{8.19}$$

$$p_{s,l,b,n}^2 + q_{s,l,b,n}^2 \leq (S_l^{\max})^2 \qquad \forall\, (l,b,n) \in \mathcal{K}, \forall\, s \in \mathcal{S} \tag{8.20}$$

$$(V_b^{\min})^2 \leq \alpha_{s,b} \leq (V_b^{\max})^2 \qquad \forall\, b \in \mathcal{B}, \forall\, s \in \mathcal{S} \tag{8.21}$$

$$P_g^{G,\min} \leq p_{s,g}^G \leq P_g^{G,\max} \qquad \forall\, g \in \mathcal{G}, \forall\, s \in \mathcal{S} \tag{8.22}$$

$$Q_g^{G,\min} \leq q_{s,g}^G \leq Q_g^{G,\max} \qquad \forall\, g \in \mathcal{G}, \forall\, s \in \mathcal{S} \tag{8.23}$$

$$-\tan(\Theta_{b,n}^{\max})\eta_{s,l,b,n} \leq \phi_{s,l,b,n} \qquad \forall \{(l,b,n) \in \mathcal{K} \mid l \in \mathcal{L}_s^D\}, (b,n) \in \mathcal{A}, \forall\, s \in \mathcal{S} \tag{8.24}$$

$$\phi_{s,l,b,n} \leq \tan(\Theta_{b,n}^{\max})\eta_{s,l,b,n} \qquad \forall \{(l,b,n) \in \mathcal{K} \mid l \in \mathcal{L}_s^D\}, (b,n) \in \mathcal{A}, \forall\, s \in \mathcal{S} \tag{8.25}$$

$$-\tan(\Theta_{b,n}^{\max})\beta_{s,b,n} \leq \gamma_{s,b,n} \qquad \forall \{(l,b,n) \in \mathcal{K} \mid l \notin \mathcal{L}_s^D\}, (b,n) \in \mathcal{A}, \forall\, s \in \mathcal{S} \tag{8.26}$$

$$\gamma_{s,b,n} \leq \tan(\Theta_{b,n}^{\max})\beta_{s,b,n} \qquad \forall \{(l,b,n) \in \mathcal{K} \mid l \notin \mathcal{L}_s^D\}, (b,n) \in \mathcal{A}, \forall\, s \in \mathcal{S} \tag{8.27}$$

$$(1-\Delta_b)P_b^L z_b + P_b^L(1-z_b) \leq p_{s,b}^L \leq P_b^L \qquad \forall\, b \in \mathcal{B}, \forall\, s \in \mathcal{S} \tag{8.28}$$

$$(1-\Delta_b)Q_b^L z_b + Q_b^L(1-z_b) \leq q_{s,b}^L \leq Q_b^L \qquad \forall\, b \in \mathcal{B}, \forall\, s \in \mathcal{S} \tag{8.29}$$

$$\sum_{b \in \mathcal{B}} z_b \leq N_z \tag{8.30}$$

$$z_b \in \{0,1\} \qquad \forall\, b \in \mathcal{B} \tag{8.31}$$

$$y_l \in \{0,1\} \qquad \forall\, l \in \mathcal{L} \tag{8.32}$$

Rather than applying a Big-M transformation directly to the constraints in (7.4), we use a similar approach to that proposed by Kocuk et al.[43] Because we typically have tight bounds on α, β, and γ, we introduce the new variables ζ, η, and ϕ and relate them to α, β, and γ through constraints (8.8) - (8.13). These constraints ensure that ζ, η, and ϕ are all equal to zero for branches that are out of service but not hardened. Thus, the power flows on transmission lines that are out of service but not hardened are also zero by constraints (8.4) and (8.5). For transmission lines that are hardened, constraints (8.8) - (8.13) ensure that ζ,

η, and ϕ equal α, β, and γ, respectively. Note that this formulation could be written without η or ϕ. However, including these variables allows extensions which include other relaxations (e.g., the QC relaxation of (6)). The next section describes how this MISOCP relaxation is used to solve the original MINLP.

Software Tools and Solution Approach

All problem formulations and solution strategies were implemented using Pyomo, a Python-based algebraic modeling language.[44] The DC formulation (5) is an MILP following big-M transformation of the disjunctions, and the extensive form is solved directly using Gurobi 7.5.2. The AC formulation (7) is an MINLP (again, following a big-M transformation) that is significantly more challenging to solve. Here, we use a tailored multi-tree solution approach similar to those presented by Liu et al.[29] and Kocuk et al.[43] The algorithm involves three main steps. First, the MISOCP (8) relaxation is solved with Gurobi 7.5.2 to obtain a lower bound and a candidate integer solution. Second the integer variables are fixed in the MINLP, and an NLP is solved with Ipopt[45] (using the HSL linear solver MA27[46]) to obtain an upper bound on the objective if the problem is feasible. Third, if the gap between the upper and lower bounds is not small enough, a "no-good" cut[47] is added to the MISOCP in order to remove already visited integer solutions from the feasible region . Given a candidate integer solution $\mathbb{X}^k = \{x_1^k, x_2^k, ..., x_N^k\}$, $\mathcal{I} = \{1, 2, ..., N\}$, $\mathcal{I}_1 = \{i \in \mathcal{I} | x_i^k = 1\}$, $\mathcal{I}_0 = \{i \in \mathcal{I} | x_i^k = 0\}$, the "no-good" cut

$$\sum_{i \in \mathcal{I}_1} x_i - \sum_{i \in \mathcal{I}_0} x_i \leq |\mathcal{I}_1| - 1 \tag{9}$$

ensures that the same integer solution ($\mathbb{X}^k$) is not obtained in subsequent iterations. The three steps are then repeated. In the worst case, the "no-good" cuts guarantee enumeration of all possible integer solutions. As described by both Liu et al.[29] and Kocuk et al.[43], if the NLP subproblems are solved to global optimality, then the algorithm will converge to global

optimality for the original MINLP. In this work, we do not solve the NLP subproblems to global optimality, so the algorithm is a heuristic with regards to optimality of the discrete decisions. Additionally, when the integer variables are fixed in the AC DR formulation, the objective is fixed. Therefore, the NLP subproblem reduces to a feasibility check. Note that proving infeasibility of the NLP subproblem still requires global optimization techniques. Proving infeasibility of the NLP subproblems is out of the scope of this paper but will be considered in future work. Rather, we terminate the algorithm when Ipopt finds a feasible solution to one of the NLP subproblems. However, in many cases, the algorithm converges in one iteration without any integer cuts, and the globally optimal solution is obtained. Additionally, when the algorithm does not converge on the first iteration, we can still compute an optimality gap using the upper bound from the best feasible solution and the lower bound obtained before any integer cuts are added. In the case study, pglib_opf_case14_ieee,[30] 83 of the 87 problems were provably solved to global optimality. For further algorithm details, see the above references. The following section presents results for both the AC and DC DR formulations and compares the results.

Numerical Results

In this section, we evaluate the tradeoff between increased DR capabilities and capital investment in infrastructure for improving resilience to weather-related events. Both the DCPF- and the ACPF-based problem formulations are stochastic programming problems that seek to find solutions that provide feasible operation across all of the scenarios. Numerous studies have focused on electric grid resilience to the worst case scenario,[48–50] but this approach is not representative of naturally occurring, severe weather events. Different types of natural disasters have different impact regions, predictability, geographical span, and impact duration.[51–53] Therefore a range of forecasting models have been proposed in the literature to model grid component damage and outage duration, as well as a range of simulation

and optimization models to address service restoration, corrective actions, and preparedness planning. When historical data is available, it can be used to generate representative scenarios regarding transmission element failure due to weather-related events.

In the absence of system-specific data, we consider failure of transmission lines only, and characterize scenarios according to the set of transmission lines that are damaged; in other words, no power transfer occurs across the line — it is essentially removed from the network model. We formulate scenarios by randomly selecting a set of transmission lines to be out of service for each weather-event scenario. Note that both formulations could be adapted to consider failure of other transmission elements, including generators and substations.

We first use the DCPF-based stochastic programming formulation to compute the minimum number of hardened transmission lines that are required to ensure feasible operation across all the scenarios. In this analysis, we vary the number of nodes to consider for demand response contracts, as well as the maximum reduction in load required should that bus be selected for demand response (written as a fraction, Δ_b, of the expected load at each bus). This provides us with a set of tradeoff curves that provide the minimum required capital investment (in terms of the number of required hardened lines) as a function of the number of demand response contracts and the load reduction fraction. This analysis is performed on a set of case studies that are described in more detail in the following section.

Following this analysis, we compare results of the DCPF- and the ACPF-based formulations. Because of the challenge associated with solution of large-scale MINLP problems, we perform this comparison on a set of smaller grid models from a standard test suite. In particular, we compare the solutions from the AC and DC problems in terms of the required reduction in number of hardened lines and the location of selected demand response nodes. We also estimate the impact of using the DC approximation by taking solutions from the DCPF-based MILP formulation and testing these for feasibility in the AC model. This allows comparison of the larger test cases and provides an indication of the degree of applicability of the DCPF-based model.

The Value of Demand Response

In this section, we evaluate the tradeoff between increased DR and required capital investment in terms of the number of hardened lines. The maximum required fractional load reduction for DR nodes, Δ_b is varied from 0 to 1, and the number of optimally selected DR node locations N_z is varied from 0 to 10. Three test cases are considered from version 17.08 of the Power Grid Lib — Optimal Power Flow repository:[30] pglib_opf_case118_ieee, pglib_opf_case162_ieee_dtc, and pglib_opf_case300_ieee. For each problem, we considered 100 scenarios with 10 randomly selected branch outages per scenario. Note that branches with only one path between the corresponding pair of buses were excluded since such a branch would likely always need to be hardened. The results of this tradeoff analysis are presented in Figure 1. The y-axis shows the minimum number of branches that need to be hardened in order to maintain feasibility. Each group of columns represents a specific value of Δ_b. Within each group of columns, N_z varies from 0 to 10 by 2. The particular value of N_z associated with each column can be seen both in the legend and above the column. The problems were typically solved in under 5 minutes, although most problems took less than 1 minute.

As expected, the minimum number of hardened branches needed to maintain feasibility decreases both as N_z increases and as Δ_b increases. All three test cases show similar trends, indicating that demand response can have a significant impact on resilience. With Δ_b=0.25, only two DR contracts are required to reduce the objective by 11%, 25%, and 21% for cases pglib_opf_case118_ieee, pglib_opf_case162_ieee_dtc, and pglib_opf_case300_ieee, respectively. Increasing Δ_b to 0.5 results in reductions of 21%, 31%, and 25%, respectively. Even more dramatic cost reductions are possible in other cases. For example, with a 50% maximum load reduction, 10 DR contracts can reduce the required number of hardened lines from 32 to 17 (pglib_opf_case162_ieee_dtc). If fully interruptable load is a possibility, even more reduction can be realized across these test cases.

The extreme weather events in question typically only occur once every 5-10 years. If

chemical, petroleum, and manufacturing plants have the ability to operate flexibly in these rare times, the capital investment needed to make the grid more resilient can be reduced dramatically. As a result, the plants with demand response contracts could gain significant financial benefits in terms of electricity cost reduction with only very rare interruptions in operations. Of course, DR and transmission line hardening are not the only ways of making the electric grid more resilient, and real systems should consider other options along with system specific models and parameters in a more detailed decision making process.

The results we have shown so far only consider the DC model, which is a linear approximation of the true system and does not consider reactive power at all. In the following section, we further validate the value of demand response by both comparing solutions obtained with the DC and AC models and evaluating the DC solutions on an AC model.

A Comparison of DCPF- and ACPF-based Solutions

We used two approaches to evaluate the accuracy and effectiveness of the DC model on the AC system. First, we solved the demand response problem with both models and compared the solutions. For this, we used pglib_opf_case14_ieee and pglib_opf_case30_as, both with 30 scenarios. Figures 2 and 3 show the minimum number of hardened branches for both the AC and DC models as functions of N_z and Δ_b. In both cases, the DC model tends to underestimate the number of branches that need to be hardened to maintain feasibility, but the overall trends are quite similar. We also compared the integer solutions of the two models for pglib_opf_case14_ieee. The detailed results are presented in the Appendix. Table 1 summarizes these results. First, we define two sets. The set $\mathcal{DR}^*_{DC}$ is the union of the sets of buses selected for DR by the DC model across all values of Δ_b and N_z. The set $\mathcal{DR}^*_{AC}$ is the union of the sets of buses selected for DR by the AC model across all values of Δ_b and N_z. Table 1 the shows the intersection of these two sets, the buses unique to $\mathcal{DR}^*_{DC}$, and the buses unique to $\mathcal{DR}^*_{AC}$. As the tables show, there is strong agreement between the AC and DC solutions. In fact, all of the buses selected by the DC model were also selected by

the AC model. There was only one bus selected by the AC model and not the DC model.

Second, for each integer solution obtained with the DC model, we evaluated the fraction of AC-feasible scenarios (that is, fraction of scenarios that were feasible when evaluated using the AC model). Table 2 summarizes the results. The table shows the fraction of AC-feasible scenarios averaged over all values of Δ_b and N_z. Note that we did not include pglib_opf_case300_ieee because there were several scenarios for which Ipopt neither converged to an optimal solution nor converged to a point of local infeasibility. Case pglib_opf_case162_ieee_dtc also had a few scenarios for which Ipopt obtained neither of these two convergence criteria, but it was less than 0.3% of the scenarios. Therefore, we simply discarded these scenarios when computing the fraction of AC-feasible scenarios. Again, a problem may be feasible even if Ipopt converges to a point of local infeasibility. However, for simplicity, we are using this criterion as an approximation. Future work will use global optimization techniques to prove infeasibility. The average fraction of feasible scenarios was over 85% for all test cases except pglib_opf_case162_ieee_dtc. These are quite high and indicate high quality solutions even for the true AC system.

Finally, Figure 4 plots the fraction of AC-feasible scenarios and the minimum number of hardened branches as a function of N_z for the four test cases with Δ_b=0.2. The results for pglib_opf_case118_ieee behave as expected. The fraction of AC-feasible scenarios generally increases as N_z increases. However, there are cases where the fraction of AC-feasible scenarios can decrease with an increase in N_z. The reason for this relates back to Figures 2 and 3. The DC model often underestimates the amount of DR needed and/or the number of branches that need hardened. In some cases, the DC formulation results in a lower number of hardened branches and smaller fraction of DR than what is actually required to ensure AC-feasibility. An implementation of such a solution in the AC system may decrease capital investment, but it may also not provide the expected resilience. Because of this, it is important to continue development of MINLP strategies that can address AC power flow problems at scale.

Conclusions

This paper presents a stochastic programming framework for estimating the value of demand response capabilities in ensuring electric grid resilience. It includes two formulations that seek to determine the minimum number of hardened transmission lines required to ensure feasible operation across a set of weather-related failure scenarios.

The first formulation (an MILP) shows similar results with all three test cases considered. On the largest test case, the addition of only two demand response contracts (each requiring only a 25% drop in consumed load) is sufficient ensure feasible operation across all scenarios while reducing the required number of hardened lines (e.g., the required capital investment) by 21%. This indicates that demand response can have a significant impact on system resilience.

These results were obtained with an MILP formulation based on the linear DC approximation for the AC power flow equations. While this approximation is widely used in power systems analysis, it can underestimate the impact of thermal limits and other system constraints. In particular, for unit commitment problems, the DC approximation can lead to solutions that are suboptimal or not even feasible for the actual AC system. Therefore, we also included results with the actual nonlinear AC power flow equations to determine consistency.

Because the second formulation (an MINLP) cannot be efficiently solved for large-scale problems, we compare the results from the DC and AC formulations on a set of smaller test cases. We use a tailored multi-tree approach that solves a sequence of MISOCP relaxations of the MINLP to find candidate integer solutions and NLP subproblems to check feasibility. Using this approach, results with the smaller test cases show that both the DC approximation and the nonlinear AC formulation have similar trends, indicating that there is value in the use of demand response for improved resilience. Furthermore, they also find similar optimal locations for demand response contracts. For case pglib_opf_case14_ieee, every bus selected for demand response by the DC model was also selected for demand response by

the AC model (cumulative across all values of Δ_b and N_z). Only one bus was selected for demand response by the AC model and not the DC model. However, the linear model often underestimates the amount of demand response or hardened lines necessary to ensure resilience of the AC system. This result shows a need for future work in improved scalability of MINLPs based on AC power flow equations.

Ultimately, our results show that there is significant value in the introduction of new demand response capabilities. The formulations presented here can help process facilities quantify their potential impact on electric grid resilience, facilitating informed negotiations between process facilites and electric utilities when developing DR contracts. Of course, the cost of increasing operational flexibility at individual process facilities must also be evaluated. The formulations presented here could be extended to include process facility models. However, this is left for future work.

Acknowledgment

Sandia National Laboratories is a multimission laboratory managed and operated by National Technology and Engineering Solutions of Sandia, LLC, a wholly owned subsidiary of Honeywell International, Inc., for the U.S. Department of Energys National Nuclear Security Administration under contract DENA0003525.

Disclaimer: This paper describes objective technical results and analysis. Any subjective views or opinions that might be expressed in the paper do not necessarily represent the views of the U.S. Department of Energy or the United States Government.

The work of Michael Bynum, Anya Castillo, Carl Laird, and Jean-Paul Watson was supported by Sandia National Laboratories Laboratory Directed Research and Development (LDRD) program.

Notation

Sets

$\mathcal{B}$	Set of all buses
$\mathcal{B}^{DR}$	Set of buses that are candidates for demand response
$\mathcal{B}_b$	Set of buses connected to bus b by a branch
$\mathcal{G}$	Set of all generators
$\mathcal{G}_b$	Set of generators at bus b
$\mathcal{L}$	Set of all branches
$\mathcal{A}$	Set of 2-tuples containing adjacent buses
$\mathcal{L}_b$	Set of branches connected to bus b
$\mathcal{L}_s^D$	Set of branches damaged in scenario s
$\mathcal{H}$	Candidate set of hardened branches
$\mathcal{K}$	Set of 3-tuples describing bi-directional connectivity;
	for each branch there are two 3-tuples in this set:
	1) (Branch index, "from" bus index, "to" bus index)
	2) (Branch index, "to" bus index, "from" bus index)
$\mathcal{S}$	Set of all line failure scenarios

Parameters

P_b^L	Real power load at bus b
Q_b^L	Reactive power load at bus b
G_b^{Sh}	Shunt conductance at bus b
B_b^{Sh}	Shunt susceptance at bus b
$P_g^{G,\min}$	Minimum real power output at generator g

$P_g^{G,\max}$	Maximum real power output at generator g
$Q_g^{G,\min}$	Minimum reactive power output at generator g
$Q_g^{G,\max}$	Maximum reactive power output at generator g
$S_l^{\max}$	Maximum power magnitude on branch l
$\Theta_l^{\max}$	Maximum voltage angle difference for branch l
G_l	Conductance of branch l
B_l	Susceptance of branch l
R_l	Resistance of branch l
X_l	Reactance of branch l
T_l^m	Transformer tap ratio for branch l
T_l^a	Transformer phase shift for branch l
B_l^c	Charging susceptance of branch l
$V_b^{\min}$	Minimum voltage magnitude at bus b
$V_b^{\max}$	Maximum voltage magnitude at bus b
Δ_b	Fraction load decrease allowed by demand response contract at bus b
N_z	Maximum number of demand response contracts

Continuous Variables

$p_{s,g}^G$	Real power output at generator g
$q_{s,g}^G$	Reactive power output at generator g
$p_{s,b}^L$	Real power delivered to bus b
$q_{s,b}^L$	Reactive power delivered to bus b
$p_{s,l,b,n}$	Real power flow on branch l from bus b to bus n
$q_{s,l,b,n}$	Reactive power flow on branch l from bus b to bus n
$v_{s,b}$	Voltage magnitude at bus b

$\theta_{s,b}$	Voltage angle at bus b
Logic Variables	
Y_l	$true$ if branch l is selected for hardening, and $false$ otherwise
Z_b	$true$ if bus b is selected for demand response, and $false$ otherwise
$X^H_{s,l,b,n}$	$true$ if branch l is present for scenario s (i.e. either branch l is not in the damage set $\mathcal{L}^D_s$ or it is in the set, but selected for hardening) and $false$ otherwise
$X^D_{s,b}$	$true$ if bus b is selected for demand response and $false$ otherwise. (Same indicator as Z_b, but allows for clear representation of disjunctions across scenarios.)
Binary Variables	
y_l	binary variable representation of Y_l
z_b	binary variable representation of Z_b

Literature Cited

1 U.S. Department of Energy. Quadrennial energy review: Energy transmission, storage, and distribution infrastructure. Technical report, U.S. Department of Energy, 2015.

2 Executive Office of the President. Economic benefits of increasing electric grid resilience to weather outages. Technical report, Presidents Council of Economic Advisers, U.S. Department of Energys Office of Electricity Delivery and Energy Reliability, with assistance from the White House Office of Science and Technology, 2013.

3 House T.W. Presidential policy directive – critical infrastructure security and resilience. `https://www.whitehouse.gov/the-press-office/2013/02/12/`

presidential-policy-directive-critical-infrastructure-security-and-resil, February 2013. Accessed: 2016-09-19.

4 Preston B.L, Backhaus S.N, Ewers M, Phillips J.A, Silva-Monroy C.A, Dagle J.E, Tarditi A.G, Looney J, and King T.J, Jr. Resilience of the U.S. electricity system: A multi-hazard perspective. Technical report, Technical report, US DOE, 2016.

5 Hoffman P, Bryan W, Lippert A, Farber-DeAnda M, Cleaver M, Lewandowski C, and Young K. Hardening and resiliency: U.s. energy industry response to recent hurricane seasons. Technical report, Technical report, US DOE, 2010.

6 Bienstock D and Mattia S. Using mixed-integer programming to solve power grid blackout problems. *Discrete Optimization*, 4:115–141, 2007.

7 Carrión M, Arroyo J.M, and Alguacil N. Vulnerability-constrained transmission expansion planning: A stochastic programming approach. *IEEE Transactions on Power Systems*, 22(4):1436–1445, 2007.

8 Adibi M and Fink L. Power system restoration planning. *IEEE Transactions on Power Systems*, 9(1):22–28, 1994.

9 Lindemeyer D, Dommel H, and Adibi M. Power system restorationa bibliographical survey. *Int. J. Electr. Power Energy Syst.*, 23(3):219–227, 2001.

10 Castillo A. Risk analysis and management in power outage and restoration: A literature survey. *Electric Power Systems Research*, 107:9–15, 2014.

11 Henrikson C.B and Brief K. Designing a successful demand response program: Its not your grandfathers load control program. Technical report, Technical report, ACEE Summer Study on Energy Efficiency in Buildings, 2008.

12 Bingyuan Y, Jiguang W, and Junyong L. Research on pricing model of congestion management considering influence of partitioned interruptible load. *Power System Technology*, 29(9):41–45, 2005.

13 Na Y, Wei F, and Ya L. Optimization model of purchasing interruptible load for network congestion constrained dispatch during the peak load periods. In *Power and Energy Engineering Conference*, pages 496–500. SciRes, 2010.

14 Aalami H, Moghaddam M.P, and Yousefi G. Demand response modeling considering interruptible/curtailable loads and capacity market programs. *Applied Energy*, 87:243–250, 2010.

15 Mitra S, Grossmann I, Pinto J, and Arora N. Optimal production planning under time-sensitive electricity prices for continuous power-intensive processes. *Computers & Chemical Engineering*, 38:171–184, 2012.

16 Mitra S, Sun L, and Grossmann I. Optimal scheduling of industrial combined heat and power plants under time-sensitive electricity prices. *Energy*, 54:194–211, 2013.

17 Zhang Q, Grossmann I, Heuberger C, Sundaramoorthy A, and Pinto J.M. Air separation with cryogenic energy storage: Optimal scheduling considering electric energy and reserve markets. *AIChE Journal*, 61(5):1547–1558, 2015.

18 Ashok S and Banerjee R. An optimization mode for industrial load management. *IEEE Transactions on Power Systems*, 16(4):879–884, 2001.

19 Zhang Q, Morari M, Grossmann I.E, Sundaramoorthy A, and Pinto J.M. A projection-based method for production planning of multiproduct facilities. *AIChE Journal*, 55(10): 2614–2630, 2009.

20 Zhang Q, Grossmann I, Sundaramoorthy A, and Pinto J. Data-driven construction of convex region surrogate models. *Optimization and Engineering*, 2015.

21 Zhang Q, Morari M, Grossmann I.E, Sundaramoorthy A, and Pinto J.M. An adjustable robust optimization approach to scheduling of continuous industrial processes providing interruptible load. *Computers & Chemical Engineering*, 86(4):106–119, 2016.

22 Vujanic R, Mariethos S, Goulart P, and Morari M. Robust integer optimization and scheduling problems for large electricity consumers. In *Proceedings of the 2012 American Control Conference*, pages 3108–3113, 2012.

23 Bynum M, Staid A, Arguello B, Castillo A, Watson J.P, and Larid C.D. Proactive operations and investment planning via stochastic optimization to enhance power systems extreme weather resilience. *Submitted to Journal of Infrastructure Systems*, 2018.

24 Land A.H and Doig A.G. An automatic method of solving discrete programming problems. *Econometrica: Journal of the Econometric Society*, pages 497–520, 1960.

25 Dakin R.J. A tree-search algorithm for mixed integer programming problems. *The computer journal*, 8(3):250–255, 1965.

26 Belotti P, Kirches C, Leyffer S, Linderoth J, Luedtke J, and Mahajan A. Mixed-integer nonlinear optimization. *Acta Numerica*, 22:1–131, 2013.

27 Pörn R, Harjunkoski I, and Westerlund T. Convexification of different classes of non-convex minlp problems. *Computers & chemical engineering*, 23(3):439–448, 1999.

28 Pörn R and Westerlund T. A cutting plane method for minimizing pseudo-convex functions in the mixed integer case. *Computers & Chemical Engineering*, 24(12):2655–2665, 2000.

29 Liu J, Castillo A, Watson J.P, and Laird C.D. Global solution strategies for the network-constrained unit commitment problem with ac transmission constraints. *Under Revision, IEEE Transactions on Power Systems*, 2018.

30 IEEE PES Task Force on Benchmarks for Validation of Emerging Power System Algorithms. Power grid lib - optimal power flow. `https://github.com/power-grid-lib/pglib-opf`, 2017.

31 Zhang Q and Grossmann I.E. Planning and scheduling for industrial demand side management: advances and challenges. In *Alternative Energy Sources and Technologies*, pages 383–414. Springer, 2016.

32 Zimmerman R.D, Murillo-Sánchez C.E, Thomas R.J, et al. Matpower: Steady-state operations, planning, and analysis tools for power systems research and education. *IEEE Transactions on power systems*, 26(1):12–19, 2011.

33 Cain M.B, Oneill R.P, and Castillo A. History of optimal power flow and formulations. Technical report, Technical report, US FERC, 2012.

34 Vecchietti A, Lee S, and Grossmann I.E. Modeling of discrete/continuous optimization problems: characterization and formulation of disjunctions and their relaxations. *Computers & chemical engineering*, 27(3):433–448, 2003.

35 Jabr R.A. Radial distribution load flow using conic programming. *IEEE transactions on power systems*, 21(3):1458–1459, 2006.

36 Kocuk B, Dey S.S, and Sun X.A. Strong socp relaxations for the optimal power flow problem. *Operations Research*, 64(6):1177–1196, 2016.

37 Hijazi H, Coffrin C, and Van Hentenryck P. Convex quadratic relaxations for mixed-integer nonlinear programs in power systems. *Mathematical Programming Computation*, 9(3):321–367, 2017.

38 Bynum M, Castillo A, Watson J.P, and Laird C.D. Tightening mccormick relaxations toward global solution of the acopf problem. *Under review, IEEE Transactions on Power Systems*, 2018.

39 Bynum M, Castillo A, Watson J.P, and Laird C.D. Strengthened socp relaxations for acopf with mccormick envelopes and bounds tightening. *to appear in PSE 2018*, 2018.

40 Liu J, Bynum M, Castillo A, Watson J.P, and Laird C.D. A multitree approach for global solution of acopf problems using piecewise outer approximations. *Computers & Chemical Engineering*, 2017.

41 Kocuk B, Dey S.S, and Sun X.A. Matrix minor reformulation and socp-based spatial branch-and-cut method for the ac optimal power flow problem. *arXiv preprint arXiv:1703.03050*, 2017.

42 Lu M, Nagarajan H, Bent R, Eksioglu S.D, and Mason S.J. Tight piecewise convex relaxations for global optimization of optimal power flow. *arXiv preprint arXiv:1803.04633*, 2018.

43 Kocuk B, Dey S.S, and Sun X.A. New formulation and strong misocp relaxations for ac optimal transmission switching problem. *IEEE Transactions on Power Systems*, 32(6): 4161–4170, Nov 2017. ISSN 0885-8950. doi: 10.1109/TPWRS.2017.2666718.

44 Hart W.E, Laird C.D, Watson J.P, Woodruff D.L, Hackebeil G.A, Nicholson B.L, and Siirola J.D. *Pyomo-optimization modeling in python*, volume 67. Springer, 2012.

45 Wächter A and Biegler L.T. On the implementation of an interior-point filter line-search algorithm for large-scale nonlinear programming. *Mathematical programming*, 106(1): 25–57, 2006.

46 HSL. A collection of fortran codes for large scale scientific computation. URL `http://www.hsl.rl.ac.uk/`.

47 DAmbrosio C, Frangioni A, Liberti L, and Lodi A. On interval-subgradient and no-good cuts. *Operations Research Letters*, 38(5):341–345, 2010.

48 Wu X and Conejo A.J. An efficient tri-level optimization model for electric grid defense planning. *IEEE Transactions on Power Systems*, 32(4):2984–2994, 2017.

49 Salmeron J, Wood K, and Baldick R. Analysis of electric grid security under terrorist threat. *IEEE Transactions on Power Systems*, 19(2):905–912, May 2004. ISSN 0885-8950. doi: 10.1109/TPWRS.2004.825888.

50 Alguacil N, Delgadillo A, and Arroyo J.M. A trilevel programming approach for electric grid defense planning. *Computers & Operations Research*, 41:282 – 290, 2014. ISSN 0305-0548. doi: https://doi.org/10.1016/j.cor.2013.06.009. URL `http://www.sciencedirect.com/science/article/pii/S0305054813001664`.

51 Wang Y, Chen C, Wang J, and Baldick R. Research on resilience of power systems under natural disasters–a review. *IEEE Transactions on Power Systems*, 31(2):1604–1613, 2016.

52 Guikema S, Davidson R, and Liu H. Statistical models of the effects of tree trimming on power system outages. *IEEE Transactions on Power Delivery*, 21(3):1549–1557, 2006.

53 Hines P, Apt J, and Talukdar S. Trends in the history of large blackouts in the united states. In *2008 IEEE Power Energy Soc. General Meeting–Convers. Del. Electr. Energy 21st Century*, pages 1–8, 2008.

Table 1: Comparison of DR locations selected by DC and AC models for pglib_opf_case14_ieee across all values of Δ_b and N_Z.

Model	DR Buses
$\mathcal{DR}^*_{DC} \cap \mathcal{DR}^*_{AC}$	2, 3, 9, 13, 14, 12
$\mathcal{DR}^*_{DC} \backslash \mathcal{DR}^*_{AC}$	-
$\mathcal{DR}^*_{AC} \backslash \mathcal{DR}^*_{DC}$	6

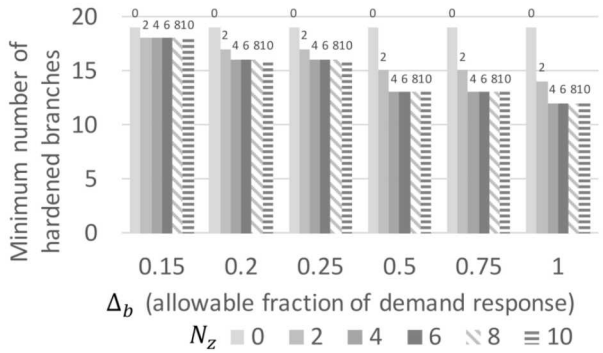

(a) pglib_opf_case118_ieee

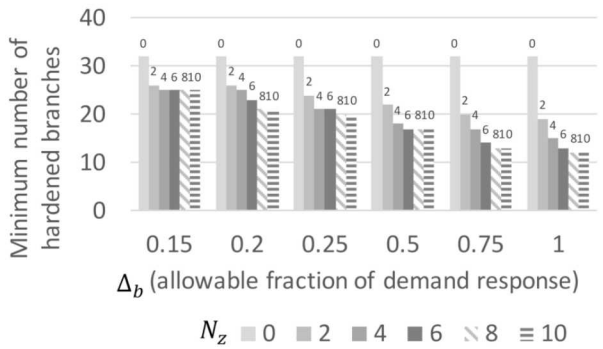

(b) pglib_opf_case162_ieee_dtc

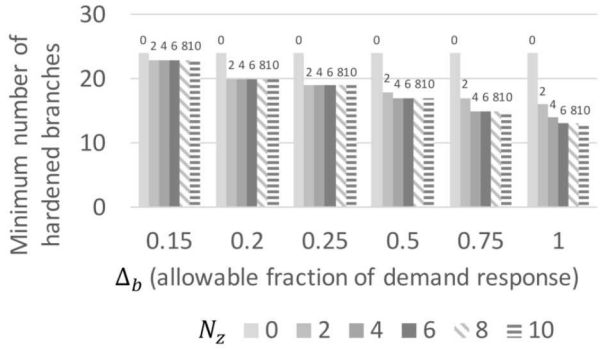

(c) pglib_opf_case300_ieee

Figure 1: The value of DR on resilience as a function of the number of demand response contracts (N_z) and the allowable fraction of DR (Δ_b) with 100 scenarios.

Table 2: Average fraction of AC-feasible scenarios when implementing DC solution

Test Case	Average fraction of AC-feasible scenarios
pglib_opf_case14_ieee	0.9
pglib_opf_case30_as	0.86
pglib_opf_case118_ieee	0.89
pglib_opf_case162_ieee_dtc	0.67

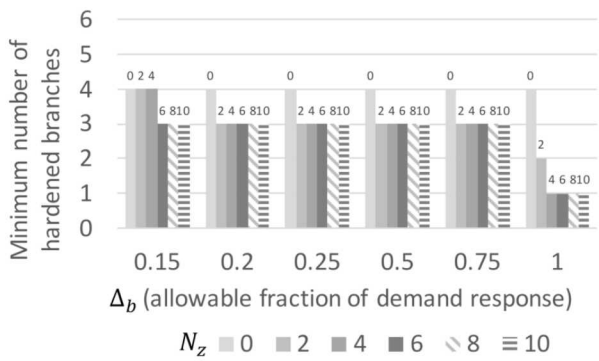

(a) DC results

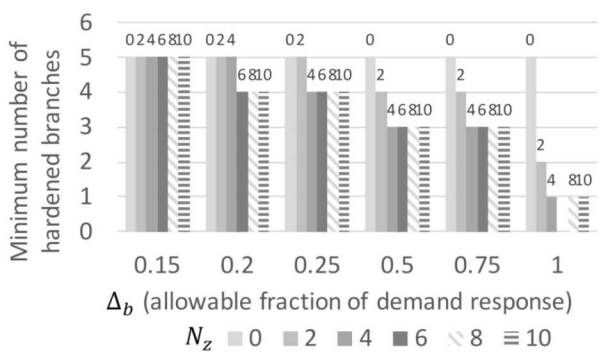

(b) AC results

Figure 2: Comparison of DC and AC results for pglib_opf_case14_ieee. Each figure shows the minimum number of hardened transmission lines as a function of Δ_b and N_z.

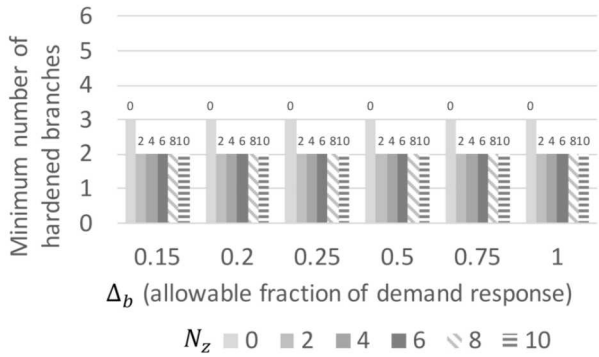

(a) DC results

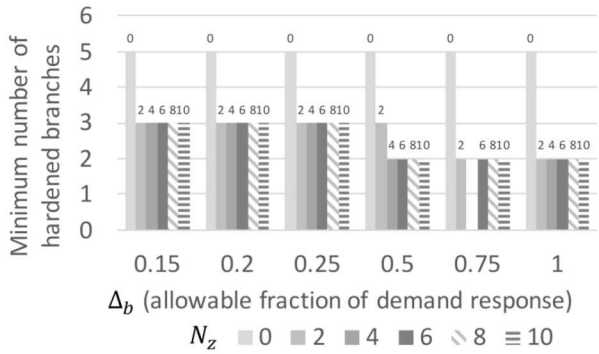

(b) AC results

Figure 3: Comparison of DC and AC results for pglib_opf_case30_as. Each figure shows the minimum number of hardened transmission lines as a function of Δ_b and N_z.

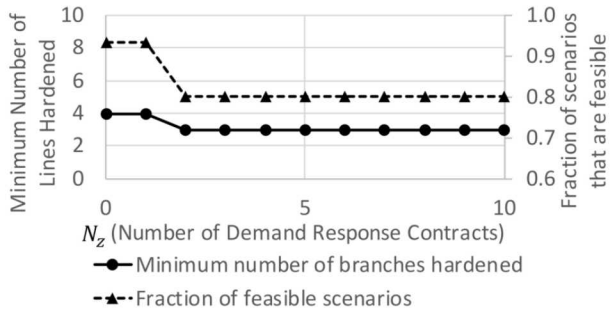

(a) pglib_opf_case14_ieee

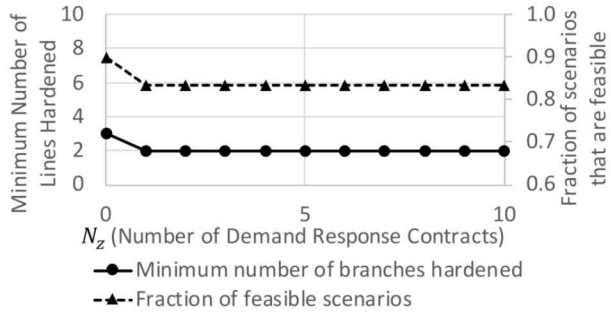

(b) pglib_opf_case30_as

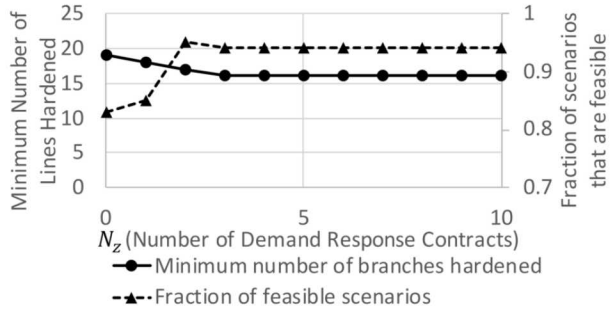

(c) pglib_opf_case118_ieee

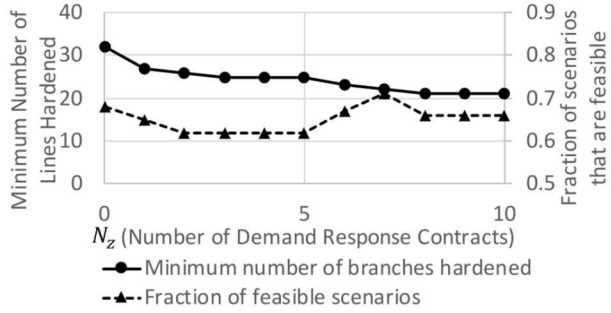

(d) pglib_opf_case162_ieee_dtc

Figure 4: Fraction of scenarios feasible when integer solutions obtained with the DC model are evaluated with the AC model ($\Delta_b = 0.2$). The solid lines show the minimum number of hardened branches and the dashed lines show the fraction of feasible scenarios, both as a function of N_z.

Power Flow Coefficients

This section provides definitions for the power flow coefficients[1].

$$C^{\alpha,p}_{l,b,n} \equiv \begin{cases} \dfrac{G_l}{(T^m_l)^2} & \text{if there is a transformer on branch } l \text{ by bus } b \\ G_l & \text{otherwise} \end{cases} \tag{1.1}$$

$$C^{\beta,p}_{l,b,n} \equiv \begin{cases} \dfrac{B_l T^m_l \sin(T^a_l) - G_l T^m_l \cos(T^a_l)}{(T^m_l)^2} & \text{if there is a transformer on branch } l \text{ by bus } b \\ \dfrac{-B_l T^m_l \sin(T^a_l) - G_l T^m_l \cos(T^a_l)}{(T^m_l)^2} & \text{if there is a transformer on branch } l \text{ by bus } n \\ -G_l & \text{otherwise} \end{cases} \tag{1.2}$$

$$C^{\gamma,p}_{l,b,n} \equiv \begin{cases} \dfrac{-B_l T^m_l \cos(T^a_l) - G_l T^m_l \sin(T^a_l)}{(T^m_l)^2} & \text{if there is a transformer on branch } l \text{ by bus } b \\ \dfrac{-B_l T^m_l \cos(T^a_l) + G_l T^m_l \sin(T^a_l)}{(T^m_l)^2} & \text{if there is a transformer on branch } l \text{ by bus } n \\ -B_l & \text{otherwise} \end{cases} \tag{1.3}$$

$$C^{\alpha,q}_{l,b,n} \equiv \begin{cases} \dfrac{-B_l - 0.5B^c_l}{(T^m_l)^2} & \text{if there is a transformer on branch } l \text{ by bus } b \\ -B_l - 0.5B^c_l & \text{otherwise} \end{cases} \tag{1.4}$$

$$C^{\beta,q}_{l,b,n} \equiv \begin{cases} \dfrac{B_l T^m_l \cos(T^a_l) + G_l T^m_l \sin(T^a_l)}{(T^m_l)^2} & \text{if there is a transformer on branch } l \text{ by bus } b \\ \dfrac{B_l T^m_l \cos(T^a_l) - G_l T^m_l \sin(T^a_l)}{(T^m_l)^2} & \text{if there is a transformer on branch } l \text{ by bus } n \\ B_l & \text{otherwise} \end{cases} \tag{1.5}$$

$$C^{\gamma,q}_{l,b,n} \equiv \begin{cases} \dfrac{B_l T^m_l \sin(T^a_l) - G_l T^m_l \cos(T^a_l)}{(T^m_l)^2} & \text{if there is a transformer on branch } l \text{ by bus } b \\ \dfrac{-B_l T^m_l \sin(T^a_l) - G_l T^m_l \cos(T^a_l)}{(T^m_l)^2} & \text{if there is a transformer on branch } l \text{ by bus } n \\ -G_l & \text{otherwise} \end{cases} \tag{1.6}$$

where

$$B_l = \frac{-X_l}{R^2_l + X^2_l} \tag{2}$$

and

$$G_l = \frac{R_l}{R_l^2 + X_l^2} \tag{3}$$

for resistance R_l and reactance X_l on branch $l \in \mathcal{L}$.

$$C^T_{l,b,n} \equiv \begin{cases} -T^a_l & \text{if there is a transformer on branch } l \text{ by bus } b \\ T^a_l & \text{otherwise} \end{cases} \tag{4}$$

Integer Solutions for pglib_opf_case14_ieee

Table 1: Integer Solutions DC - pglib_opf_case14_ieee

Δ_b	N_z	Branches Hardened	Demand Response Buses
0	0	1, 6, 18, 19	-
0.05	1-10	1, 6, 18, 19	-
0.1	1-10	1, 6, 18, 19	-
0.15	1-4	1, 6, 18, 19	-
0.15	5-10	3, 18, 19	2, 3, 9, 13, 14
0.2	1	1, 6, 18, 19	-
0.2	2-10	6, 18, 19	3, 9
0.25	1	1, 6, 18, 19	-
0.25	2-10	6, 18, 19	3, 9
0.5	1-10	6, 18, 19	3
0.75	1-10	6, 18, 19	3
1	1-3	18, 19	3
1	4-10	18	3, 12, 13, 14

Table 2: Integer Solutions AC - pglib_opf_case14_ieee

Δ_b	N_z	Branches Hardened	Demand Response Buses
0	0	1, 6, 11, 17, 19	-
0.05	1-10	1, 6, 11, 17, 19	-
0.1	1-10	1, 6, 11, 17, 19	-
0.15	1-10	1, 6, 11, 17, 19	-
0.2	1-5	1, 6, 11, 17, 19	-
0.2	6-10	6, 11, 17, 19	2, 3, 6, 9, 13, 14
0.25	1-2	1, 6, 11, 17, 19	-
0.25	3-10	6, 17, 18, 19	2, 3, 9
0.5	1-2	3, 11, 17, 19	3
0.5	3-10	3, 11, 19	3, 13, 14
0.75	1-2	3, 11, 13, 19	3
0.75	3-10	3, 11, 19	9, 13, 14
1	1	13, 18, 19	3
1	2-3	13, 18	3, 12
1	4-10	18	3, 12, 13, 14

References

[1] Zimmerman R.D, Murillo-Sánchez C.E, Thomas R.J, et al. Matpower: Steady-state operations, planning, and analysis tools for power systems research and education. *IEEE Transactions on power systems*, 26(1):12–19, 2011.

1.2. Strengthened SOCP relaxations for ACOPF with McCormick envelopes and bounds tightening

Strengthened SOCP Relaxations for ACOPF with McCormick Envelopes and Bounds Tightening

Michael Bynum[a], Anya Castillo[b], Jean-Paul Watson[b], Carl D. Laird[a,b*]

[a]*Purdue University, Davidson School of Chemical Engineering, 480 Stadium Mall Drive, West Lafayette, IN 47907, United States*
[b]*Center for Computing Research, Sandia National Laboratories, Albuquerque, NM 87185, United States*
cdlaird@sandia.gov

Abstract

The solution of the Optimal Power Flow (OPF) and Unit Commitment (UC) problems (i.e., determining generator schedules and set points that satisfy demands) is critical for efficient and reliable operation of the electricity grid. For computational efficiency, the alternating current OPF (ACOPF) problem is usually formulated with a linearized transmission model, often referred to as the DCOPF problem. However, these linear approximations do not guarantee global optimality or even feasibility for the true nonlinear alternating current (AC) system. Nonlinear AC power flow models can and should be used to improve model fidelity, but successful global solution of problems with these models requires the availability of strong relaxations of the AC optimal power flow constraints. In this paper, we use McCormick envelopes to strengthen the well-known second-order cone (SOC) relaxation of the ACOPF problem. With this improved relaxation, we can further include tight bounds on the voltages at the reference bus, and this paper demonstrates the effectiveness of this for improved bounds tightening. We present results on the optimality gap of both the base SOC relaxation and our Strengthened SOC (SSOC) relaxation for the National Information and Communications Technology Australia (NICTA) Energy System Test Case Archive (NESTA). For the cases where the SOC relaxation yields an optimality gap more than 0.1 %, the SSOC relaxation with bounds tightening further reduces the optimality gap by an average of 67 % and ultimately reduces the optimality gap to less than 0.1 % for 58 % of all the NESTA cases considered. Stronger relaxations enable more efficient global solution of the ACOPF problem and can improve computational efficiency of MINLP problems with AC power flow constraints, e.g., unit commitment.

Keywords: ACOPF, Second-order cone programming, McCormick, Bounds tightening.

1. Introduction

Reliable and economic operation of the electricity grid is vital for the economy, public safety, and health. Key practical problems relating to the operation of the grid include the Optimal Power Flow (OPF) and the Unit-Commitment (UC) problems. The OPF, also referred to as the ACOPF problem, seeks to find generator operating conditions for a single time period that minimize the total operating cost while satisfying physical power flow laws and other operational constraints, such as generator and transmission limits. The UC problem solves for a generator on/off schedule across multiple time periods, introducing discrete variables for these scheduling decisions. Both problems require a model for the AC power flow (ACPF), giving rise to a large number of nonlinear, non-

convex constraints. To remove these nonlinearities, the ACOPF problem is typically simplified to a linear approximation known as the DCOPF problem. This approximation is more computationally efficient; however, it does not guarantee global optimality or even feasibility for the system under consideration. For this reason, there has recently been extensive research in convex relaxations for the ACOPF model to support global optimization of ACOPF and UC with ACOPF constraints.

Lavaei and Low (2012) present a semidefinite programming (SDP) formulation for the dual of the ACOPF problem and provide a rank-one sufficient condition under which the duality gap is guaranteed to be zero. Coffrin et al. (2017) propose a quadratic relaxation on the polar form of the ACOPF problem. Jabr (2006) introduced a convex second-order Cone (SOC) programming relaxation of the ACOPF problem. Kocuk et al. (2016) proposed extensions to the SOC relaxation including (1) relaxations on the arctangent constraints relating the SOC variables to voltage angles differences and (2) linear cutting planes to incorporate information from the SDP relaxation. Liu et al. (2017) propose a piecewise outer approximation based global optimization algorithm for solving the ACOPF problem.

In this paper, we propose a strengthened SOC (SSOC) relaxation that relates the auxiliary variables in the SOC relaxation to the real and imaginary components of the voltages in the rectangular form through McCormick envelopes. The ACOPF problem has an infinite number of solutions unless the voltage angle is specified at an arbitrary bus, typically referred to as the reference bus. By relating the SOC auxiliary variables to the rectangular voltages, this reference bus specification may now be included in the proposed relaxation, providing tighter bounds on the voltage variables at the reference bus. Results for several widely studied ACOPF test cases demonstrate that this approach improves the effectiveness of optimality-based bounds tightening (OBBT) and strengthens the SOC relaxation significantly. In the next section, we present a review of the SOC relaxation; our SSOC relaxation is described in Section 3. Computational results comparing the optimality gap of the SOC and SSOC relaxations are presented along with results showing the impact of the reference bus on bounds tightening.

2. ACOPF Second-Order Cone Relaxation

A power system is modeled with a set of buses connected by transmission lines and/or transformers. Each bus may have one or more generators and loads. The rectangular form of the ACOPF includes real and imaginary components of the voltage, v^r and v^j respectively, at each bus. With the following definitions,

$$c_{b,b} \equiv (v_b^r)^2 + (v_b^j)^2 = v_b^2, \;\; c_{b,k} \equiv v_b^r v_k^r + v_b^j v_k^j, \;\; s_{b,k} \equiv v_b^r v_k^j - v_k^r v_b^j \tag{1}$$

the SOC relaxation of the ACOPF problem can be written as follows:

$$\min \sum_{g \in \mathcal{G}} [A_g^2 (p_g^G)^2 + A_g^1 p_g^G + A_g^0]$$

s.t.

$$\sum_{(b,k) \in \mathcal{L}_b^{in}} p_{b,k}^t + \sum_{(b,k) \in \mathcal{L}_b^{out}} p_{b,k}^f + G_b^{sh} c_{b,b} + P_b^D - \sum_{g \in \mathcal{G}_b} p_g^G = 0 \qquad \forall\, b \in \mathcal{B}$$

$$
\begin{aligned}
&\sum_{(b,k)\in\mathcal{L}_b^{in}} q_{b,k}^t + \sum_{(b,k)\in\mathcal{L}_b^{out}} q_{b,k}^f - B_b^{sh} c_{b,b} + Q_b^D - \sum_{g\in\mathcal{G}_b} q_g^G = 0 && \forall\, b \in \mathcal{B} \\
&p_{b,k}^f = G_{b,k}^{ff} c_{b,b} + G_{b,k}^{ft} c_{b,k} - B_{b,k}^{ft} s_{b,k} && \forall\, (b,k) \in \mathcal{L} \\
&q_{b,k}^f = -B_{b,k}^{ff} c_{b,b} - B_{b,k}^{ft} c_{b,k} - G_{b,k}^{ft} s_{b,k} && \forall\, (b,k) \in \mathcal{L} \\
&p_{b,k}^t = G_{b,k}^{tt} c_{k,k} + G_{b,k}^{tf} c_{k,b} - B_{b,k}^{tf} s_{k,b} && \forall\, (b,k) \in \mathcal{L} \\
&q_{b,k}^t = -B_{b,k}^{tt} c_{k,k} - B_{b,k}^{tf} c_{k,b} - G_{b,k}^{tf} s_{k,b} && \forall\, (b,k) \in \mathcal{L} \qquad (2) \\
&(p_{b,k}^f)^2 + (q_{b,k}^f)^2 \le (S_{b,k}^{max})^2,\ (p_{b,k}^t)^2 + (q_{b,k}^t)^2 \le (S_{b,k}^{max})^2 && \forall\, (b,k) \in \mathcal{L} \\
&(V_b^{min})^2 \le c_{b,b} \le (V_b^{max})^2 && \forall\, b \in \mathcal{B} \\
&P_g^{G,min} \le p_g^G \le P_g^{G,max},\ Q_g^{G,min} \le q_g^G \le Q_g^{G,max} && \forall\, g \in \mathcal{G} \\
&c_{b,k} = c_{k,b},\ s_{b,k} = -s_{k,b} && \forall\, (b,k) \in \mathcal{L} \\
&c_{b,k}^2 + s_{b,k}^2 \le c_{b,b} c_{k,k} && \forall\, (b,k) \in \mathcal{L}
\end{aligned}
$$

Here, capitalized symbols represent parameters and lower-case symbols represent variables. Real power is denoted by $\boldsymbol{p}$, reactive power by $\boldsymbol{q}$, and the relaxation variables by $\boldsymbol{s}$ and $\boldsymbol{c}$. The superscripts *G* and *D* denote generation and demand, and *f* and *t* denote the "from" and "to" ends of transmission lines. Subscripts denote indices of the sets of buses $\boldsymbol{\mathcal{B}}$, generators $\boldsymbol{\mathcal{G}}$, and transmission lines $\boldsymbol{\mathcal{L}}$. The optimization objective is to minimize the aggregate operating cost of all the generators. The constraints enforce real power balances at all the buses and reactive power balances at all of the buses, model real and reactive power flow on transmission lines at the "from" and "to" ends of the transmission lines, and enforce thermal limits on the transmission lines, voltage limits at the buses, and generator limits on real and reactive power. The last two constraints are derived from the definitions of *s* and *c*, while the final constraint is relaxed to be an inequality, forming the SOC relaxation. Eq.(2) is a convex optimization problem that may be solved efficiently with off-the-shelf solvers, e.g., Ipopt.

Note that bounds tightening does not improve the relaxation as written since none of the relaxations depend on variable bounds, as is the case when using McCormick envelopes. Further, the voltage variables have been removed from the model, so there is no direct way to incorporate a specification of the voltage angle at the reference bus. In the following section, we present our SSOC relaxation that incorporates McCormick envelopes for Eq.(1) into the SOC relaxation, allowing specification of the reference bus angle and providing a mechanism to effectively tighten the relaxation with OBBT.

3. McCormick Envelopes for Strengthening the SOC Relaxation

First, let $\widehat{xy}$ be an auxiliary variable for the bilinear term xy. We represent the set of McCormick envelopes for the bilinear term as $\widehat{xy} \in MCC(x,y)$. With this notation, Eq.(1) may be relaxed with McCormick Envelopes, as follows:

$$
\begin{aligned}
&c_{b,b} = \widehat{v_b^r} + \widehat{v_b^j}, \;\; c_{b,k} = \widehat{v_b^r v_k^r} + \widehat{v_b^j v_k^j}, \;\; s_{b,k} = \widehat{v_b^r v_k^j} - \widehat{v_b^j v_k^r} \\
&(v_b^r)^2 \leq \widehat{v_b^r} \leq (V_b^{r,\max} + V_b^{r,\min}) v_b^r - V_b^{r,\max} V_b^{r,\min} \\
&(v_b^j)^2 \leq \widehat{v_b^j} \leq (V_b^{j,\max} + V_b^{j,\min}) v_b^j - V_b^{j,\max} V_b^{j,\min} \\
&\widehat{v_b^r v_k^r} \in MCC(v_b^r, v_k^r), \;\; \widehat{v_b^j v_k^j} \in MCC(v_b^j, v_k^j) \\
&\widehat{v_b^r v_k^j} \in MCC(v_b^r, v_k^j), \;\; \widehat{v_b^j v_k^r} \in MCC(v_b^j, v_k^r)
\end{aligned}
\tag{3}
$$

The initial bounds on the real and imaginary voltage components are determined by the voltage magnitude limits provided in the problem specification. However, at the reference bus, the imaginary component is fixed to zero (i.e., the voltage angle is fixed to zero), and the bounds on the real component of the voltage at the reference bus can be tightened as with Eq.(4). The SSOC relaxation is then given by Eqs.(2-4).

$$
\begin{aligned}
&-V_b^{\max} \leq v_b^r, v_b^j \leq V_b^{\max} \\
&V_{ref}^{\min} \leq v_{ref}^r \leq V_{ref}^{\max}, \;\; v_{ref}^j = 0
\end{aligned}
\tag{4}
$$

To Further tighten the SSOC relaxation, OBBT is performed on the voltage variables at each bus. The relaxations in Eq.(3) are then updated, the SSOC relaxation is solved, and the process is repeated until either the optimality gap is less than 0.1 % or 20 iterations are performed with a cumulative reduction in the optimality gap of less than 0.1 %.

4. Results

4.1. Performance of the SSOC Relaxation

Table 1 compares the optimality gap for the SOC and SSOC relaxations for several of the NESTA test cases (Coffrin et al., 2014). The relaxations were modelled in Python 3.5.2 with Pyomo (Hart, 2011) and solved with Ipopt 3.12.5 (Wächter, 2006). The results show that the SSOC relaxation tightens the SOC relaxation significantly. Of the cases for which the optimality gap with the SOC relaxation is greater than 0.1 %, the SSOC relaxation with bounds tightening further reduces the optimality gap by an average of 67 % and overall reduces the optimality gap to less than 0.1 % for 58 % of the NESTA cases.

4.2. The Impact of the Reference Bus on Bounds Tightening

Figure 1 shows the importance of the reference bus and the corresponding bounds in Eq.(4). The figure shows the variable bound ranges for the real and imaginary components of the voltages averaged over all buses of the same shortest path in terms of the number of transmission lines from the reference bus. The iteration count for OBBT is shown on the x-axis. The figure shows the first four iterations of bounds tightening for nesta_case24_ieee_rts__api. As shown in the figure, before any bounds tightening is performed, the reference bus is the only bus with good bounds on the voltage. After one iteration of bounds tightening, the bounds on the voltages at buses connected directly to the reference bus are tightened dramatically. On the second iteration of bounds tightening, the bounds on the voltages at buses a distance of 2 from the reference bus

Table 1: Comparison of optimality gap of SOC and SSOC with OBBT.

Nesta Case	Optimality Gap (%)					
	Standard		Active Power Increase		Small Angle Difference	
	SOC	SSOC	SOC	SSOC	SOC	SSOC
case3_lmbd	1.32	0.40	3.30	0.07	4.28	0.05
case4_gs	0.00	0.00	0.65	0.07	4.90	0.01
case5_pjm	14.54	4.94	0.28	0.06	3.61	0.03
case6_ww	0.63	0.09	-	-	0.80	0.05
case6_c	0.30	0.10	0.35	0.05	1.36	0.01
case9_wscc	0.00	0.00	0.00	0.00	1.50	0.01
case14_ieee	0.11	0.06	1.34	0.17	0.06	0.06
case24_ieee_rts	0.01	0.01	20.75	1.98	11.42	0.06
case29_edin	0.14	0.11	0.44	0.43	34.47	2.02
case30_as	0.06	0.06	4.76	0.21	9.16	0.18
case30_fsr	0.39	0.29	45.97	41.53	0.62	0.14
case30_ieee	15.88	0.08	1.01	0.08	5.84	0.08
case39_epri	0.05	0.05	2.99	0.21	0.11	0.05
case57_ieee	0.06	0.06	0.21	0.09	0.11	0.09
case73_ieee_rts	0.03	0.03	14.39	14.36	8.37	2.51
case89_pegase	0.17	0.10	20.43	20.11	0.28	0.17
case118_ieee	2.07	1.75	44.15	29.89	12.89	5.16

are tightened more than the bounds on variables at other buses. The trend continues through all four iterations of bounds tightening shown. In this figure, it is clear that the effectiveness of bounds tightening at a given iteration is directly related to the distance of the corresponding bus from the reference bus. Additionally, although not shown in Table 1, the SSOC relaxation was solved with the bounds tightening procedure described in Section 3 but without the tight bounds on the reference bus voltages. The optimality gap did not improve at all beyond the gap obtained with the SOC relaxation for any of the test cases. This further indicates the necessity of the tight voltage bounds at the reference bus for effective bounds tightening.

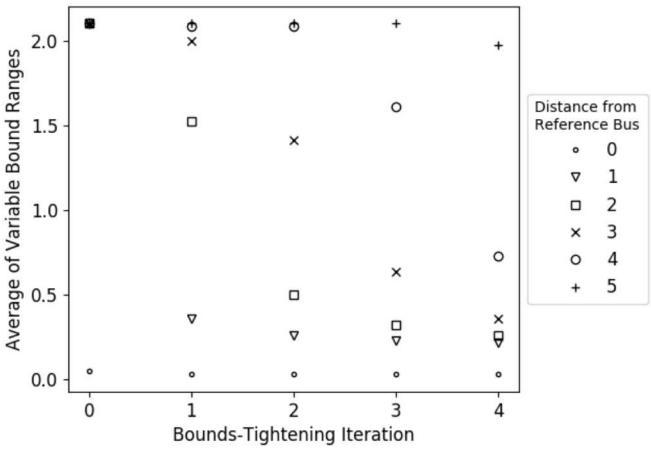

Figure 1: Impact of the reference bus on bounds tightening for nesta_case24_ieee_rts__api. The abscissa shows the iteration count, and the ordinate shows the average range between the upper and lower variable.

5. Conclusions

We describe the use of McCormick envelopes and OBBT to strengthen the well-known second-order cone (SOC) relaxation of the ACOPF problem. With the proposed relaxation, tight bounds on the voltages at the reference bus can be specified, and we demonstrate the necessity of this specification for bounds tightening to be effective. In Section 4.1, we showed that, of the NESTA test cases for which the optimality gap with the SOC relaxation is greater than 0.1 %, the SSOC relaxation with bounds tightening further reduces the optimality gap by an average of 67 % and ultimately reduces the optimality gap to less than 0.1 % for 58 % of all the cases considered. In Section 4.2, we demonstrated that the effectiveness of OBBT at a given iteration is directly related to the distance of the corresponding bus from the reference bus. In future work, this relationship may be exploited to develop more efficient strategies for bounds tightening.

6. Acknowledgements

Sandia National Laboratories is a multimission laboratory managed and operated by National Technology and Engineering Solutions of Sandia, LLC, a wholly owned subsidiary of Honeywell International, Inc., for the U.S. Department of Energy's National Nuclear Security Administration under contract DENA0003525.

The work of Michael Bynum, Carl Laird, and Jean-Paul Watson was supported in part by the U.S. Department of Energy, Office of Science, Office of Advanced Scientific Computing Research, Applied Mathematics program under contract number KJ0401000 through the project "Multifaceted Mathematics for Complex Energy Systems". The work of Michael Bynum, Anya Castillo, Carl Laird, and Jean-Paul Watson was also supported in part by Sandia National Laboratories' Laboratory Directed Research and Development (LDRD) program.

References

C. Coffrin, D. Gordon, and P. Scott, 2014, NESTA, the NICTA Energy System Test Case Archive, arXiv preprint arXiv:1411.0359.

W. Hart, J.P. Watson, and D. Woodruff, 2011, Pyomo: Modeling and Solving Mathematical Programs in Python, Math Program Comput, 3, 3, 219-260.

H. Hijazi, C. Coffrin, and P. Hentenryck, 2017, Convex Quadratic Relaxations for Mixed-Integer Nonlinear Programs in Power Systems, Math Program Comput, 9, 3, 321-367.

R. Jabr, 2006, Radial Distribution Load Flow using Conic Programming, IEEE Trans Power Syst, 21, 3, 1458-1459.

B. Kocuk, S. Dey, and X. Sun, 2016, Strong SOCP Relaxations for the Optimal Power Flow Problem, Oper Res, 64, 6, 1177-1196.

J. Lavaei and S. Low, 2012, Zero Duality Gap in Optimal Power Flow Problem, IEEE Trans Power Syst, 27, 1, 92-107.

J. Liu, M. Bynum, A. Castillo, J.P. Watson, and C. Laird, A Multitree Approach for Global Solution of ACOPF Problems Using Piecewise Outer Approximations, Comput Chem Eng (2017), https://doi.org/10.1016/j.compchemeng.2017.10.018.

A. Wächter, and L. Biegler, 2006, On the Implementation of an Interior-Point Filter Line-Search Algorithm for Large-Scale Nonlinear Programming, Math Program, 106, 1, 25-57.

1.3. Tightening McCormick relaxations toward global solution of the ACOPF problem

Tightening McCormick Relaxations Toward Global Solution of the ACOPF Problem

Michael Bynum, *Student Member, IEEE,* Anya Castillo, *Member, IEEE,* Jean-Paul Watson, *Member, IEEE,* and Carl D. Laird, *Member, IEEE*

***Abstract*—We show that a strong upper bound on the objective of the alternating current optimal power flow (ACOPF) problem can significantly improve the effectiveness of optimization-based bounds tightening (OBBT) on a number of relaxations. We additionally compare the performance of relaxations of the ACOPF problem, including the rectangular form without reference bus constraints, the rectangular form with reference bus constraints, and the polar form. We find that relaxations of the rectangular form significantly strengthen existing relaxations if reference bus constraints are included. Overall, relaxations of the polar form perform the best. However, neither the rectangular nor the polar form dominates the other. Ultimately, with these strategies, we are able to reduce the optimality gap to less than 0.1% on all but 5 NESTA test cases with up to 300 buses by performing OBBT alone.**

***Index Terms*—ACOPF, bounds tightening, convex relaxation**

I. Introduction

THE alternating current optimal power flow (ACOPF), also referred to as the OPF, is a fundamental problem for reliable and efficient operation of the electric grid and is the basis of more complex operations problems such as unit commitment. Global optimization of the OPF guarantees revenue adequacy of the locational marginal prices (LMPs) by closing the duality gap. Moreover, OPF problems with discrete decision variables, including unit commitment, are modeled as mixed integer nonlinear programming (MINLP) problems, where global solution of the nonlinear ACOPF is a required subproblem for many algorithms. Therefore, efficient global optimization of the ACOPF problem is a critical step towards incorporating higher fidelity models into practical grid operations.

Kocuk et al. [1] proved that the second order cone (SOC) relaxation is tighter than a linear McCormick relaxation of the rectangular OPF (RM) under certain assumptions on variable bounds. As a result, they initially strengthen the SOC relaxation with arctangent constraints, cycle constraints, and semidefinite programming (SDP) cuts, and later with matrix minor reformulations [2]. However, we demonstrate that a quadratic form of the RM relaxation, in combination with explicit reference bus constraints and optimization-based bounds tightening (OBBT) [3], can also be quite effective in practice for improving the performance of the existing SOC [4] and quadratic convex (QC) [5] OPF relaxations since this produces tighter bounds on the variables than those assumed in Theorem 3.1 of [1]. Specifically, we extend our findings in [6] and demonstrate that neither the RM nor the QC (with McCormick envelopes, reference bus constraints, and OBBT) relaxation dominates the other, and, between the two approaches, we close 91% of the NESTA archive [7] test cases up to 300 buses. This result requires no branching or piecewise refinement, and therefore is a promising foundation for future work. The remainder of this paper first reviews these relaxations, and then presents significant improvements to the numerical results reported in [1] and [8].

M. Bynum is with the Davidson School of Chemical Engineering, Purdue University, West Lafayette, IN, 47907 USA e-mail: bynumm@purdue.edu and with Sandia National Laboratories, Albuquerque, NM, 87185 USA email: mlbynum@sandia.gov

A. Castillo is with Sandia National Laboratories, Albuquerque, NM, 87185 USA e-mail: arcasti@sandia.gov.

J.P. Watson is with Sandia National Laboratories, Livermore, CA, 94550 USA e-mail: jwatson@sandia.gov.

C. Laird is with the Davidson School of Chemical Engineering, Purdue University, West Lafayette, IN, 47907 USA and with Sandia National Laboratories, Albuquerque, NM, 87185 USA e-mail: cdlaird@sandia.gov.

Manuscript received XXX; revised XXX.

II. ACOPF Relaxations

We use lower case symbols to represent variables, upper case symbols to represent parameters, and upper case script symbols to represent index sets. The sets $\mathcal{G}$, $\mathcal{G}_b$, and $\mathcal{B}$ represent the sets of all generators, generators connected to bus b, and buses, respectively. The set $\mathcal{A}$ contains all connected bus pairs. The set $\mathcal{K}$ is a set of three-tuples containing both (transmission line index, "from" bus, "to" bus) and (transmission line index, "to" bus, "from" bus) 3-tuples for each transmission line. Finally, $\mathcal{K}_b = \{(l,i,j) \in \mathcal{K} \mid i{=}b\}$. The superscripts G, D, and Sh represent generation, demand, and shunt, respectively. The parameters $C^{\alpha,p}_{l,b,n}$, $C^{\beta,p}_{l,b,n}$, $C^{\gamma,p}_{l,b,n}$, $C^{\alpha,q}_{l,b,n}$, $C^{\beta,q}_{l,b,n}$, and $C^{\gamma,q}_{l,b,n}$ are functions of branch characteristics [9].

We explore three relaxations with the following base formulation in (1) for co-optimizing real and reactive power, p and q, respectively.

$$\min \sum\nolimits_{g\in\mathcal{G}} [A^2_g (p^G_g)^2 + A^1_g p^G_g + A^0_g] \tag{1a}$$
$$\sum_{g\in\mathcal{G}_b} p^G_g - \sum_{(l,i,j)\in\mathcal{K}_b} p_{l,i,j} = p^L_b + G^{Sh}_b \alpha_b \qquad \forall b \in \mathcal{B} \tag{1b}$$
$$\sum_{g\in\mathcal{G}_b} q^G_g - \sum_{(l,i,j)\in\mathcal{K}_b} q_{l,i,j} = q^L_b - B^{Sh}_b \alpha_b \qquad \forall b \in \mathcal{B} \tag{1c}$$
$$p_{l,b,n} = C^{\alpha,p}_{l,b,n}\alpha_b + C^{\beta,p}_{l,b,n}\beta_{b,n} + C^{\gamma,p}_{l,b,n}\gamma_{b,n} \qquad \forall (l,b,n) \in \mathcal{K} \tag{1d}$$
$$q_{l,b,n} = C^{\alpha,q}_{l,b,n}\alpha_b + C^{\beta,q}_{l,b,n}\beta_{b,n} + C^{\gamma,q}_{l,b,n}\gamma_{b,n} \qquad \forall (l,b,n) \in \mathcal{K} \tag{1e}$$
$$p^2_{l,b,n} + q^2_{l,b,n} \le (S^{\max}_l)^2 \qquad \forall (l,b,n) \in \mathcal{K} \tag{1f}$$
$$(V^{\min}_b)^2 \le \alpha_b \le (V^{\max}_b)^2 \qquad \forall b \in \mathcal{B} \tag{1g}$$
$$P^{G,\min}_g \le p^G_g \le P^{G,\max}_g \qquad \forall g \in \mathcal{G} \tag{1h}$$
$$Q^{G,\min}_g \le q^G_g \le Q^{G,\max}_g \qquad \forall g \in \mathcal{G} \tag{1i}$$
$$\tan(\Theta^{\min}_{b,n})\beta_{b,n} \le \gamma_{b,n} \le \tan(\Theta^{\max}_{b,n})\beta_{b,n} \qquad \forall (b,n) \in \mathcal{A} \tag{1j}$$
$$\beta_{b,n} = \beta_{n,b}, \gamma_{b,n} = -\gamma_{n,b} \qquad \forall (b,n) \in \mathcal{A} \tag{1k}$$

The *rectangular OPF* (i.e., where v^r and v^j represent the real and imaginary components of the nodal voltages, respectively) is defined with the following substitutions for α, β, and γ:

$$\alpha_b \to (v^r_b)^2 + (v^j_b)^2 \qquad \forall\, b \in \mathcal{B} \tag{2a}$$
$$\beta_{b,n} \to v^r_b v^r_n + v^j_b v^j_n \qquad \forall\, (b,n) \in \mathcal{A} \tag{2b}$$
$$\gamma_{b,n} \to v^j_b v^r_n - v^r_b v^j_n \qquad \forall\, (b,n) \in \mathcal{A} \tag{2c}$$

with $v^r, v^j \in [-V^{max}, V^{max}]$. The *polar OPF* (i.e., v and θ represent nodal voltage magnitude and angle, respectively) is defined with the following substitutions into (1):

$$\alpha_b \to v^2_b \qquad \forall\, b \in \mathcal{B} \tag{3a}$$
$$\beta_{b,n} \to v_b v_n \cos(\theta_b - \theta_n) \qquad \forall\, (b,n) \in \mathcal{A} \tag{3b}$$
$$\gamma_{b,n} \to v_b v_n \sin(\theta_b - \theta_n) \qquad \forall\, (b,n) \in \mathcal{A}. \tag{3c}$$

Constraints (1b) and (1c) enforce power balances, (1d)-(1e) compute power flows, (1f) enforces thermal limits, (1g) enforces voltage magnitude bounds, (1h) and (1i) enforce generator limits, and (1j) limits the voltage angle difference for interconnected buses.

The solution to both forms of the OPF problem is non-unique without fixing a reference voltage angle at one of the buses, $ref \in \mathcal{B}$. In the polar form, this reference bus constraint is

$$\theta_{ref} = 0. \tag{4}$$

In rectangular form, there is a domain reduction for v^r_{ref}:

$$v^j_{ref} = 0 \tag{5a}$$
$$V^{min}_{ref} \leq v^r_{ref} \leq V^{max}_{ref}. \tag{5b}$$

The choice of reference bus does not impact the optimal solution of the ACOPF problem, but it may impact the quality of the relaxation [6], [10]. For comparison purposes, we used the reference bus location specified in the test cases.

There is a SOC equality relationship amongst α, β, and γ that may be relaxed to the following convex inequality:

$$\beta^2_{b,n} + \gamma^2_{b,n} \leq \alpha_b \alpha_n \quad \forall\, (b,n) \in \mathcal{A}. \tag{6}$$

The SOC problem [4] is given by (1) and (6).

McCormick envelopes can be applied to (2), yielding

$$\alpha_b = \widehat{v^r_b} + \widehat{v^j_b},\ \beta_{b,n} = \widehat{v^r_b v^r_n} + \widehat{v^j_b v^j_n},\ \gamma_{b,n} = \widehat{v^j_b v^r_n} - \widehat{v^r_b v^j_n} \tag{7a}$$
$$(v^r_b)^2 \leq \widehat{v^r_b} \leq (V^{r,max}_b + V^{r,min}_b) v^r_b - V^{r,max}_b V^{r,min}_b \tag{7b}$$
$$(v^j_b)^2 \leq \widehat{v^j_b} \leq (V^{j,max}_b + V^{j,min}_b) v^j_b - V^{j,max}_b V^{j,min}_b \tag{7c}$$
$$\widehat{v^r_b v^r_n} \in MCC(v^r_b, v^r_n),\ \widehat{v^j_b v^j_n} \in MCC(v^j_b, v^j_n) \tag{7d}$$
$$\widehat{v^j_b v^r_n} \in MCC(v^j_b, v^r_n),\ \widehat{v^r_b v^j_n} \in MCC(v^r_b, v^j_n) \tag{7e}$$

where $\widehat{xy} \in MCC(x,y)$ denotes the McCormick envelopes for the bilinear term xy. The RM problem is given by (1) and (5)-(7).

The QC formulation [5] is a quadratic convex relaxation of the polar form in (3):

$$v^2_b \leq \alpha_b \leq (V^{max}_b + V^{min}_b) v_b - V^{max}_b V^{min}_b \tag{8a}$$
$$\beta_{b,n} \in MCC(\widehat{v_b v_n}, \widehat{cos\theta_{b,n}}),\ \gamma_{b,n} \in MCC(\widehat{v_b v_n}, \widehat{sin\theta_{b,n}}) \tag{8b}$$
$$\widehat{v_b v_n} \in MCC(v_b, v_n) \tag{8c}$$
$$\widehat{cos\theta_{b,n}} \in CR(\theta_{b,n}),\ \widehat{sin\theta_{b,n}} \in SR(\theta_{b,n}) \tag{8d}$$
$$\theta_{b,n} = \theta_b - \theta_n \tag{8e}$$
$$\Theta^{\min}_{b,n} \leq \theta_{b,n} \leq \Theta^{\max}_{b,n},\ V^{min}_b \leq v_b \leq V^{max}_b. \tag{8f}$$

Here, $\widehat{cosx} \in CR(x)$ and $\widehat{sinx} \in SR(x)$ denote relaxations of the cosine and sine functions, respectively [5]. Additionally, when $\Theta^{min}_{b,n} \geq 0$ ($\Theta^{max}_{b,n} \leq 0$), the sine function is concave (convex) and requires two linear over (under) estimators; this is the linear variant of S-CONV in [8]. The QC problem is given by (1), (4), (6), and (8).

III. Numerical Results

To analyze the strength of the different relaxations, we iteratively solve the specified relaxation and perform OBBT to compute valid bounds for the specified convex relaxation $\mathcal{R}$ of the ACOPF feasible region by minimizing (for the lower bound) and maximizing (for the upper bound) each variable, i.e.,

$$\min / \max \{x_i | x \in \mathcal{R}, f(x) \leq UB\}. \tag{9}$$

Here, $f(x)$ denotes the objective function in (1a) and UB denotes the objective value of the best-known solution to the NLP. Note that any of the relaxations may define $\mathcal{R}$. A more efficient approach to OBBT is to optimize only over a subset of the constraints in $\mathcal{R}$ (e.g., corresponding to a subset of the network [1]). However, this can lead to weaker bounds. Our bounds tightening procedure is similar to the *minimal continuous constraint relaxation network algorithm* presented in [8] but includes the UB constraint.

To evaluate the impact of the UB constraint, we implement OBBT with and without the UB constraint, denoted as OBBT(UB) and OBBT, respectively. All problems were modeled with Pyomo [11] and solved with IPOPT [12] using the linear solver MA27 [13]. OBBT was performed in parallel on a cluster with 24 64-GB-RAM nodes and 16 2.6 GHz Intel Sandy Bridge cores per node. We used 12 processes per node. The relaxations compared and summary results are as follows:

Relaxation	Description	Cases Closed[a]
SOC	Eqs (1), (6)	16%
RM^{o}	Eqs (1), (6)-(7) & OBBT(UB)	16%
RM^{r}	Eqs (1), (5)-(7) & OBBT	52%
$\mathrm{RM}^{\mathrm{ro}}$	Eqs (1), (5)-(7) & OBBT(UB)	67%
QC^{r}	Eqs (1), (4), (6), (8) & OBBT	67%
$\mathrm{QC}^{\mathrm{ro}}$	Eqs (1), (4), (6), (8) & OBBT(UB)	90%

We note that because the reference bus selection does not result in further domain reduction for polar OPF, QC^{o} was omitted.

Detailed results are reported in Table I for the NESTA archive [7], including the optimality gap, wallclock time, and total iterations. We define a single iteration as performing OBBT once on all appropriate variables. Our stopping criteria are as follows: (1) optimality gap less than 0.1%, (2) wallclock time exceeds one hour, or (3) optimality gap improved less than 0.1% in 20 iterations of OBBT. For (3), the gap and wallclock time reported were obtained by the last iteration prior to stalling.

Out major findings are that the OBBT(UB) significantly improves performance across relaxations, and neither the $\mathrm{RM}^{\mathrm{ro}}$ nor the $\mathrm{QC}^{\mathrm{ro}}$ dominates the other. Overall, the $\mathrm{QC}^{\mathrm{ro}}$ formulation performs best. However, the $\mathrm{RM}^{\mathrm{ro}}$ formulation can significantly tighten the SOC relaxation and may be improved by adjusting the location of the reference bus [10]. This is left for future work. Across all relaxations tested, only 5 cases did not solve to less than a 0.1% optimality gap. This is a *significant improvement* to the results reported in [1] and [8]. Note that this advancement requires no branching or piecewise refinement, which is a promising foundation for future work on the global optimization of the OPF. We recognize that the full OBBT approach considered here will not scale well to larger cases, and integration of these techniques (and those described in [1] and [8]) within a scalable global optimization framework will be the subject of future work.

Acknowledgment

This work was supported by Sandia National Laboratories' Laboratory Directed Research and Development program. Sandia National Laboratories is a multimission laboratory managed and operated by National Technology and Engineering Solutions of Sandia, LLC, a wholly owned subsidiary of Honeywell International, Inc., for the U.S. Department of Energy's National Nuclear Security Administration under contract DENA0003525. This paper describes objective technical results and analysis. Any subjective views or opinions that might be expressed in the paper do not necessarily represent the views of the U.S. Department of Energy or the United States Government.

[a]Percentage of 58 NESTA cases with less than 0.1% optimality gap.

[b]Initializing the NLP from the updated solution to the relaxation and recomputing the UB between iterations of OBBT results in an optimality gap reduction from 0.5% to less than 0.1% for both $\mathrm{RM}^{\mathrm{ro}}$ and $\mathrm{QC}^{\mathrm{ro}}$.

TABLE I

NUMERICAL RESULTS FOR RELAXATIONS OF NESTA ARCHIVE CASES UP TO 300 BUSES (58 CASES TOTAL). HIGHLIGHTING INDICATES CASES NOT CLOSED TO LESS THAN 0.1% GAP. NINE CASES ARE NOT LISTED DUE TO THE SOC RELAXATION ALONE REDUCING THE GAP BELOW 0.1%.

Case	Optimality Gap(%)						Wallclock Time(s) / # Iterations					
	SOC	RM^{o}	RM^{r}	RM^{ro}	QC^{r}	QC^{ro}	SOC	RM^{o}	RM^{r}	RM^{ro}	QC^{r}	QC^{ro}
3_lmbd	1.3	1.3	0.5	0.0	0.2	0.0	0/0	0/0	1/4	1/3	1/3	1/3
5_pjm	14.5	14.5	5.0	0.1	9.3	5.7	0/0	0/0	3/6	35/84	3/6	7/15
6_c	0.3	0.3	0.1	0.0	0.1	0.1	0/0	0/0	4/9	2/3	1/2	1/1
6_ww	0.6	0.6	0.1	0.1	0.0	0.0	0/0	0/0	1/1	1/1	1/1	1/1
14_ieee	0.1	0.1	0.1	0.1	0.0	0.0	1/0	2/0	3/1	3/1	4/1	3/1
29_edin	0.1	0.1	0.1	0.1	0.1	0.1	3/0	4/0	38/9	16/3	4/0	4/0
30_fsr	0.4	0.4	0.4	0.1	0.1	0.1	1/0	2/0	2/0	16/7	8/3	6/2
30_ieee	15.9	15.9	0.1	0.0	0.0	0.1	1/0	1/0	18/8	12/5	8/3	6/2
118_ieee	1.8	1.8	1.6	0.7	0.5	0.1	4/0	7/0	217/10	253/18	59/2	83/3
162_ieee_dtc	4.0	4.0	4.0	4.0	0.7	0.1	7/0	12/0	13/0	13/0	430/7	488/8
189_edin	0.2	0.2	0.2	0.2	0.2	0.1	5/0	9/0	9/0	9/0	10/0	46/1
300_ieee	1.2	1.2	1.2	1.2	0.2	0.0	14/0	23/0	22/0	23/0	290/2	284/2
3_lmbd__api	3.3	3.3	0.1	0.1	0.1	0.0	0/0	0/0	2/7	1/3	2/6	1/3
4_gs__api	0.7	0.7	0.1	0.0	0.0	0.1	0/0	0/0	1/3	1/3	1/3	1/2
5_pjm__api	0.3	0.3	0.1	0.0	0.0	0.0	0/0	0/0	1/2	1/2	1/2	1/2
6_c__api	0.3	0.3	0.1	0.0	0.1	0.0	0/0	0/0	3/5	1/2	2/3	1/2
14_ieee__api	1.3	1.3	0.2	0.0	0.3	0.1	0/0	1/0	9/8	8/7	4/3	5/4
24_ieee_rts__api	20.8	20.8	2.0	0.6	0.3	0.1	1/0	1/0	21/10	27/13	8/3	8/3
29_edin__api	0.4	0.4	0.4	0.4	0.1	0.1	7/0	5/0	5/0	5/0	25/3	35/3
30_as__api	4.8	4.8	0.3	0.1	0.0	0.0	1/0	2/0	25/11	25/11	9/3	8/3
30_fsr__api	46.0	46.0	41.6	41.2	2.4	0.1	1/0	1/0	57/25	63/28	27/11	27/11
30_ieee__api	1.0	1.0	0.1	0.1	0.1	0.0	1/0	1/0	27/12	18/8	11/4	11/4
39_epri__api	3.0	3.0	0.3	0.1	0.1	0.0	1/0	2/0	63/24	45/17	7/2	7/2
57_ieee__api	0.2	0.2	0.1	0.1	0.0	0.1	1/0	3/0	61/13	25/5	16/2	9/1
73_ieee_rts__api	14.4	14.4	14.4	14.4	0.2	0.0	3/0	5/0	5/0	5/0	29/2	40/3
89_pegase__api	20.4	20.4	20.2	20.2	18.9	9.1	5/0	11/0	179/10	208/11	1663/24	3604/55
118_ieee__api	43.9	43.9	26.9	26.4	9.3	8.7	4/0	8/0	1102/75	1074/74	318/10	301/11
162_ieee_dtc__api	1.3	1.3	1.0	0.9	0.1	0.1	7/0	12/0	824/24	785/23	799/13	433/7
189_edin__api	5.7	5.7	5.5	2.9	0.3	0.1	5/0	9/0	276/9	746/28	83/2	85/2
300_ieee__api	0.7	0.7	0.7	0.7	0.1	0.0	14/0	23/0	23/0	23/0	346/2	291/2
3_lmbd__sad	4.3	4.3	0.1	0.0	0.0	0.0	0/0	0/0	1/3	1/3	1/1	1/1
4_gs__sad	4.9	4.9	0.0	0.0	0.0	0.0	0/0	0/0	1/2	1/2	1/1	1/1
5_pjm__sad	3.6	3.6	0.0	0.0	0.0	0.0	0/0	0/0	2/3	2/3	1/1	1/1
6_c__sad	1.4	1.4	0.0	0.0	0.0	0.0	0/0	0/0	2/4	2/3	1/1	1/1
6_ww__sad	0.8	0.8	0.0	0.0	0.0	0.0	0/0	0/0	1/1	1/1	1/1	1/1
9_wscc__sad	1.5	1.5	0.0	0.0	0.0	0.0	0/0	0/0	3/3	2/3	2/1	1/1
24_ieee_rts__sad	11.4	11.4	0.1	0.0	0.1	0.0	1/0	2/0	17/8	15/7	8/3	6/2
29_edin__sad	34.7	34.7	2.4	0.5^{b}	1.2	0.5^{b}	3/0	5/0	72/14	78/14	40/4	33/4
30_as__sad	9.2	9.2	0.2	0.1	0.1	0.0	1/0	2/0	19/8	17/7	6/2	6/2
30_fsr__sad	0.6	0.6	0.2	0.0	0.1	0.0	1/0	1/0	20/8	14/6	6/2	6/2
30_ieee__sad	5.8	5.8	0.1	0.1	0.0	0.0	1/0	1/0	12/5	10/4	6/2	6/2
39_epri__sad	0.1	0.1	0.0	0.0	0.0	0.0	1/0	2/0	25/9	17/6	2/0	2/0
57_ieee__sad	0.1	0.1	0.1	0.1	0.1	0.1	1/0	3/0	25/5	16/3	3/0	3/0
73_ieee_rts__sad	8.4	8.4	2.6	2.0	0.1	0.0	3/0	4/0	124/16	169/21	28/2	28/2
89_pegase__sad	0.3	0.3	0.3	0.1	0.1	0.1	5/0	9/0	57/3	162/10	91/2	43/1
118_ieee__sad	12.8	12.8	5.1	1.5	1.4	0.1	4/0	8/0	516/34	520/33	113/4	248/9
162_ieee_dtc__sad	7.1	7.1	7.1	7.1	0.5	0.0	7/0	13/0	13/0	13/0	674/11	563/9
189_edin__sad	2.3	2.3	2.2	1.8	1.0	0.8	5/0	9/0	155/5	214/8	46/1	46/1
300_ieee__sad	1.3	1.3	1.3	1.3	0.2	0.0	14/0	23/0	23/0	23/0	162/1	281/2

REFERENCES

[1] B. Kocuk, S. S. Dey, and X. A. Sun, "Strong SOCP relaxations for the optimal power flow problem," *Operations Research*, vol. 64, no. 6, pp. 1177–1196, 2016.

[2] B. Kocuk, S. S. Dey, and X. Sun, "Matrix minor reformulation and SOCP-based spatial branch-and-cut method for the AC optimal power flow problem," *arXiv preprint arXiv:1703.03050*, 2017.

[3] A. Caprara and M. Locatelli, "Global optimization problems and domain reduction strategies," *Mathematical Programming*, no. 125, pp. 123–137, 2010.

[4] R. Jabr, "A conic quadratic format for the load flow equations of meshed networks," *IEEE Trans. on Power Syst.*, vol. 22, no. 4, pp. 2285–2286, 2007.

[5] H. Hijazi, C. Coffrin, and P. Van Hentenryck, "Convex quadratic relaxations for mixed-integer nonlinear programs in power systems," *Math. Prog. Comp.*, vol. 9, no. 3, pp. 321–367, 2017.

[6] M. Bynum, A. Castillo, J.-P. Watson, and C. D. Laird, "Strengthened SOCP relaxations for ACOPF with mccormick envelopes and bounds tightening," in *13th International Symposium on Process Systems Engineering (PSE 2018)*, ser. Computer Aided Chemical Engineering. Elsevier, 2018, vol. 44, pp. 1555 – 1560.

[7] C. Coffrin, D. Gordon, and P. Scott, "NESTA, the NICTA energy system test case archive," *CoRR*, vol. abs/1411.0359, 2014.

[8] C. Coffrin, H. L. Hijazi, and P. Van Hentenryck, "Strengthening convex relaxations with bound tightening for power network optimization," in *International Conference on Principles and Practice of Constraint Programming*. Springer, 2015, pp. 39–57.

[9] J. A. Momoh, *Electric power system applications of optimization*. Markel Dekker, 2001.

[10] D. Bienstock and G. Munoz, "On linear relaxations of opf problems," *arXiv preprint arXiv:1411.1120*, 2014.

[11] W. E. Hart, C. D. Laird, J.-P. Watson, D. L. Woodruff, G. A. Hackebeil, B. L. Nicholson, and J. D. Siirola, *Pyomo-optimization modeling in python*. Springer, 2012, vol. 67.

[12] A. Wächter and L. T. Biegler, "On the implementation of an interior-point filter line-search algorithm for large-scale nonlinear programming," *Math. Prog.*, vol. 106, no. 1, pp. 25–57, 2006.

[13] HSL, "A collection of Fortran codes for large scale scientific computation," 2007. [Online]. Available: http://www.hsl.rl.ac.uk

1.4. A multitree approach for global solution of ACOPF problems using piecewise outer approximations

A Multitree Approach for Global Solution of ACOPF Problems Using Piecewise Outer Approximations

Jianfeng Liu[a], Michael Bynum[a], Anya Castillo[b], Jean-Paul Watson[b], Carl D. Laird[a,b,*]

[a] *Davidson School of Chemical Engineering, Purdue University, West Lafayette, IN 47907*
[b] *Center for Computing Research, Sandia National Laboratories, Albuquerque, NM 87185*

Abstract

Electricity markets rely on the rapid solution of the *optimal power flow* (OPF) problem to determine generator power levels and set nodal prices. Traditionally, the OPF problem has been formulated using linearized, approximate models, ignoring nonlinear alternating current (AC) physics. These approaches do not guarantee global optimality or even feasibility in the real ACOPF problem.

We introduce an outer-approximation approach to solve the ACOPF problem to global optimality based on alternating solution of upper- and lower-bounding problems. The lower-bounding problem is a piecewise relaxation based on strong second-order cone relaxations of the ACOPF, and these piecewise relaxations are selectively refined at each major iteration through increased variable domain partitioning. Our approach is able to efficiently solve all but one of the test cases considered to an optimality gap below 0.1%. Furthermore, this approach opens the door for global solution of MINLP problems with AC power flow equations.

Keywords: `optimal power flow, outer-approximation, piecewise relaxation, global optimization, second-order cone relaxation, ACOPF`

*Corresponding author
Email address: `cdlaird@sandia.gov` (Carl D. Laird)

Notation

Sets

$\mathcal{B}$	Set of all buses
$\mathcal{B}_b$	Set of all buses connected to bus b
$\mathcal{L}$	Set of all branches (transmission lines)
$\mathcal{L}_b^{in}$	Set of all *inbound* branches to bus b
$\mathcal{L}_b^{out}$	Set of all *outbound* branches from bus b
$\mathcal{G}$	Set of all generators
$\mathcal{G}_b$	Set of all generators at bus b
$\mathcal{C}$	Set of simple cycles
$\mathcal{L}_c$	Set of branches in cycle c
$\mathcal{Z}_{b,k}^{cs}$	Set of all possible combinations of partitions for $s_{b,k}$ and $c_{b,k}$
$\mathcal{Z}_{b,k}^{cc}$	Set of all possible combinations of partitions for $c_{b,b}$ and $c_{k,k}$

Parameters

$B_{b,k}, G_{b,k}$	Susceptance and conductance matrices for branch (b,k)
B_b^{sh}, G_b^{sh}	Shunt susceptance and conductance at bus b
$P_b^D,\ Q_b^D$	Real (P) and reactive (Q) power demand (or load) at bus b
$P_g^{G,min},\ P_g^{G,max}$	Minimum/maximum real power output of generator g
$Q_g^{G,min},\ Q_g^{G,max}$	Minimum/maximum reactive power output of generator g
V_b^{min}, V_b^{max}	Minimum/maximum voltage magnitude at bus b
$S_{b,k}^{max}$	Apparent power magnitude limit on branch (b,k)
$A_g^0,\ A_g^1,\ A_g^2$	Coefficients of quadratic production cost function of generator g

Variables

$p_g^G,\ q_g^G$	Real (p) and reactive (q) power output of generator g
$p_{b,k}^f,\ q_{b,k}^f$	Real (p) and reactive (q) power flow at the *from* end of branch (b,k)
$p_{b,k}^t,\ q_{b,k}^t$	Real (p) and reactive (q) power flow at the *to* end of branch (b,k)
$v_b^r,\ v_b^j$	Real and imaginary part of complex voltage at bus b
$\theta_{b,k}$	Voltage phase angle difference between ends of branch (b,k)
$c_{b,k}, s_{b,k}$	Auxillary variables used in relaxations
$cc_{b,k}, cs_{b,k}$	Auxillary variables used in relaxations
$y_{b,k,i,j}, \delta_{b,k,i,j}$	Binary variables used in piecewise relaxations

1. Introduction

The field of power systems engineering deals with the generation, transmission, and distribution of electric power. A power grid is an electric system that transfers power from generators to demand (i.e., load), and includes ancillary devices that enable control to ensure security, stability, and reliability in operations. In Figure 1, we show a "one-line" diagram of a widely used benchmark test system that illustrates a power grid using a simplified notation, intended for power flow analysis. Nodes in the graph correspond to buses in the transmission system, each of which may have associated generators and loads that respectively represent sources and sinks in the network. Nodes are connected by branches that represent transmission elements in the network. For purposes of planning analyses and operations, a circuit-based mathematical model of the network is typically applied in order to accurately characterize power and current flows.

The U.S. electric grid is mostly an alternating current (AC) system. In an AC system, voltages V – energy/charges quantified in Volts (V) – and currents I

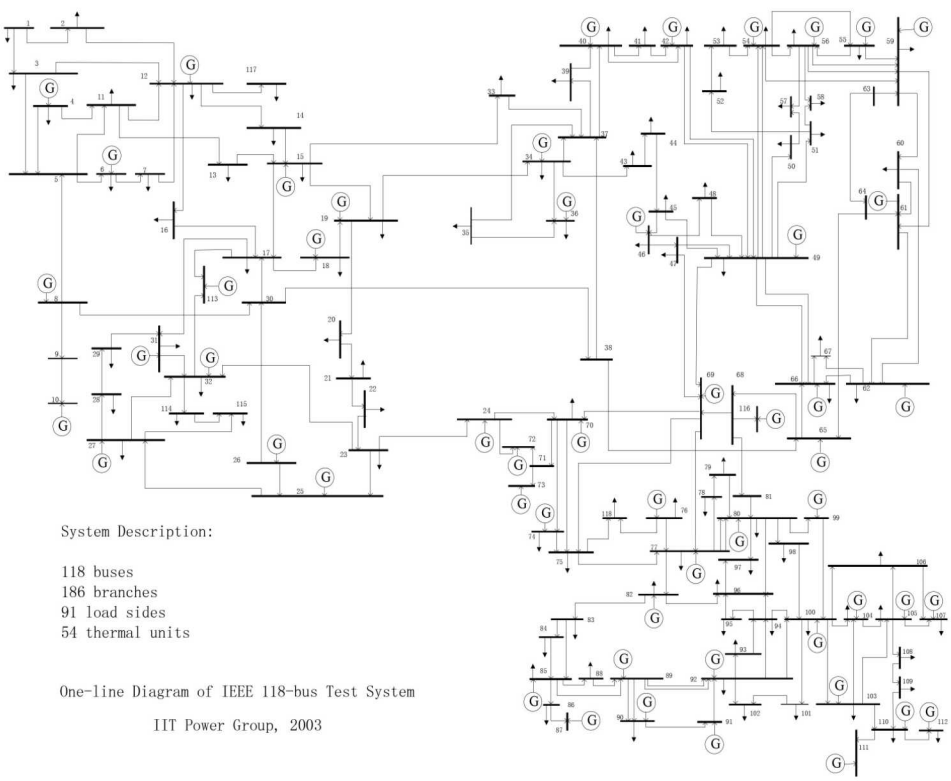

Figure 1: The IEEE 118-bus benchmark system topology.

– charge flows quantified in Amperes (A) – are assumed to be sinusoidal waves that cycle at a constant of 60 times per second (i.e., 60 Hertz). Under the assumption of constant frequency, the power system can be represented with phasors, which is a complex number representing a sinusoid, and the need for modeling short-term dynamics is removed. The result is an algebraic model of the cyclic steady-state behavior for AC power flows.

Building on a base AC power flow model, the objective of the AC optimal power flow (ACOPF) problem is to determine generator set points (i.e., power output levels) that minimize total operating costs of the system while meeting the existing loads subject to key operational limits and physical power flow laws. First formulated over half a century ago in 1962 by Carpentier [6], the ACOPF is the most representative mathematical program of steady-state operations in AC power networks. Due to the complex number representations of voltage and current phasors and alternative strategies for calculating power and/or current flows, there are a number of different possible formulations for the ACOPF [5]. These formulations are, however, universally nonlinear and non-convex, such that the ACOPF is currently not solved in practice due to perceived concerns over computational efficiency, solver reliability, and the strong desire to identify global solutions (which is known to be NP-hard [71] even for networks with tree topologies [49]). Instead, the least-cost economic dispatch for operating actual power grids is determined using numerous simplifications of the ACOPF constraint set, the most common being the linearized "DC" power flow constraints.

A broad range of solution techniques have been applied to solve the ACOPF problem, as surveyed in [7, 23, 24, 26, 35, 50, 51, 60, 61]. General software tools exist to solve the ACOPF problem [20, 76] and many of these tools are based on general platforms for algebraic modeling (e.g., AIMMS [44], Ampl [22], GAMS [65], and Pyomo [30, 31]) that interface with nonlinear optimization solvers (e.g., CONOPT [17], IPOPT [73], KNITRO [4], MINOS [62], and SNOPT [27]). While these nonlinear solvers do not provide any guarantee of global optimality, and do not provide any quantification of the optimality gap, prior analyses have shown these techniques to be scalable and reliable depending upon the initialization conditions, data set parameterization, and ACOPF problem formulation [8]. However, given the importance of these formulations to power systems operations and electricity pricing – wholesale prices are computed as the duals of power balance constraints at buses – there is a need for optimization techniques that can both locate globally optimal solutions and prove their global optimality, quickly and at scale.

A handful of recent approaches focus on development of relaxations of the ACOPF problem to compute lower bounds on the global optima. These relaxations are convex and can provide a (ideally tight) lower bound, certify problem infeasibility and, in some cases, can even be provably exact under certain conditions [34, 47, 51] related to the underlying physics and network structure [48, 69]. Such relaxations are based on semidefinite programming (SDP) [2, 26, 37, 47, 52, 57–59] and second-order cone programming (SOCP) [11, 12, 41, 42]. While these relaxations may provide effective lower bounds on the objective function, when the relaxation is not exact, the solution

may not be feasible or even physically meaningful. Consequently, the Lasserre hierarchy [46] that incorporates sum-of-square polynomials has been applied to tighten the SDP relaxation and guarantee global optimality [26, 37, 57, 58]; however, this approach presents practical difficulties for efficient implementation within a branch-and-cut algorithm and becomes numerically intractable for large-scale networks. Kuang et al. [42, 43] propose LP and SOCP hierarchies that alleviate the computational burden of solving the polynomial optimization problems proposed in [26, 37, 57, 58]. Alternatively, local search techniques or penalty approaches can be applied to recover ACOPF feasible solutions, but global optimality is not guaranteed [53]. Phan [64] proposes a Lagrangian duality-based branch-and-bound specifically to solve the ACOPF to global optimality, and Chen et al. [9] develop a spatial branch-and-cut approach for QCQP problems, and some of their test problems are taken from the ACOPF literature.

Here, we focus on developing rigorous deterministic optimization algorithms for ACOPF that provide a guarantee of optimality and that can also be feasibly embedded into optimization algorithms for solving variants of the ACOPF with discrete decision variables – which result in very difficult mixed-integer nonlinear optimization models. The latter arise in numerous real-world power systems applications, including unit commitment, transmission switching, and contingency analysis. Global solution techniques for nonconvex optimization problems can be generally classified into approximation/relaxation techniques, cutting plane (valid inequality) techniques, and branch-and-bound techniques where deterministic algorithms may leverage more than a single strategy. Branch-and-bound methods [13, 45] seek to solve a lower-bounding (relaxed) problem and an upper-bounding problem, progressively partitioning the search space to improve tightness of the lower bound and allow fathoming of the search space when the lower bound is already larger than a known upper bound. These methods have seen significant success with the introduction of Branch-and-Reduce [19, 66–68, 70] and other variants [38, 39, 75].

In contrast, multitree methods [3] iteratively solve a sequence of lower-bounding and upper-bounding problems with a variety of strategies designed to close the gap. A promising class of multitree methods are known as outer-approximation (OA) methods [18, 21]. While first used for convex NLPs and mixed-integer problems with convex relaxations, these methods can also be used for non-convex problems. Typically, mixed-integer linear programming (MILP) relaxations are formulated for the lower-bounding problem and the responsibility of branching is pushed to an MILP solver. An important feature of multitree approaches is that the lower-bounding problem need not be convex. Rather, the primary requirements are that that the lower bounding problem can be solved to global optimality and can be refined in some way to an arbitrary level of accuracy. Further efficiency gains are possible with increased integration between the global optimization approach and the MILP solver [54].

In this paper, we present an OA-based multitree approach for global solution of the ACOPF problem. The upper-bounding problem is the well-known rectangular power-voltage (RPQV) formulation of the ACOPF problem. The

lower-bounding problem is a piecewise outer approximation based on the SOCP relaxation of the ACOPF problem originally introduced by Jabr [36] and later extended by Kocuk et al. [40]. In the next section, we introduce the RPQV formulation and the classic SOCP-based relaxation. We then introduce a new piecewise outer approximation for the ACOPF problem based on SOCP relaxations that includes piecewise McCormick envelopes for the second-order cone surface constraint, and piecewise relaxations for multivariate arctangent functions. This piecewise relaxation forms the lower-bounding problem in the outer approximation algorithm. The OA-based multitree algorithm is discussed in Section 3. In Section 4 we discuss the performance of this approach in terms of computational time and in terms of relative gap when compared with current state-of-the-art in convex ACOPF relaxations. Finally, we close with conclusions and future work in Section 5.

2. Problem Formulation and Piecewise Relaxations

The OA multitree approach used in this paper is described in detail in Section 3. The approach relies on an upper-bounding problem that can be used to find candidate solutions of the ACOPF problem. Here, we make use of the RPQV formulation with IPOPT to obtain solutions to the upper-bounding problem. The lower-bounding problem must be a relaxation of the original problem, but it need not be convex. Rather, it must be solvable to global optimality with the ability to refine the relaxation to arbitrary tightness. In this paper, we develop a piecewise outer approximation based on the SOCP relaxation introduced by Jabr [36] and extended by Kocuk et al. [40]. This relaxation can be refined by progressively adding smaller intervals in the piecewise representation as the algorithm progresses.

Section 2.1 shows the RPQV formulation used for the upper-bounding problem, and Section 2.2 describes the traditional (non-piecewise) SOCP relaxation. Sections 2.3 and 2.4 show our piecewise relaxation of the ACOPF problem.

2.1. Rectangular Power-Voltage (RPQV) Formulation

The ACOPF problem can be formulated many different ways [5]. The polar formulation considers power flow balances at the buses, and the transmission line equations are written in terms of power, voltage magnitudes, and voltage angles. The RPQV formulation replaces the voltage magnitudes and angles with real and complex voltages, removing trigonometric functions in the power balance, but introducing additional bilinear terms in the tranmission line equations and the voltage limits. The rectangular-current-voltage formulation [7] writes the transmission line equations in terms of current and voltage, and has the favorable property that there are fewer nonlinear terms, since the bilinearities appear at each bus instead of each branch. Each of these different formulations are discussed in detail in Castillo and O'Neill [7] and computational performance is compared in Castillo and O'Neill [8].

The RPQV model is widely used to formulate ACOPF problems and is selected for the upper-bounding problem in this work because it also forms the

basis for the SOCP-based relaxations used in the lower-bounding problem. The RPQV problem formulation is given by,

$$\min \sum_{g\in\mathcal{G}} [A_g^2 (p_g^G)^2 + A_g^1 p_g^G + A_g^0] \tag{1a}$$

s.t.

$$\sum_{(b,k)\in\mathcal{L}_b^{in}} p_{b,k}^t + \sum_{(b,k)\in\mathcal{L}_b^{out}} p_{b,k}^f + G_b^{sh} v_b^2 + P_b^D - \sum_{g\in\mathcal{G}_b} p_g^G = 0 \qquad \forall\, b\in\mathcal{B} \tag{1b}$$

$$\sum_{(b,k)\in\mathcal{L}_b^{in}} q_{b,k}^t + \sum_{(b,k)\in\mathcal{L}_b^{out}} q_{b,k}^f - B_b^{sh} v_b^2 + Q_b^D - \sum_{g\in\mathcal{G}_b} q_g^G = 0 \qquad \forall\, b\in\mathcal{B} \tag{1c}$$

$$p_{b,k}^f = G_{b,k}^{ff} v_b^2 + G_{b,k}^{ft}(v_b^r v_k^r + v_b^j v_k^j) - B_{b,k}^{ft}(v_b^r v_k^j - v_b^j v_k^r) \qquad \forall\, (b,k)\in\mathcal{L} \tag{1d}$$

$$q_{b,k}^f = -B_{b,k}^{ff} v_b^2 - B_{b,k}^{ft}(v_b^r v_k^r + v_b^j v_k^j) - G_{b,k}^{ft}(v_b^r v_k^j - v_b^j v_k^r) \qquad \forall\, (b,k)\in\mathcal{L} \tag{1e}$$

$$p_{b,k}^t = G_{b,k}^{tt} v_k^2 + G_{b,k}^{tf}(v_k^r v_b^r + v_k^j v_b^j) - B_{b,k}^{tf}(v_k^r v_b^j - v_k^j v_b^r) \qquad \forall\, (b,k)\in\mathcal{L} \tag{1f}$$

$$q_{b,k}^t = -B_{b,k}^{tt} v_k^2 - B_{b,k}^{tf}(v_k^r v_b^r + v_k^j v_b^j) - G_{b,k}^{tf}(v_k^r v_b^j - v_k^j v_b^r) \qquad \forall\, (b,k)\in\mathcal{L} \tag{1g}$$

$$(p_{b,k}^f)^2 + (q_{b,k}^f)^2 \le (S_{b,k}^{max})^2,\ (p_{b,k}^t)^2 + (q_{b,k}^t)^2 \le (S_{b,k}^{max})^2 \qquad \forall\, (b,k)\in\mathcal{L} \tag{1h}$$

$$(V_b^{min})^2 \le v_b^2 = (v_b^r)^2 + (v_b^j)^2 \le (V_b^{max})^2 \qquad \forall\, b\in\mathcal{B} \tag{1i}$$

$$P_g^{G,min} \le p_g^G \le P_g^{G,max},\ Q_g^{G,min} \le q_g^G \le Q_g^{G,max} \qquad \forall\, g\in\mathcal{G} \tag{1j}$$

The objective (1a) is to minimize the production cost, which is usually written as a quadratic function of the real power generation. Here A_g^2, A_g^1, and A_g^0 are known coefficients associated with a specific generator g. Equations (1b, 1c) are the balance equations for both real power and reactive power at each bus b. The power flow in the "from" and "to" ends of the transmission lines are modeled with equations (1d-1g). Here, a branch (transmission line) is denoted as $l{\equiv}(b,k)$, where b is the index of the bus at the *from* end of branch l and k is the index of the bus at the *to* end. Real and reactive power injections at either end of a branch are explicitly expressed in terms of complex voltages. These power flow constraints are based on the RPQV model, where

$$G_l = \begin{bmatrix} G_l^{ff}, G_l^{ft} \\ G_l^{tf}, G_l^{tt} \end{bmatrix}, B_l = \begin{bmatrix} B_l^{ff}, B_l^{ft} \\ B_l^{tf}, B_l^{tt} \end{bmatrix}$$

are the real and imaginary parts of the admittance matrix of branch l. Parameters G_b^{sh} and B_b^{sh} are the shunt conductance and susceptance at bus b, respectively. A discussion of the relationship between these power flow constraints and the π-transmission model is given in Appendix B. Thermal limits on the lines are enforced in equations (1h) through bounds on the square of the apparent power flow at both ends of branch l. Equations (1i) and (1j) provide bounds on the voltage magnitudes and the generator real and reactive power respectively. More details on the RPQV model can be found in Castillo and O'Neill [7] and the MATPOWER user manual. MATPOWER is a commonly-

used MATLAB-based power system analysis tool [76].

Any solution of the RPQV formulation given by equations (1) provides a valid upper bound of the ACOPF problem, and this formulation is used as the upper-bounding problem in this work. For the lower-bounding problem, we require a relaxation of the ACOPF problem, and we base our approach on ideas from existing SOCP relaxations, discussed next.

2.2. SOCP-based Reformulation of the ACOPF Problem

The formulation (1) is a non-convex optimization problem due to quadratic and bilinear terms. To support development of tight convex relaxations, Jabr [36] was the first to reformulate this problem through the introduction of a set of new variables defined as,

$$\begin{aligned} c_{b,b} &\equiv (v_b^r)^2 + (v_b^j)^2 = v_b^2 \\ c_{b,k} &\equiv v_b^r v_k^r + v_b^j v_k^j = |v_b||v_k| \cos\theta_{b,k} \\ s_{b,k} &\equiv v_b^r v_k^j - v_k^r v_b^j = -|v_b||v_k| \sin\theta_{b,k} \end{aligned}$$

With this transformation, the quadratic and bilinear terms can be replaced by the new variables, $c_{b,k}$ and $s_{b,k}$, leading to the reformulation

$$\min \sum_{g\in\mathcal{G}} [A_g^2 (p_g^G)^2 + A_g^1 p_g^G + A_g^0] \tag{2a}$$

$$\text{s.t.} \tag{2b}$$

$$\sum_{(b,k)\in\mathcal{L}_b^{in}} p_{b,k}^t + \sum_{(b,k)\in\mathcal{L}_b^{out}} p_{b,k}^f + G_b^{sh} c_{b,b} + P_b^D - \sum_{g\in\mathcal{G}_b} p_g^G = 0 \qquad \forall\, b\in\mathcal{B} \tag{2c}$$

$$\sum_{(b,k)\in\mathcal{L}_b^{in}} q_{b,k}^t + \sum_{(b,k)\in\mathcal{L}_b^{out}} q_{b,k}^f - B_b^{sh} c_{b,b} + Q_b^D - \sum_{g\in\mathcal{G}_b} q_g^G = 0 \qquad \forall\, b\in\mathcal{B} \tag{2d}$$

$$p_{b,k}^f = G_{b,k}^{ff} c_{b,b} + G_{b,k}^{ft} c_{b,k} - B_{b,k}^{ft} s_{b,k} \qquad \forall\,(b,k)\in\mathcal{L} \tag{2e}$$

$$q_{b,k}^f = -B_{b,k}^{ff} c_{b,b} - B_{b,k}^{ft} c_{b,k} - G_{b,k}^{ft} s_{b,k} \qquad \forall\,(b,k)\in\mathcal{L} \tag{2f}$$

$$p_{b,k}^t = G_{b,k}^{tt} c_{k,k} + G_{b,k}^{tf} c_{k,b} - B_{b,k}^{tf} s_{k,b} \qquad \forall\,(b,k)\in\mathcal{L} \tag{2g}$$

$$q_{b,k}^t = -B_{b,k}^{tt} c_{k,k} - B_{b,k}^{tf} c_{k,b} - G_{b,k}^{tf} s_{k,b} \qquad \forall\,(b,k)\in\mathcal{L} \tag{2h}$$

$$(p_{b,k}^f)^2 + (q_{b,k}^f)^2 \le (S_{b,k}^{max})^2,\ (p_{b,k}^t)^2 + (q_{b,k}^t)^2 \le (S_{b,k}^{max})^2 \qquad \forall\,(b,k)\in\mathcal{L} \tag{2i}$$

$$(V_b^{min})^2 \le c_{b,b} \le (V_b^{max})^2 \qquad \forall\, b\in\mathcal{B} \tag{2j}$$

$$P_g^{G,min} \le p_g^G \le P_g^{G,max},\ Q_g^{G,min} \le q_g^G \le Q_g^{G,max} \qquad \forall\, g\in\mathcal{G} \tag{2k}$$

where the power balance and branch injection constraints are all linear. It is worthwhile to point out that the reformulation (2), as written, is not mathematically equivalent to the original formulation (1), and additional constraints are required for equivalence. First, according to the definitions of $c_{b,k}$ and $s_{b,k}$, we have

$$c_{b,k} = c_{k,b},\ s_{b,k} = -s_{k,b} \quad \forall\,(b,k)\in\mathcal{L} \tag{3}$$

and

$$c_{b,k}^2 + s_{b,k}^2 = c_{b,b}c_{k,k} \quad \forall\, (b,k) \in \mathcal{L} \tag{4}$$

Note that constraint (4) is non-convex since it indicates the surface of a rotated second-order cone in $\mathcal{R}^4$, and we call this the *second-order cone surface constraint*.

In addition, we need to consider the *cycle constraints*, which ensure that the sum of angle differences along each cycle (or loop) equals zero.

$$\sum_{(b,k)\in\mathcal{L}_c} \theta_{b,k} = 0 \qquad \forall\, c \in \mathcal{C} \tag{5a}$$

$$\theta_{b,k} = -\arctan\left(\frac{s_{b,k}}{c_{b,k}}\right) \qquad \forall\, (b,k) \in \mathcal{L} \tag{5b}$$

Here $\mathcal{L}_c$ denotes a simple cycle in the network. Previous work has shown that cycle constraints can be neglected for radial networks; however, for general meshed networks, these constraints have to be enforced. Therefore, an equivalent ACOPF problem formulation in the space of the new variables is given by equations,

$$(2), (3), (4), (5) \tag{6}$$

Note that the reformulation (6) is still a non-convex optimization problem due to the second-order cone surface constraints (4) and the arctangent functions in the cycle constraints (5).

Equations (2) formed the basis for development of strong SOCP relaxations of the ACOPF problem. Jabr [36] first proposed an SOCP relaxation, where the non-convex constraint (4) is relaxed with the inequality,

$$c_{b,k}^2 + s_{b,k}^2 \leq c_{b,b}c_{k,k} \quad \forall\, (b,k) \in \mathcal{L} \tag{7}$$

Though quadratic and bilinear terms are included, constraint (7), known as the second-order cone constraint, is convex since the corresponding feasible region is the surface and the inner space of a rotated second-order cone (note that $c_{b,b}$ and $c_{k,k}$ are non-negative). The classic SOCP-based convex relaxation proposed in Jabr [36] includes equations (2) and (7) only, excluding the cycle constraints. To further improve the tightness of this formulation, Kocuk et al. [40] proposed three strong SOCP-based relaxations, including different relaxations of the cycle constraints (5), and additional SDP-based cuts. Numerical results have shown that these strong SOCP relaxations are tighter than the classic formulation [36]. Moreover, they can provide even tighter relaxations than the SDP approach in several benchmark problems. Although the SDP-based separation cuts provide stronger relaxations on most of their test problems, the generation of these cuts requires solution of a number of SDP subproblems.

While these relaxations have been shown to be quite strong, they are not appropriate for the OA multitree approach as written. That is, they cannot be refined to produce increasingly tight relaxations. Because of the favorable tradeoff between tightness of the relaxation and computational cost, the lower-bounding

problem used in this paper builds from ideas in the SOCPA formulation. The next subsections focus on the development of piecewise representations of the second-order cone surface constraints (4) and the arctangent cycle constraints (5).

2.3. Piecewise Relaxation of the Second-Order Cone Surface Constraint

In a typical SOCP-based relaxation, equation (4) is directly relaxed with the one-sided second-order cone inequality (7). For a large number of benchmark problems, this relaxation is tight enough and the residual of $c_{b,b}c_{k,k}-c_{b,k}^2-s_{b,k}^2$ is negligible. This means the optimal solution of the relaxation problem automatically converges to some point very close to or even on the surface of the second-order cone. However, there exist counter examples where this relaxation is not tight. In these cases, the optimal solution of the relaxation problem lies in the interior of the second-order cone and equation (7) alone is not enough to provide tight relaxation of the ACOPF problem. The existence of these examples illustrates the need to enforce the full second-order cone surface constraint (4) instead of (7) alone.

To ensure a tight relaxation, the equality constraints (4) needs to be considered directly. As others have done, we continue to relax the convex side of this constraint with the second-order cone inequality (7), but also add a relaxation for the other side of the inequality based on McCormick envelopes [55] on the bilinear terms.

Introducing two new variables,

$$\begin{aligned} cs_{b,k} &= c_{b,k}^2 + s_{b,k}^2 \\ cc_{b,k} &= c_{b,b}c_{k,k}, \end{aligned}$$

the non-convex equality constraint (4) can be written as,

$$cs_{b,k} = cc_{b,k} \quad \forall\, (b,k) \in \mathcal{L} \tag{8}$$

Both new variables can be relaxed using standard outer approximation techniques which give a set of linear over- and under-estimators. Since $c_{b,k}^2 + s_{b,k}^2$ is a convex function, the linear over-estimator of $cs_{b,k}$ is given as

$$cs_{b,k} \leq (c_{b,k}^L + c_{b,k}^U)c_{b,k} + (s_{b,k}^L + s_{b,k}^U)s_{b,k} - c_{b,k}^L c_{b,k}^U - s_{b,k}^L s_{b,k}^U, \tag{9}$$

providing a single linear over-estimator for the entire domain $[c_{b,k}^L, c_{b,k}^U] \times [s_{b,k}^L, s_{b,k}^U]$. Note that under-estimators for $cs_{b,k}$ are not needed because we are directly including (7).

For variable $cc_{b,k}$, the well-known McCormick envelopes [55] provide the tightest linear envelopes. Particularly, for the domain $[c_{b,b}^L, c_{b,b}^U] \times [c_{k,k}^L, c_{k,k}^U]$, we have two under-estimators

$$\begin{aligned} cc_{bk} &\geq c_{b,b}c_{k,k}^U + c_{b,b}^U c_{k,k} - c_{b,b}^U c_{k,k}^U \\ cc_{bk} &\geq c_{b,b}c_{k,k}^L + c_{b,b}^L c_{k,k} - c_{b,b}^L c_{k,k}^L \end{aligned} \tag{10}$$

Again, note that the over-estimators are not required because we directly include (7).

It is worthwhile to point out that the tightness of these over- and under-estimators are strongly dependent on the upper and lower bounds of variables, and while the OA multitree approach makes use of bounds tightening methods, further refinement is still necessary with piecewise relaxations where the feasible domain is split into a set of smaller regions with over- and under-estimators constructed for each region.

In this piecewise outer approximation approach, discrete variables are required to indicate which region is active. For this reason, the resulting relaxations are formulated as mixed-integer programming problems. There exist a number of different mathematical representations for piecewise over- and under-estimators [25, 32, 56, 72, 74]. Previous studies have indicated that the choice of representation can strongly impact computational performance. Comprehensive comparisons for piecewise bilinear representations can be found in the literature [25, 29, 32]. Such an analysis for the ACOPF relaxation is beyond the scope of this paper. Here, a bivariate partitioning is used [32] (i.e., both variables in the bilinear terms are partitioned). Using $[s^L_{b,k,i}, s^U_{b,k,i}]$ to refer to the i-th interval for $s_{b,k}$ and $[c^L_{b,k,j}, c^U_{b,k,j}]$ to refer to the j-th interval of $c_{b,k}$, we can write the following piecewise over-estimators for $cs_{b,k}$ as,

$$\begin{aligned}
cs_{b,k,i,j} \leq\ & (c^L_{b,k,j} + c^U_{b,k,j})c_{b,k,i,j} \\
& + (s^L_{b,k,i} + s^U_{b,k,i})s_{b,k,i,j} && \forall\ (i,j) \in \mathcal{Z}^{cs}_{b,k}\ \ \forall\ (b,k) \in \mathcal{L} && \text{(11a)} \\
& - (c^L_{b,k,j}c^U_{b,k,j} + s^L_{b,k,i}s^U_{b,k,i})y_{b,k,i,j} \\
cs_{b,k} =\ & \sum_{(i,j)\in\mathcal{Z}^{cs}_{b,k}} cs_{b,k,i,j} && \forall\ (b,k) \in \mathcal{L} && \text{(11b)} \\
s_{b,k,i,j} \leq\ & s^U_{b,k,i}y_{b,k,i,j} && \forall\ (i,j) \in \mathcal{Z}^{cs}_{b,k}\ \ \forall\ (b,k) \in \mathcal{L} && \text{(11c)} \\
s_{b,k,i,j} \geq\ & s^L_{b,k,i}y_{b,k,i,j} && \forall\ (i,j) \in \mathcal{Z}^{cs}_{b,k}\ \ \forall\ (b,k) \in \mathcal{L} && \text{(11d)} \\
s_{b,k} =\ & \sum_{(i,j)\in\mathcal{Z}^{cs}_{b,k}} s_{b,k,i,j} && \forall\ (b,k) \in \mathcal{L} && \text{(11e)} \\
c_{b,k,i,j} \leq\ & c^U_{b,k,j}y_{b,k,i,j} && \forall\ (i,j) \in \mathcal{Z}^{cs}_{b,k}\ \ \forall\ (b,k) \in \mathcal{L} && \text{(11f)} \\
c_{b,k,i,j} \geq\ & c^L_{b,k,j}y_{b,k,i,j} && \forall\ (i,j) \in \mathcal{Z}^{cs}_{b,k}\ \ \forall\ (b,k) \in \mathcal{L} && \text{(11g)} \\
c_{b,k} =\ & \sum_{(i,j)\in\mathcal{Z}^{cs}_{b,k}} c_{b,k,i,j} && \forall\ (b,k) \in \mathcal{L} && \text{(11h)} \\
& \sum_{(i,j)\in\mathcal{Z}^{cs}_{b,k}} y_{b,k,i,j} = 1 && \forall\ (b,k) \in \mathcal{L} && \text{(11i)} \\
& y_{b,k,i,j} \in \{0,1\} && \forall\ (i,j) \in \mathcal{Z}^{cs}_{b,k}\ \ \forall\ (b,k) \in \mathcal{L} && \text{(11j)}
\end{aligned}$$

The binary variables $y_{b,k,i,j}$ are used to indicate which subregion $[s^L_{b,k,i}, s^U_{b,k,i}]$ $\times$ $[c^L_{b,k,j}, c^U_{b,k,j}]$ is active for each branch (b,k). The set $\mathcal{Z}^{cs}_{b,k}$ is the set of all subre-

gions $[s^L_{b,k,i}, s^U_{b,k,i}] \times [c^L_{b,k,j}, c^U_{b,k,j}]$ for each branch (b,k). The variable $cs_{b,k,i,j}$ is the value of $cs_{b,k}$ within the corresponding subregion. It is equal to 0 if the subregion is not active and equal to $cs_{b,k}$ if the subregion is active. Similarly, $s_{b,k,i,j}$ and $c_{b,k,i,j}$ are the values of $s_{b,k}$ and $c_{b,k}$ within the corresponding subregions.

Constraint (11a) is the over-estimator for each subregion. Constraints (11c), (11d), (11f), and (11g) force $s_{b,k,i,j}$ and $c_{b,k,i,j}$ to be zero if the subregion is not active and within the bounds of the subregion if the subregion is active. Note that if the subregion is not active, these constraints along with (11a) force $cs_{b,k,i,j}$ to be less than or equal to 0. Constraint (11i) ensures that only one subregion can be active for each branch.

We used the following for the under-estimators for $cc_{b,k}$.

$$\begin{aligned} cc_{b,k,i,j} \geq\ & cb_{b,k,i,j} c^U_{k,k,j} \\ & + c^U_{b,b,i} ck_{b,k,i,j} && \forall\ (i,j) \in \mathcal{Z}^{cc}_{b,k}\ \ \forall\ (b,k) \in \mathcal{L} && \text{(12a)} \\ & - c^U_{b,b,i} c^U_{k,k,j} \delta_{b,k,i,j} \\ cc_{b,k,i,j} \geq\ & cb_{b,k,i,j} c^L_{k,k,j} \\ & + c^L_{b,b,i} ck_{b,k,i,j} && \forall\ (i,j) \in \mathcal{Z}^{cc}_{b,k}\ \ \forall\ (b,k) \in \mathcal{L} && \text{(12b)} \\ & - c^L_{b,b,i} c^L_{k,k,j} \delta_{b,k,i,j} \\ cc_{b,k} =\ & \sum_{(i,j)\in\mathcal{Z}^{cc}_{b,k}} cc_{b,k,i,j} && \forall\ (b,k) \in \mathcal{L} && \text{(12c)} \\ cb_{b,k,i,j} \leq\ & c^U_{b,b,i} \delta_{b,k,i,j} && \forall\ (i,j) \in \mathcal{Z}^{cc}_{b,k}\ \ \forall\ (b,k) \in \mathcal{L} && \text{(12d)} \\ cb_{b,k,i,j} \geq\ & c^L_{b,b,i} \delta_{b,k,i,j} && \forall\ (i,j) \in \mathcal{Z}^{cc}_{b,k}\ \ \forall\ (b,k) \in \mathcal{L} && \text{(12e)} \\ c_{b,b} =\ & \sum_{(i,j)\in\mathcal{Z}^{cc}_{b,k}} cb_{b,k,i,j} && \forall\ (b,k) \in \mathcal{L} && \text{(12f)} \\ ck_{b,k,i,j} \leq\ & c^U_{k,k,j} \delta_{b,k,i,j} && \forall\ (i,j) \in \mathcal{Z}^{cc}_{b,k}\ \ \forall\ (b,k) \in \mathcal{L} && \text{(12g)} \\ ck_{b,k,i,j} \geq\ & c^L_{k,k,j} \delta_{b,k,i,j} && \forall\ (i,j) \in \mathcal{Z}^{cc}_{b,k}\ \ \forall\ (b,k) \in \mathcal{L} && \text{(12h)} \\ c_{k,k} =\ & \sum_{(i,j)\in\mathcal{Z}^{cc}_{b,k}} ck_{b,k,i,j} && \forall\ (b,k) \in \mathcal{L} && \text{(12i)} \\ & \sum_{(i,j)\in\mathcal{Z}^{cc}_{b,k}} \delta_{b,k,i,j} = 1 && \forall\ (b,k) \in \mathcal{L} && \text{(12j)} \\ & \delta_{b,k,i,j} \in \{0,1\} && \forall\ (i,j) \in \mathcal{Z}^{cc}_{b,k}\ \ \forall\ (b,k) \in \mathcal{L}. && \text{(12k)} \end{aligned}$$

Similar to above, the binary variables $\delta_{b,k,i,j}$ are used to indicate which subregion $[c^L_{b,b,i}, c^U_{b,b,i}] \times [c^L_{k,k,j}, c^U_{k,k,j}]$ is active for each branch (b,k). The set $\mathcal{Z}^{cc}_{b,k}$ is the set of all subregions $[c^L_{b,b,i}, c^U_{b,b,i}] \times [c^L_{k,k,j}, c^U_{k,k,j}]$ for each branch (b,k). The variable $cc_{b,k,i,j}$ is the value of $cc_{b,k}$ within the corresponding subregion. It is equal to 0 if the subregion is not active and equal to $cc_{b,k}$ if the subregion is active. Similarly, $cb_{b,k,i,j}$ and $ck_{b,k,i,j}$ are the values of $c_{b,b}$ and $c_{k,k}$ within the corresponding subregions.

Constraints (12a) and (12b) are the under-estimators for each subregion. Constraints (12d), (12e), (12g), and (12h) force $cb_{b,k,i,j}$ and $ck_{b,k,i,j}$ to be zero if the subregion is not active and within the bounds of the subregion if the subregion is active. Note that if the subregion is not active, these constraints along with (12a) and (12b) force $cc_{b,k,i,j}$ to be greater than or equal to 0. Constraint (12j) ensures that only one subregion can be active for each branch.

The combined constraints,

$$(7), (8), (11), (12), \tag{13}$$

form the piecewise relaxation of the second-order cone surface constraints.

2.4. Piecewise Relaxation of the Arctangent Function in the Cycle Constraints

To obtain a convex relaxation of the reformulation (6), we also need to relax the nonlinear arctangent terms in the cycle constraints (5). Similarly, we are interested in constructing linear over- and under-estimators for these expressions.

Given the domain $[c^L_{b,k}, c^U_{b,k}] \times [s^L_{b,k}, s^U_{b,k}]$ one approach to derive piecewise relaxations is to identify the "tightest" hyperplanes which pass through each of the vertices and lie strictly above or below the arctangent function over the domain. The two over-estimators and two under-estimators for each arctan term can be parameterized,

$$\begin{aligned} \arctan\left(\frac{s_{b,k}}{c_{b,k}}\right) &\geq \alpha^u_i s_{b,k} + \beta^u_i c_{b,k} + \gamma^u_i \quad \forall\, i \in \{1,2\} \\ \arctan\left(\frac{s_{b,k}}{c_{b,k}}\right) &\leq \alpha^o_i s_{b,k} + \beta^o_i c_{b,k} + \gamma^o_i \quad \forall\, i \in \{1,2\} \end{aligned} \tag{14}$$

where the values of parameters α, β, and γ, are based on different feasible domains of $s_{b,k}$ and $c_{b,k}$ [40]. In Kocuk et al. [40], relaxations of the arctangent functions are computed by solving four optimization problems for each arctangent function to lift the linear planes and ensure none of the feasible region is violated. In our approach, piecewise relaxations are desired over a number of subintervals, and we derive linear envelopes that pass through the arctangent function at each of the four corners. The expressions for the parameters from our approach are provided in Appendix A.

As before, piecewise representations are used to improve tightness as the algorithm progresses. In particular, for each arctan term, we partition the domains of variables $c_{b,k}$ and $s_{b,k}$, leading to small sub-regions $[s^L_{b,k,m}, s^U_{b,k,m}] \times [c^L_{b,k,n}, c^U_{b,k,n}]$, where m=1, $\cdots$, M and n=1, $\cdots$, N. Note that the binary variables introduced for $c_{b,k}$ and $s_{b,k}$ can be shared with those used in the over-estimators introduced for variable $cs_{b,k}$. We use the following piecewise relaxations for the

cycle constraints in (5).

$$
\begin{aligned}
-\theta_{b,k,i,j} \geq\ & \alpha^u_{b,k,i,j,n} s_{b,k,i,j} \\
& + \beta^u_{b,k,i,j,n} c_{b,k,i,j} && \forall\, n \in \{1,2\}\ \ \forall\, (i,j) \in \mathcal{Z}^{cs}_{b,k}\ \ \forall\, (b,k) \in \mathcal{L} \quad (15a) \\
& + \gamma^u_{b,k,i,j,n} y_{b,k,i,j} \\
-\theta_{b,k,i,j} \leq\ & \alpha^o_{b,k,i,j,n} s_{b,k,i,j} \\
& + \beta^o_{b,k,i,j,n} c_{b,k,i,j} && \forall\, n \in \{1,2\}\ \ \forall\, (i,j) \in \mathcal{Z}^{cs}_{b,k}\ \ \forall\, (b,k) \in \mathcal{L} \quad (15b) \\
& + \gamma^o_{b,k,i,j,n} y_{b,k,i,j} \\
\theta_{b,k} =\ & \sum_{(i,j) \in \mathcal{Z}^{cs}_{b,k}} \theta_{b,k,i,j} && \forall\, (b,k) \in \mathcal{L} \quad (15c)
\end{aligned}
$$

$$
(11c) - (11j)
$$

Note that we only need to impose cycle constraints for a set of simple cycles, which is called a *cycle basis* [40]. For instance, in a connected graph with n buses and m branches, the cycle basis contains a number of $m-n+1$ simple cycles. In larger networks, $m-n+1$ may still be quite large. Therefore, the relaxations of the arctangent fucntions are initialized with only a single interval (no piecewise components), and then selectively refined as described in Section 3.

3. Global Solution Framework for ACOPF

The global solution approach developed for the ACOPF problem in this paper is a multitree method [3] that iteratively solves a sequence of upper-bounding and lower-bounding problems. The upper bound at each iteration is found by solving the original nonconvex problem to local optimality. For the ACOPF problem in this paper, the RPQV formulation in equations (1) is used for the upper-bounding problem. The lower bound at each iteration is computed using a piecewise outer-approximation of (1) based on the variables in the classic SOCP relaxation. Outer-approximation [18, 21] is traditionally used for convex NLP problems or MINLP problems with convex binary relaxations, however, convexity is not required. The lower-bounding problem must represent a true relaxation of the original problem, it must be solvable to global optimality, and it must be possible to refine the relaxation to sufficient accuracy for the desired optimality gap. In this paper, the lower-bounding problem is the piecewise SOCP-based relaxation of the ACOPF problem given by,

$$
(2), (3), (5a), (7), (8), (11), (12), (15), \qquad \text{(PW-ACOPF-R)}
$$

where the selection of intervals for each of the constraints is managed by the algorithm described below. If none of the variables are partitioned (initial relaxation), this is a convex SOCP problem and can be solved to global optimality by local solvers. However, if internal points (i.e., additional intervals) are

added to the piecewise representation, the resulting relaxation is formulated as a mixed-integer second-order cone programming (MISOCP) problem, which can be solved by commonly-used mixed-integer programming solvers.

Theoretically, one can achieve arbitrary tightness by simply increasing the number of segment points. However, the resulting relaxation, formulated as a large-scale MISOCP problem, can be very challenging to solve or even become intractable. Therefore, the overall algorithm iteratively solves a sequence of lower- and upper-bounding problems, where the lower-bounding problem is progressively and selectively refined as the algorithm proceeds. The goal is to provide strong improvement in the tightness of the relaxation while ensuring efficient solution of the lower-bounding problem by introducing fewer discrete variables.

Note that the lower-bounding problem (PW-ACOPF-R) is a true relaxation of the original ACOPF problem. Therefore, if the lower-bounding problem is ever infeasible, then the original ACOPF problem is also infeasible and the algorithm terminates. Otherwise, the solution provides a valid lower bound of the optimal objective function value for the ACOPF problem.

In each iteration, the upper-bounding problem is reinitialized with the solution obtained from the lower-bounding problem and solved with a local NLP solver to search for a better candidate solution and upper bound. If the gap between the upper and lower bound closes, then a provably global solution has been found. While there is no guarantee that the upper-bounding problem will converge to the global minimum, in practice this approach has been effective. Furthermore, since the lower-bounding problem is progressively refined, in the limit, the solution of the lower-bounding problem will approach the global solution of the original ACOPF problem and eventually meet the desired tolerance criteria. The algorithm terminates when the relative optimality gap is below a given tolerance or the computational time exceeds the desired threshold.

The performance of this global solution framework depends strongly on the tightness of the lower-bounding problem, and it is well known that reducing the bounds on key variables can have a significant impact. In this work, optimization-based bounds tightening (OBBT) is used to reduce the domain of the variables and improve the relaxation. This optimization-based strategy solves two optimization problems for each selected variable to find the smallest lower bound and the largest upper bound where the problem is still feasible. Global optimality is required for the OBBT problems (so as not to improperly cut off a valid part of the feasible region), and they are derived directly from our lower-bounding problem by modifying the objective function and adding the *objective cut-off* constraint based on the current upper bound. This OBBT approach is described well in several sources [3, 28, 70]. The OBBT approach is computationally expensive. Therefore, it is only implemented on all $s_{b,k}$ and $c_{b,k}$ variables in the initial step of the algorithm, and applied selectively thereafter. To further improve computational time, these problems are solved in parallel using Pyomo [30, 31] and mpi4py [14–16].

The following algorithm is used for global optimization of the ACOPF problem:

0. **Initialization:** The upper bounding problem (1) is solved to local optimality. If the upper bounding problem is feasible, the corresponding objective function value is used as the initial upper bound. Otherwise, the initial upper bound is set to a sufficiently large value. An initial lower-bounding problem (PW-ACOPF-R) with no partitioning (e.g., lower and upper bounds only are used in the relaxation) is generated. Optimization-based bound tightening (OBBT) is performed for selected variables, including $s_{b,k}$ and $c_{b,k}$, based on the initial upper bound and the lower-bounding problem.

1. **Solve the Lower-Bounding Problem:** The lower-bounding problem (PW-ACOPF-R) is solved to global optimality. If this relaxation is infeasible, the original ACOPF problem is infeasible, and the algorithm terminates. Otherwise, the lower bound on the problem is updated as needed and the algorithm proceeds to Step 2.

2. **Solve the Upper-Bounding Problem:** The original non-convex ACOPF problem (1) is solved to local optimality with the variables initialized from the solution of the lower-bounding problem. If the problem is feasible and the objective is lower than the best known feasible solution, the upper bound is updated. If the optimality gap between the current upper and lower bounds is below the given tolerance, the algorithm terminates with the global solution. If the algorithm execution time is larger than the maximum execution time, then the algorithm terminates with the best solution found. Otherwise, proceed to Step 3.

3. **Refining the Lower-Bounding Problem:** In this step, additional intervals are added to the piecewise representations. Given the solution of the lower-bounding problem, the second-order cone surface constraints with residuals greater than a specified tolerance are identified, and the corresponding variable domains are further partitioned by adding new segment points according to the solution of the lower-bounding problem. As well, the network solution is examined, and we identify simple cycles within the cycle basis that have the largest cycle constraint violations. Similarly, the corresponding variable domains are further partitioned by adding new segment points based on the solution of the lower-bounding problem. Bounds for variables associated with these modified constraints are tightened using OBBT. Proceed to Step 1.

This algorithm is used to converge ACOPF problems to global optimality as demonstrated on a number of test cases in the next section.

4. Numerical Results

The primary purpose of this work is to provide an algorithm to quickly identify global solutions to the ACOPF problem, which requires a rigorous approach

to closing any remaining optimality gap and proving global optimality of candidate solutions. Our OA-based approach solves a sequence of upper- and lower-bounding problems where the lower bounding problem is a piecewise relaxation of ACOPF that allows further refinement as the algorithm progresses. Here, we compare the performance of our approach against the current state-of-the-art reported in the literature for convex relaxations of the ACOPF problem.

Comparisons are made with the quadratic convex (`QC`) relaxation proposed by [12] and refined in [11], the classic SOCP [36] formulation (`SOCP`), and three strong relaxations (`SOCPA`, `S34A`, and `SSDP`) proposed by [40]. Recall that the `SOCPA` is `SOCP` strengthened by cycle constraints with linear cuts around the arctangent functions, the `S34A` is further strengthened by imposing polynomial-based relaxations for cycle constraints arising in 3- and 4-node cycles, and the `SSDP` is `SOCP` strengthened by generation of SDP separation cuts.

We observe that all of these relaxations (`QC`, `SOCP`, `SOCPA`, `S34A`, and `SSDP`) are single relaxations and are therefore not global optimization approaches. Computational results in Kocuk et al. [40] do include up-front computations for bounds tightening and generation of improved cuts. However, they are still single-pass approaches and do not *iteratively* refine or tighten the relaxation. This difference makes it difficult to compare the performance of these approaches with our global approach, which does provide iterative tightening of the relaxation. Therefore, when presenting experimental results below, we report solution quality and run time of our approach executed to termination as well as the corresponding statistics for the first iteration of our OA approach, i.e., a single pass that includes solution of the lower-bounding relaxation and the upper-bounding problem.

We test our approach on 14 benchmark ACOPF test cases, including 6 standard IEEE instances from MATPOWER [76] and 8 instances (under 'typical operating conditions') from the NESTA test case archive [10]. The NESTA test cases are designed to contain more realistic operating data and can be more computationally challenging than standard IEEE test cases. Our global solution framework is implemented in Python 2.7 with Pyomo 5.1 [30, 31]. All experiments are executed on a 64-bit server with 48 CPUs (Intel(R) Xeon(R) CPU E5-2697 v2 @ 2.70GHz) and total memory of 264 GB. All lower-bounding problems are solved with GUROBI 6.5.2 [63], with the thread option set to 24. The NLP problems are solved with IPOPT 3.12.6 [73] configured using the MA27 sparse linear solver [33].

The relative optimality gap of the global algorithm is defined as $\left(z^{UB}-z^{LB}\right)/z^{UB}\times 100$ where z^{UB} and z^{LB} are the current "best" values of the upper and lower bounds on the objective function, respectively. The convergence tolerance for the relative optimality gap is set to 0.1%, the total computational time limit is 3600 seconds, and the maximum outer iteration number limit is set to 100.

4.1. Comparison of Optimality Gap

In Table 1, we report optimality gaps resulting from both our global OA approach (including the first iteration of our OA approach) and the single-pass

Table 1: *Percentage relative optimality gap.* The '-' indicates no results were reported by the authors on this test case; the '*' indicates results that are reported to the tenth decimal place only. Note that the optimality tolerance for our Global OA Approach is set to 0.1%, and no additional refinement is done after this gap is acheived.

Case Name	Global OA Approach	Single-Pass Relaxations					
		1st OA	QC	SOCP	SOCPA	S34A	SSDP
nesta_case3_lmbd	0.00	0.89	1.24	1.32	1.25	0.97	0.43
nesta_case5_pjm	0.09	14.35	14.54	14.54	14.47	14.26	6.22
case6ww	0.02	0.02	-	0.63	0.02	0.01	0.00
nesta_case6_ww	0.02	0.02	0.6*	0.63	0.02	0.01	0.00
case14	0.01	0.01	-	0.08	0.08	0.06	0.00
nesta_case14_ieee	0.00	0.00	0.1*	0.11	0.11	0.07	0.00
case30	0.08	0.26	-	0.57	0.37	0.34	0.07
nesta_case30_ieee	0.09	2.24	15.64	15.65	5.24	4.79	0.00
case39	0.00	0.00	-	0.02	0.01	0.01	0.01
nesta_case39_epri	0.01	0.01	0.0*	0.05	0.02	0.02	0.01
case57	0.02	0.02	-	0.06	0.06	0.06	0.00
nesta_case57_ieee	0.01	0.01	0.1*	0.06	0.06	0.06	0.00
case118	0.08	0.10	-	0.25	0.24	0.16	0.03
nesta_case118_ieee	0.59[1]	0.87	1.72	2.10	1.12	0.94	0.25

[1] This case failed to solve to a gap of 0.1% in the allotted time (3600s). The reported gap of 0.59% was achieved in 423 seconds.

convex relaxations reported in the literature.

As shown in the table, our global approach achieves the specified target optimality gap (less than 0.1%) for all but one test case. Comparing with specific single-pass convex relaxations, our global approach obtains equal or smaller optimality gaps than the `QC`, `SOCP`, and `SOCPA` relaxations for all test cases considered. Note that the optimality gap tolerance is set to 0.1%, and the global approach does not refine further after this tolerance is met. Therefore, it is more important to take note of the more challenging problems where the single-pass relaxations do not achieve tight relaxation on their own. Although our global approach is based on similar relaxations as the SOCP-based methods, our implementation further refines these relaxations with the piecewise outer approximations and therefore improves the tightness of the lower bounding problem. Finally, our proposed approach is competitive with the tightest SOCP-based relaxation, `SSDP`, and yields significant improvements over `SSDP` on the `nesta_case3_lmbd` and `nesta_case5_pjm` cases. For the `nesta_case3_lmbd` and `nesta_case5_pjm` test cases, the first iteration of the OA approach finds a solution that is in the interior of the second-order cone inequality, and it is likely that this harms the quality of the other single-pass relaxations as well. However, our global approach explicitly addresses this violation through refinement of the piecewise outer approximations and additional bounds tightening. These results show that our OA-based multitree approach is able to effectively close the gap and solve even the more challenging problems to global optimality.

Comparing the optimality gap from the first iteration of our OA approach with those obtained by the other relaxations shows that the relaxations proposed in this work are competitive with all the reported relaxations except for those based on generating SDP cuts. While `SSDP` relaxations are tighter than the initial OA relaxation, this comes with an increased computational cost to solve the SDP subproblems and generate these cuts. Furthermore, these additional cuts could be included with our lower-bounding problem. However, the improvement in the relaxation would need to be weighed against the increased computational cost associated with generating the cuts.

4.2. Comparison of Computational Performance

One of our key objectives is to quickly generate globally optimal solutions to the ACOPF quickly. To assess the degree to which we achieve this objective, we report computational timing results for each of the test cases in Table 2. In this table, we report the best upper bound and lower bound identified, the relative optimality gap (in %), the solver CPU time (in s), and the number of outer iterations. Consistent with other reported timing in the literature, this table shows only the cumulative time required by the solvers (on both the upper- and lower-bounding problems), and omits the overhead associated with data processing, model construction, and OBBT. All the benchmark test cases with the exception of `nesta_case118_ieee` can be solved to under the 0.1% optimality gap within the time allotted, and out of that set only the `nesta_case30_ieee` takes longer than one minute to solve. Many of the instances were solved within

Table 2: *Computational Performance.* Note that the solver CPU time does not include overhead computational costs related to data processing, model construction, and OBBT.

Case Name	Upper Bound	Lower Bound	Gap (%)	CPU Time (s)	Iteration
nesta_case3_lmbd	5812.64	5812.64	0.00	0.25	3
nesta_case5_pjm	17551.89	17536.94	0.09	50.37	16
case6ww	3143.97	3142.55	0.02	0.07	1
nesta_case6_ww	3143.97	3143.43	0.02	0.11	1
case14	8081.52	8081.10	0.01	0.10	1
nesta_case14_ieee	244.05	244.04	0.00	0.07	1
case30	576.89	576.45	0.08	33.01	6
nesta_case30_ieee	204.97	204.78	0.09	250.02	8
case39	41864.12	41862.14	0.00	2.76	1
nesta_case39_epri	96505.52	96499.21	0.01	0.72	1
case57	41737.79	41731.17	0.02	0.92	1
nesta_case57_ieee	1143.27	1143.10	0.01	0.27	1
case118	129660.69	129562.20	0.08	53.83	3
nesta_case118_ieee	3718.64	3696.81	0.59	423.13[1]	4

[1] This case failed to solve to a gap of 0.1% in the allotted time (3600s). The reported gap of 0.59% was achieved in 423 seconds.

a single iteration, due to the tight variable bounds obtained by the initial OBBT process and the strength of the SOCP-based relaxations used.

For one of the test cases, `nesta_case118_ieee`, our global approach fails to converge to the threshold gap of 0.1% within the allotted time, and terminates with an optimality gap of 0.59% after 4 outer iterations. The time reported in this table is the time to obtain the listed optimality gap. In this instance, the initial relaxation is not very strong, and the size of the lower-bounding problem (PW-ACOPF-R) grows dramatically as points are added to many of the piecewise relaxations. In future work, we will explore more targeted, adaptive refinement strategies to control this growth and increase refinement only where necessary. With the exception of the final test case, the computational times for these problems are short enough to allow global solution of the ACOPF problem in a real-time context. However, the problem sizes are still below those considered in practice, and further development of our gobal approach is necessary to ensure reliable, efficient convergence for larger systems.

Table 3 compares the computational performance of our global approach with the reported solution times for the single-pass convex relaxations from the literature. The times reported for the solution of these relaxations are taken from Kocuk et al. [40] directly, and were not run on the same computing hardware or software platform as those reported for our approach, and are therefore not directly comparable. However, all experiments are conducted on modern

Table 3: *Comparison of computational time between global approach and solution of single relaxations.*

Case Name	Global OA Approach	Single-Pass Relaxations				
		1st OA	SOCP	SOCPA	S34A	SSDP
nesta_case3_lmbd	0.25	0.03	0.02	0.13	0.31	0.21
nesta_case5_pjm	50.37	0.05	0.02	0.13	0.15	0.21
case6ww	0.07	0.07	0.06	0.26	0.32	0.46
nesta_case6_ww	0.11	0.11	0.02	0.22	0.24	0.51
case14	0.10	0.10	0.05	0.38	0.41	0.61
nesta_case14_ieee	0.07	0.07	0.02	0.45	0.48	0.67
case30	33.01	0.38	0.06	0.78	0.81	1.03
nesta_case30_ieee	250.02	0.21	0.04	0.88	1.03	1.08
case39	2.76	2.76	0.09	0.91	0.99	0.82
nesta_case39_epri	0.72	0.72	0.04	0.89	0.97	0.64
case57	0.92	0.92	0.11	1.45	1.51	1.93
nesta_case57_ieee	0.27	0.27	0.08	2.04	2.09	2.17
case118	53.83	1.21	0.30	3.64	5.12	5.04
nesta_case118_ieee	423.13[1]	1.04	0.25	4.98	5.57	5.97

[1] This case failed to solve to a gap of 0.1% in the allotted time (3600s). The reported gap of 0.59% was achieved in 423 seconds.

computing platforms, making the qualitative comparison instructive. We further reinforce that these are solve times for the solution of a single relaxation and upper-bounding problem only. Therefore, computational time between these approaches and our global approach are not directly comparable since these single-pass relaxations do not include progressive refinement to close the gap. Nevertheless, the computational timing results show that the first iteration of our OA approach (a single pass through our algorithm) is comparable to the times reported for these SOCP-based relaxations.

Of course, for challenging problems where the initial relaxation was not sufficiently tight and further iterations of the OA approach are required, the computational time of the global approach is larger than the single-pass relaxations. This shows the additional computational cost required to refine the initial relaxation and provide global solutions within the desired optimality gap.

5. Summary and Conclusions

The optimal power flow problem is a critical component in modern electricity markets where it is used to determine generator operating points and nodal electricity prices. Although linear approximations of the OPF (e.g., the so-called "DCOPF") provide improved computational performance and solver reliability over the nonlinear ACOPF formulations, these approximate formulations do

not yield globally optimal solutions to the nonlinear AC power flow system, and are not even guaranteed to be AC feasible. Similarily, linear approximations of the ACOPF seem attractive when addressing power systems operations and planning optimization problems with discrete decision variables, e.g., the unit commitment and transmission switching problems. However, such mixed-integer linear programming approximations suffer the same problems as above, yielding soluitons that may not even be AC feasible, yet alone optimal. Given the huge potential cost savings and the use of these models in market pricing, there is significant industrial and academic interest in developing fast, global solution algorithms for the ACOPF.

Current research in this area has focused mainly on the development of tight convex relaxations for the ACOPF problem. While semidefinite programming relaxations have received significant interest, exact relaxations of the ACOPF can only be guaranteed for certain network structures[40]. Furthermore the computational cost of these approaches can be quite high, and they present practical difficulties for efficient implementation within a branch-and-cut algorithm framework. In contrast, approaches based on quadratic envelopes or second-order cone relaxations[11, 12, 36, 40] are significantly more computationally efficient, even on large-scale test problems. While these approaches yield strong relaxations on many of the standard test problems, there are several standard test cases where significant optimality gaps remain, and there is a need to further refine these relaxations in the context of branch-and-bound or piecewise outer-approximation strategies.

We seek an optimization approach that can provide can provide rapid solution of NLP ACOPF problems to global optimality (i.e., close the optimality gap), while employing a strategy that is appropriate for extension to MINLP problems with many discrete variables. In this work we introduce a multitree global optimization algorithm based on piecewise outer approximation for global solution of the ACOPF problem. As an OA method, this approach alternates between solving an upper-bounding problem (the original non-convex ACOPF) and a lower-bounding problem to reduce the optimality gap.

This approach provides several important contributions. While most existing work in the area has focused on the development of tighter "single-pass" relaxations, our multitree approach for ACOPF makes use of piecewise outer approximations that can be further tightened to reduce the optimality gap beyond the initial relaxation. While tightening these relaxations introduced additional binary variables to the the problem, the iterative OA approach allows for targetted refinement to reduce the optimality gap while controlling the growth in problem size. At each iteration, we refine the domain partitioning of problem variables selectively, and perform parallel OBBT on the associated variables. The piecewise relaxations used in the lower-bounding problem are based on the successful family of second-order cone relaxations[36, 40]. In this paper, we derive piecewise outer approximations of the SOCP-based relaxations, including new expressions for piecewise outer approximations of the multivariate arctangent constraint that do not require the solution of additional optimization problems for computation of the necessary parameters.

The OA-based multitree approach developed in this paper is able to close the optimality gap to under 1% on all test problems considered and to 0.1% on all but one of the test problems within the allotted time. As shown in the numerical results, the approach is able to close the gap effectively, and even outperforms the `SSDP` relaxations on traditionally challenging test problems where significant optimality gaps remain for the single-pass relaxations. The computational time of a single iteration of our OA approach is comparable to the solution times for the single-pass relaxations, and the overall time required to solve to global optimality is under one minute for all but two of the test cases considered.

As an OA method, the approach developed in this paper does not perform spatial branching and does not need to manage a branch-and-bound tree. Rather, the responsibility of branching is pushed to the MILP solver used for the lower-bounding problem. While one must manage the growth of the problem size as further piecewise refinements are made, this approach makes use of the highly efficient, commercial MILP solvers as the primary workhorse. Because of this, the approach is directly applicable for extension from NLP problems to MINLP problems with many discrete variables like those arising in unit commitment or transmission switching with AC power flow constraints.

Future work will focus on strategies for improving the performance of our approach on larger test cases. Examples of possible strategies include heuristics for effective partitioning of variable domains (e.g., non-uniformly spaced partitions and relocating partitions) and improved bounds tightening procedures. For example, more computationally efficient feasibility-based bounds tightening techniques could be used in combination with OBBT. We will also explore alternative formulations for the piecewise relaxations and other relaxation strengthening ideas. For example, the power loss constraints used to strengthen the QC relaxation in Coffrin et al. [12] could be utilized in our approach.

Future work will also include integration of our outer approximation approach with other NLP problems involving AC power flow (e.g., contingency analysis and voltage stability) and other MINLP problems involving AC power flow (e.g., unit commitment and transmission switching).

Acknowledgements

Sandia National Laboratories is a multimission laboratory managed and operated by National Technology and Engineering Solutions of Sandia, LLC, a wholly owned subsidiary of Honeywell International, Inc., for the U.S. Department of Energy's National Nuclear Security Administration under contract DE-NA0003525.

The work of Jianfeng Liu, Carl Laird, and Jean-Paul Watson was supported in part by the U.S. Department of Energy, Office of Science, Office of Advanced Scientific Computing Research, Applied Mathematics program under contract number KJ0401000 through the project "Multifaceted Mathematics for Complex Energy Systems". The work of Michael Bynum, Anya Castillo, Carl Laird, and Jean-Paul Watson was also supported in part by Sandia National Laboratories' Laboratory Directed Research and Development (LDRD) program.

Disclaimer: This paper describes objective technical results and analysis. Any subjective views or opinions that might be expressed in the paper do not necessarily represent the views of the U.S. Department of Energy or the United States Government.

References

[1] G. Andersson. Modelling and analysis of electric power systems. Technical report, Eidgenössische Technische Hochschule Zürich, 2008.

[2] Xiaoqing Bai, Hua Wei, Katsuki Fujisawa, and Yong Wang. Semidefinite programming for optimal power flow problems. *International Journal of Electrical Power & Energy Systems*, 30(6):383–392, 2008.

[3] Pietro Belotti, Christian Kirches, Sven Leyffer, Jeff Linderoth, James Luedtke, and Ashutosh Mahajan. Mixed-integer nonlinear optimization. *Acta Numerica*, 22:1–131, 2013.

[4] Richard H. Byrd, Jorge Nocedal, and Richard A. Waltz. KNITRO: An integrated package for nonlinear optimization. In *Large Scale Nonlinear Optimization*, pages 35–59. Springer Verlag, 2006.

[5] M. B. Cain, R. P. O'Neill, and A. Castillo. Optimal power flow papers: Paper 1. History of optimal power flow and formulations. Technical report, Federal Energy Regulatory Commission, 2013.

[6] J. Carpentier. Contribution to the economic dispatch problem. *Bulletin de la Societe Francoise des Electriciens*, 3(8):431–447, 1962.

[7] A. Castillo and R. P. O'Neill. Survey of approaches to solving the ACOPF. Technical report, Federal Energy Regulatory Commission, 2013.

[8] A. Castillo and R. P. O'Neill. Computational performance of solution techniques applied to the ACOPF. Technical report, Federal Energy Regulatory Commission, 2013.

[9] Chen Chen, Alper Atamturk, and Shmuel S. Oren. A spatial branch-and-cut method for nonconvex QCQP with bounded complex variables. *https://arxiv.org/pdf/1705.09057.pdf*, 2016.

[10] Carleton Coffrin, Dan Gordon, and Paul Scott. NESTA, the NICTA energy system test case archive. *arXiv preprint arXiv:1411.0359*, 2014.

[11] Carleton Coffrin, Hassan L. Hijazi, and Pascal Van Hentenryck. Strengthening convex relaxations with bound tightening for power network optimization. In *Principles and Practice of Constraint Programming*, pages 39–57. Springer, 2015.

[12] Carleton Coffrin, Hassan L Hijazi, and Pascal Van Hentenryck. The QC relaxation: A theoretical and computational study on optimal power flow. *IEEE Transactions on Power Systems*, 31(4):3008–3018, 2016.

[13] Robert J. Dakin. A tree-search algorithm for mixed integer programming problems. *The Computer Journal*, 8(3):250–255, 1965.

[14] Lisandro Dalcin, Rodrigo Paz, and Mario Storti. MPI for Python. *Journal of Parallel and Distributed Computing*, 65(9):1108–1115, 2005.

[15] Lisandro Dalcín, Rodrigo Paz, Mario Storti, and Jorge DâĂŹElía. MPI for Python: Performance improvements and MPI-2 extensions. *Journal of Parallel and Distributed Computing*, 68(5):655–662, 2008.

[16] Lisandro D Dalcin, Rodrigo R Paz, Pablo A Kler, and Alejandro Cosimo. Parallel distributed computing using Python. *Advances in Water Resources*, 34(9):1124–1139, 2011.

[17] Arne. Drud. CONOPT: A GRG code for large sparse dynamic nonlinear optimization problems. *Mathematical Programming*, 31(2):153–191, 1985.

[18] Marco A. Duran and Ignacio E. Grossmann. An outer-approximation algorithm for a class of mixed-integer nonlinear programs. *Mathematical programming*, 36(3):307–339, 1986.

[19] Thomas GW Epperly and Efstratios N. Pistikopoulos. A reduced space branch and bound algorithm for global optimization. *Journal of Global Optimization*, 11(3):287–311, 1997.

[20] Michael C. Ferris, Zev Friedman, Daniel Molzahn, Chris DeMarco, and Bernie Lesieutre. Optimal power flow, 2013. URL `https://neos-guide.org/content/optimal-power-flow`.

[21] Roger Fletcher and Sven Leyffer. Solving mixed integer nonlinear programs by outer approximation. *Mathematical programming*, 66(1):327–349, 1994.

[22] Robert Fourer, David M. Gay, and Brian W. Kernighan. AMPL, 1993.

[23] S. Frank, I. Steponavice, and S. Rebennack. Optimal power flow: A bibliographic survey I. *Energy Syst.*, 3:221–258, 2012.

[24] S. Frank, I. Steponavice, and S. Rebennack. Optimal power flow: A bibliographic survey II. *Energy Syst.*, 3:259–289, 2012.

[25] Björn Geißler, Alexander Martin, Antonio Morsi, and Lars Schewe. Using piecewise linear functions for solving MINLPs. In *Mixed Integer Nonlinear Programming*, pages 287–314. Springer, 2012.

[26] Bissan Ghaddar, Jakub Marecek, and Martin Mevissen. Optimal power flow as a polynomial optimization problem. *IEEE Transactions on Power Systems*, 31(1):539–546, 2016.

[27] Philip E. Gill, Walter Murray, and Michael A. Saunders. SNOPT: An SQP algorithm for large-scale constrained optimization, 2002.

[28] Ambros M Gleixner, Timo Berthold, Benjamin Müller, Stefan Weltge, et al. Three enhancements for optimization-based bound tightening. *J. Global Optimization*, 67(4):731–757, 2017.

[29] Chrysanthos E. Gounaris, Ruth Misener, and Christodoulos A. Floudas. Computational comparison of piecewise- linear relaxations for pooling problems. *Industrial & Engineering Chemistry Research*, 48(12):5742–5766, 2009.

[30] William E Hart, Jean-Paul Watson, and David L Woodruff. Pyomo: Modeling and solving mathematical programs in Python. *Mathematical Programming Computation*, 3(3):219–260, 2011.

[31] William E Hart, Carl Laird, Jean-Paul Watson, and David L. Woodruff. *Pyomo–Optimization Modeling in Python, Second Edition*, volume 67 of *Springer Optimization and Its Applications (Book 67)*. Springer Science & Business Media; 2nd ed. 2017 edition (May 27, 2017), 2017.

[32] M. M. Hasan and I. A. Karimi. Piecewise linear relaxation of bilinear programs using bivariate partitioning. *AIChE journal*, 56(7):1880–1893, 2010.

[33] HSL. A collection of Fortran codes for large scale scientific computation http://www.hsl.rl.ac.uk/, 2013.

[34] Shaojun Huang, Qiuwei Wu, Jianhui Wang, and Haoran Zhao. A sufficient condition on convex relaxation of AC optimal power flow in distribution networks. *IEEE Transactions on Power Systems*, 32(2):1359–1368, 2017.

[35] M. Huneault and F. D. Galiana. A survey of the optimal power flow literature. *IEEE Trans. Power Syst.*, 6(2):762–770, 1991.

[36] Rabih A. Jabr. Radial distribution load flow using conic programming. *IEEE Transactions on Power Systems*, 21(3):1458–1459, 2006.

[37] Cédric Josz, Jean Maeght, Patrick Panciatici, and Jean Charles Gilbert. Application of the moment-sos approach to global optimization of the opf problem. *IEEE Transactions on Power Systems*, 30(1):463–470, 2015.

[38] Padmanaban Kesavan and Paul I. Barton. Generalized branch-and-cut framework for mixed-integer nonlinear optimization problems. *Computers & Chemical Engineering*, 24(2):1361–1366, 2000.

[39] Polyxeni-Margarita Kleniati and Claire S. Adjiman. Branch-and-sandwich: A deterministic global optimization algorithm for optimistic bilevel programming problems. part i: Theoretical development. *Journal of Global Optimization*, pages 1–34, 2014.

[40] Burak Kocuk, Santanu S Dey, and X Andy Sun. Strong SOCP relaxations for the optimal power flow problem. *Operations Research*, 64(6):1177–1196, 2016.

[41] Burak Kocuk, Santanu S. Dey, and Xu Andy Sun. Inexactness of SDP relaxation and valid inequalities for optimal power flow. *IEEE Transactions on Power Systems*, 31(1):642–651, 2016.

[42] Xiaolong Kuang, Luis F. Zuluaga, Bissan Ghaddar, and Joe Naoum-Sawaya. Approximating the ACOPF problem with a hierarchy of SOCP problems. In *IEEE PES General Meeting*, pages 1–5. IEEE, 2015.

[43] Xiaolong Kuang, Bissan Ghaddar, Joe Naoum-Sawaya, and Luis F. Zuluaga. Alternative LP and SOCP hierarchies for ACOPF problems. *IEEE Transactions on Power Systems*, 32(4):2828–2836, 2016.

[44] Chris Kuip. The modeling system aimms for developing mathematical programming and constraint programming applications., 2013.

[45] Ailsa H. Land and Alison G. Doig. An automatic method of solving discrete programming problems. *Econometrica: Journal of the Econometric Society*, pages 497–520, 1960.

[46] J. B. Lasserre. A global optimization with polynomials and the problem of moments. *SIAM J. Optimiz.*, 11(3):796–817, 2001.

[47] Javad Lavaei and Steven H. Low. Zero duality gap in optimal power flow problem. *IEEE Transactions on Power Systems*, 27(1):92–107, 2012.

[48] Javad Lavaei, David Tse, and Baosen Zhang. Geometry of power flows and optimization in distribution networks. *IEEE Transactions on Power Systems*, 29(2):572–583, 2014.

[49] K. Lehmann, A. Grastien, and P. Van Hentenryck. AC-feasibility on tree networks is NP-hard. *IEEE Trans. on Power Syst.*, PP(99):1–4, 2015.

[50] S. H. Low. Convex relaxation of optimal power flow, part I: Formulations and equivalence. *IEEE Trans. Control Netw. Syst.*, 1(1):15–27, 2014.

[51] S. H. Low. Convex relaxation of optimal power flow, part II: Exactness. *IEEE Trans. Control Netw. Syst.*, 1(2):177–189, 2014.

[52] Ramtin Madani, Samira Sojoudi, and Javad Lavaei. Convex relaxation for optimal power flow problem: Mesh networks. *IEEE Transactions on Power Systems*, 30(1):199–211, 2015.

[53] Ramtin Madani, Morteza Ashraphijuo, and Javad Lavaei. Promises of conic relaxation for contingency-constrained optimal power flow problem. *IEEE Transactions on Power Systems*, 31(2):1297–1307, 2016.

[54] A. Mahajan, S. Leyffer, J. Linderoth, J. Luedtke, and T. Munson. MINOTAUR: A Toolkit for Solving Mixed-Integer Nonlinear Optimization. *Wikipage http://wiki. mcs. anl. gov/minotaur*, 2011.

[55] G. P. McCormick. Computability of Gloabl Solutions to Factorable Nonconvex Programs: Part I-Convex Underestimating Problems. *Mathematical programming*, 10:147–175, 1976.

[56] Ruth Misener and Christodoulos A. Floudas. Global Optimization of Mixed-Integer Quadratically-Constrained Quadratic Programs (MIQCQP) through Piecewise-Linear and Edge-Concave Relaxations. *Mathematical programming*, 136(1):155–182, 2012.

[57] Daniel K. Molzahn and Ian A. Hiskens. Moment-based relaxation of the optimal power flow problem. In *18th Power Syst. Comput. Conf. (PSCC)*, pages 18–22. IEEE, 2014.

[58] Daniel K. Molzahn and Ian A. Hiskens. Sparsity-exploiting moment-based relaxations of the optimal power flow problem. *IEEE Transactions on Power Systems*, 30(6):3168–3180, 2015.

[59] Daniel K. Molzahn, Jesse T. Holzer, Bernard C. Lesieutre, and Christopher L. DeMarco. Implementation of a large-scale optimal power flow solver based on semidefinite programming. *IEEE Transactions on Power Systems*, 28(4):3987–3998, 2013.

[60] J.A. Momoh, M.E. El-Hawary, and R. Adapa. A review of selected optimal power flow literature to 1993. part I: Nonlinear and quadratic programming approachs. *IEEE Trans. Power Syst.*, 14(1):96–104, 1999.

[61] J.A. Momoh, M.E. El-Hawary, and R. Adapa. A review of selected optimal power flow literature to 1993. part II: Newton, linear programming, and interior point methods. *IEEE Trans. Power Syst.*, 14(1):105–111, 1999.

[62] Bruce A. Murtagh and Michael A. Saunders. MINOS 5.5 user's guide. In *Technical Report SOL 83-20R*, pages 1–145. Stanford University, 1983.

[63] Gurobi Optimization and Others. Gurobi optimizer reference manual. *URL: http://www. gurobi. com*, 2012.

[64] D. T. Phan. Lagrangian duality and branch-and-bound algorithms for optimal power flow. *Operations Research*, 60(2):275–285, 2012.

[65] E Rosenthal. Gams-a userâĂŹs guide. In *GAMS Development Corporation*, pages –. Citeseer, 2008.

[66] Hong S. Ryoo and Nikolaos V. Sahinidis. Global Optimization of Nonconvex NLPs and MINLPs with Applications in Process Design. *Computers & Chemical Engineering*, 19(5):551–566, 1995.

[67] Hong S. Ryoo and Nikolaos V. Sahinidis. A branch-and-reduce approach to global optimization. *Journal of Global Optimization*, 8(2):107–138, 1996.

[68] Nikolaos V. Sahinidis. BARON: A General Purpose Global Optimization Software Package. *Journal of Global Optimization*, 8(2):201–205, 1996.

[69] Samira Sojoudi and Javad Lavaei. Physics of power networks makes hard optimization problems easy to solve. In *Power and Energy Society General Meeting, 2012 IEEE*, pages 1–8. IEEE, 2012.

[70] Mohit Tawarmalani and Nikolaos V Sahinidis. *Convexification and global optimization in continuous and mixed-integer nonlinear programming: theory, algorithms, software, and applications*, volume 65. Springer, 2002.

[71] A. Verma. *Power Grid Security Analysis: An Optimization Approach*. PhD thesis, Columbia University, 2009.

[72] Juan Pablo Vielma, Shabbir Ahmed, and George Nemhauser. Mixed-integer models for nonseparable piecewise-linear optimization: Unifying framework and extensions. *Operations research*, 58(2):303–315, 2010.

[73] Andreas Wächter and Lorenz T. Biegler. On the implementation of an interior-point filter line-search algorithm for large-scale nonlinear programming. *Mathematical programming*, 106(1):25–57, 2006.

[74] Danan Suryo Wicaksono and I. A. Karimi. Piecewise milp under-and over-estimators for global optimization of bilinear programs. *AIChE Journal*, 54(4):991–1008, 2008.

[75] Juan M. Zamora and Ignacio E. Grossmann. A branch and contract algorithm for problems with concave univariate, bilinear and linear fractional terms. *Journal of Global Optimization*, 14(3):217–249, 1999.

[76] Ray Daniel Zimmerman, Carlos Edmundo Murillo-Sánchez, and Robert John Thomas. MATPOWER: Steady-state operations, planning, and analysis tools for power systems research and education. *IEEE Transactions on Power Systems*, 26(1):12–19, 2011.

Appendix A. Parameters for Actan Over- and Under-Estimators

If $s^L_{b,k} \geq 0$, we have

$$
\begin{aligned}
\alpha^u_1 &= \frac{\arctan\left(\frac{s^U_{b,k}}{c^L_{b,k}}\right) - \arctan\left(\frac{s^L_{b,k}}{c^L_{b,k}}\right)}{s^U_{b,k} - s^L_{b,k}} \\
\alpha^u_2 &= \frac{\arctan\left(\frac{s^U_{b,k}}{c^U_{b,k}}\right) - \arctan\left(\frac{s^L_{b,k}}{c^U_{b,k}}\right)}{s^U_{b,k} - s^L_{b,k}} \\
\alpha^o_1 &= \frac{c^U_{b,k}}{\left(s^U_{b,k}\right)^2 + \left(c^U_{b,k}\right)^2} \\
\alpha^o_2 &= \frac{c^L_{b,k}}{\left(s^L_{b,k}\right)^2 + \left(c^L_{b,k}\right)^2} \\
\beta^u_1 &= \frac{-s^U_{b,k}}{\left(s^U_{b,k}\right)^2 + \left(c^L_{b,k}\right)^2} \\
\beta^u_2 &= \frac{-s^L_{b,k}}{\left(s^L_{b,k}\right)^2 + \left(c^U_{b,k}\right)^2} \\
\beta^o_1 &= \frac{\arctan\left(\frac{s^U_{b,k}}{c^U_{b,k}}\right) - \arctan\left(\frac{s^U_{b,k}}{c^L_{b,k}}\right)}{c^U_{b,k} - c^L_{b,k}} \\
\beta^o_2 &= \frac{\arctan\left(\frac{s^U_{b,k}}{c^U_{b,k}}\right) - \arctan\left(\frac{s^L_{b,k}}{c^L_{b,k}}\right)}{c^U_{b,k} - c^L_{b,k}}
\end{aligned}
\tag{A.1}
$$

and γ can be calculated from corresponding α and β.

If $s^U_{b,k} \leq 0$, we have

$$
\begin{aligned}
\alpha^u_1 &= \frac{c^L_{b,k}}{\left(s^U_{b,k}\right)^2 + \left(c^L_{b,k}\right)^2} \\
\alpha^u_2 &= \frac{c^U_{b,k}}{\left(s^L_{b,k}\right)^2 + \left(c^U_{b,k}\right)^2} \\
\alpha^o_1 &= \frac{\arctan\left(\frac{s^U_{b,k}}{c^U_{b,k}}\right) - \arctan\left(\frac{s^U_{b,k}}{c^L_{b,k}}\right)}{c^U_{b,k} - c^L_{b,k}} \\
\alpha^o_2 &= \frac{\arctan\left(\frac{s^L_{b,k}}{c^U_{b,k}}\right) - \arctan\left(\frac{s^L_{b,k}}{c^L_{b,k}}\right)}{c^U_{b,k} - c^L_{b,k}} \\
\beta^u_1 &= \frac{\arctan\left(\frac{s^U_{b,k}}{c^U_{b,k}}\right) - \arctan\left(\frac{s^L_{b,k}}{c^U_{b,k}}\right)}{s^U_{b,k} - s^L_{b,k}} \\
\beta^u_2 &= \frac{\arctan\left(\frac{s^U_{b,k}}{c^L_{b,k}}\right) - \arctan\left(\frac{s^L_{b,k}}{c^L_{b,k}}\right)}{s^U_{b,k} - s^L_{b,k}} \\
\beta^o_1 &= \frac{-s^U_{b,k}}{\left(s^U_{b,k}\right)^2 + \left(c^U_{b,k}\right)^2} \\
\beta^o_2 &= \frac{-s^L_{b,k}}{\left(s^L_{b,k}\right)^2 + \left(c^L_{b,k}\right)^2}
\end{aligned}
\tag{A.2}
$$

If $s^U_{b,k} \geq 0$ and $s^L_{b,k} \leq 0$, we have

$$
\begin{aligned}
\alpha^u_1 &= \frac{\arctan\left(\frac{s^U_{b,k}}{c^L_{b,k}}\right) - \arctan\left(\frac{s^L_u}{c^L_{b,k}}\right)}{s^U_{b,k} - s^L_u} \\
\alpha^u_2 &= \frac{\arctan\left(\frac{s^U_u}{c^U_{b,k}}\right) - \arctan\left(\frac{s^L_{b,k}}{c^U_{b,k}}\right)}{s^U_u - s^L_{b,k}} \\
\alpha^o_1 &= \frac{\arctan\left(\frac{s^U_{b,k}}{c^U_{b,k}}\right) - \arctan\left(\frac{s^L_o}{c^U_{b,k}}\right)}{s^U_{b,k} - s^L_o} \\
\alpha^o_2 &= \frac{\arctan\left(\frac{s^U_o}{c^L_{b,k}}\right) - \arctan\left(\frac{s^L_{b,k}}{c^L_{b,k}}\right)}{s^U_o - s^L_{b,k}} \\
\beta^u_1 &= \frac{-s^U_{b,k}}{\left(s^U_{b,k}\right)^2 + \left(c^L_{b,k}\right)^2} \\
\beta^u_2 &= \frac{\arctan\left(\frac{s^L_{b,k}}{c^U_{b,k}}\right) - \arctan\left(\frac{s^L_{b,k}}{c^L_{b,k}}\right)}{c^U_{b,k} - c^L_{b,k}} \\
\beta^o_1 &= \frac{\arctan\left(\frac{s^U_{b,k}}{c^U_{b,k}}\right) - \arctan\left(\frac{s^U_{b,k}}{c^L_{b,k}}\right)}{c^U_{b,k} - c^L_{b,k}} \\
\beta^o_2 &= \frac{-s^L_{b,k}}{\left(s^L_{b,k}\right)^2 + \left(c^L_{b,k}\right)^2}
\end{aligned}
\tag{A.3}
$$

where $s^L_u = \max(s^L_{b,k}, x^*)$ and x^* is the solution of

$$
\frac{\arctan\left(\frac{s^U_{b,k}}{c^L_{b,k}}\right) - \arctan\left(\frac{x}{c^L_{b,k}}\right)}{s^U_{b,k} - x} - \frac{c^L_{b,k}}{x^2 + \left(c^L_{b,k}\right)^2} = 0
$$

$s^U_u = \max(s^U_{b,k}, x^*)$ and x^* is the solution of

$$
\frac{\arctan\left(\frac{x}{c^U_{b,k}}\right) - \arctan\left(\frac{s^L_{b,k}}{c^L_{b,k}}\right)}{x - s^L_{b,k}} - \frac{c^U_{b,k}}{\left(s^L_{b,k}\right)^2 + \left(c^U_{b,k}\right)^2} = 0
$$

$s_o^L = \min(s_{b,k}^L, x^*)$ and x^* is the solution of

$$\frac{\arctan\left(\frac{s_{b,k}^U}{c_{b,k}^U}\right) - \arctan\left(\frac{x}{c_{b,k}^U}\right)}{s_{b,k}^U - x} - \frac{c_{b,k}^U}{\left(s_{b,k}^U\right)^2 + \left(c_{b,k}^U\right)^2} = 0$$

$s_o^U = \min(s_{b,k}^U, x^*)$ and x^* is the solution of

$$\frac{\arctan\left(\frac{x}{c_{b,k}^L}\right) - \arctan\left(\frac{s_{b,k}^L}{c_{b,k}^L}\right)}{x - s_{b,k}^L} - \frac{c_{b,k}^L}{x^2 + \left(c_{b,k}^L\right)^2} = 0$$

Appendix B. AC Network Characteristics

Assuming balanced three-phase, steady-state conditions, we can model each branch of the AC network with the generalized π-model as shown in Figure B.2. The series admittance $y_l = g_l + \mathbf{j}b_l$ is equivalent to the inverse of the branch impedance z_l where the series conductance g_l and series susceptance b_l are determined as:

$$g_l = r_l \Big/ \left(r_l^2 + x_l^2\right), \tag{B.1}$$

$$b_l = -x_l \Big/ \left(r_l^2 + x_l^2\right) \tag{B.2}$$

for all transmission branches $l \in \mathcal{L}$. Actual transmission lines that are medium and long distance overhead lines or underground cables can have significant charging currents due to the separation of the conductive material by an insulating medium; as a result there is an effective capacitance between the conductors and potentially a conductance, which is the result of leakage over the surface of the insulating medium. These line characteristics are accounted for with a shunt component $y_l^s = g_l^s + \mathbf{j}b_l^s$ to represent the shunt susceptance b_l^s (i.e., the reactive capacitance) and the shunt conductance g_l^s. This line shunt is incorporated into the generalized π-model as two equal shunt elements $y_{l,b}^s$ and $y_{l,k}^s$ distributed at each end of line l, assuming homogeneous line parameters along the length of l. Typically the shunt conductance is negligible, which leads to the assumption that only the shunt susceptance is nonnegative, i.e., $g_{l,b}^s = g_{l,k}^s = 0$ and $b_{l,b}^s, b_{l,k}^s \geq 0$.

The π-model can be generalized to incorporate an in-phase or phase-shifting transformer at either the bus b-side or the k-side of branch l; therefore the generalized π-model is defined for each branch $l \in \mathcal{L}$ interconnecting buses b and k where $k \in \mathcal{B}_b$ and $b \in \mathcal{B}_k$. A practical transformer that is located on the bus b-side of l can be modeled as an ideal transformer with turns ratio $\tau_{l,b}$ in series with admittance y_l, in order to characterize the resistive losses and leakage flux (i.e., self-resistance). Depending on if $\tilde{\tau}_{l,b}$ is real or complex, the transformer is in-phase or phase-shifting. If in-phase on the bus b-side of l, then

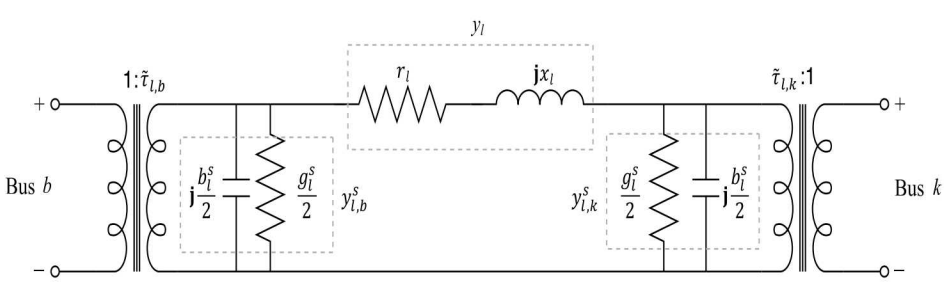

Figure B.2: The generalized π-model diagram for branch l.

$\tilde{\tau}_{l,b} = \tau_{l,b}$; otherwise for a phase-shift of $\phi_{l,b}$ radians, then $\tilde{\tau}_{l,b} = \tau_{l,b}e^{\mathbf{j}\phi_{l,b}} = \tau_{l,b}\cos\phi_{l,b} + \mathbf{j}\tau_{l,b}\sin\phi_{l,b}$ (by Euler's formula). Therefore the generalized branch (primitive) admittance matrix [1] for a π-model for a line or transformer is defined as

$$Y_l = \begin{bmatrix} Y_l^{ff} & Y_l^{ft} \\ Y_l^{tf} & Y_l^{tt} \end{bmatrix} := \begin{bmatrix} \tau_{l,b}^2\left(y_l + y_{l,b}^s\right) & -\tilde{\tau}_{l,b}{*}\tilde{\tau}_{l,k}y_l \\ -\tilde{\tau}_{l,b}\tilde{\tau}_{l,k}^{*}y_l & \tau_{l,k}^2\left(y_l + y_{l,k}^s\right) \end{bmatrix} \tag{B.3}$$

for all $l \in \mathcal{L}$ where $Y_l = G_l + \boldsymbol{j}B_l$. Note that for modeling a transmission line, $\tau_{l,b} = \tau_{l,k} = 1$ and $\phi_{l,b} = \phi_{l,k} = 0$; for an in-phase transformer on the b-side of l, then $y_{l,b}^s = y_{l,k}^s = 0$, $\tau_{l,k} = 1$, and $\phi_{l,b} = \phi_{l,k} = 0$; and for a phase-shifting transformer on the b-side of l, then $y_{l,b}^s = y_{l,k}^s = 0$, $\tau_{l,k} = 1$, and $\phi_{l,k} = 0$. Furthermore, the above representation models a two-winding transformer; generally for a P-winding ($P > 1$) transformer at branch l, the Y_l matrix would be of size $P \times P$.

1.5. A global stochastic programming approach for the optimal placement of gas detectors with nonuniform unavailabilities

A Global Stochastic Programming Approach for the Optimal Placement of Gas Detectors with Nonuniform Unavailabilities

Jianfeng Liu[1], Carl D. Laird[2]

Abstract

Optimal design of a gas detection systems is challenging because of the numerous sources of uncertainty, including weather and environmental conditions, leak location and characteristics, and process conditions. Rigorous CFD simulations of dispersion scenarios combined with stochastic programming techniques have been successfully applied to the problem of optimal gas detector placement; however, rigorous treatment of sensor failure and nonuniform unavailability has received less attention. To improve reliability of the design, this paper proposes a problem formulation that explicitly considers nonuniform unavailabilities and all backup detection levels. The resulting sensor placement problem is a large-scale mixed-integer nonlinear programming (MINLP) problem that requires a tailored solution approach for efficient solution. We have developed a multitree method which depends on iteratively solving a sequence of upper-bounding master problems and lower-bounding subproblems. The tailored global solution strategy is tested on a real data problem and the encouraging numerical results indicate that our solution framework is promising in solving sensor placement problems. This paper was selected for the special issue in JLPPI from the 2016 International Symposium of the MKO Process Safety Center.

1 Introduction

To rapidly detect release events and minimize the corresponding damages, efficient detection and mitigation depends on appropriate design of the gas detector system, including type, number, and placement of sensors. However, the optimal design of these systems is very challenging because significant uncertainty must be taken into account, including weather and environmental conditions, leak location and characteristics, and process conditions. Prescriptive or semi-quantitative approaches have been widely used in detector system design [15,17,22]; however, these heuristic techniques do not make full use of the information from dispersion simulations and fail to provide a rigorous proof of the solution quality.

A number of stochastic programming (SP) approaches have been proposed and implemented to solve various real-world sensor placement problems [1,5,6,19,20]. Most of these previously proposed SP formulations have assumed perfect sensors. In reality, however, detectors are imperfect and subject to unpredictable failures caused by, for example, poor maintenance, erroneous calibration, or power outage. In many practical cases, these imperfections can significantly impact the performance of the entire detector system. To improve the reliability of the optimal design, therefore, it is important and necessary to explicitly consider sensor

[1] Ph.D. Candidate, School of Chemical Engineering, Purdue University
[2] Assoc. Professor, School of Chemical Engineering, Purdue University; PMTS, Discrete Mathematics and Optimization, Sandia National Laboratories

imperfection, which is measured in terms of unavailability, i.e., the probability of a false-negative detection. Berry et al. [5] first proposed an SP-based imperfect-sensor model for the contamination warning system design in water networks. Inspired by this research, Benavides-Serrano et al. [1,3] presented SP formulations for flammable gas detection and mitigation systems considering sensor unavailabilities. However, the resulting sensor placement problems, formulated as large-scale mixed-integer nonlinear programming (MINLP) problems, are very challenging to solve due to the presence of nonlinearities and discrete variables. To solve these problems efficiently, Benavides-Serrano et al. [3] approximated the MINLP as a mixed-integer quadratic programming problem (MIQP) by considering only one or two levels of redundancy. In this paper, we provide a rigorous problem formulation and solution approach for optimal sensor placement that does not require this approximation.

Sensor placement problems considering nonuniform unavailabilities are formulated as MINLP problems. Two major categories of solution techniques have been used to solve MINLP problems. Stochastic approaches, such as random search, simulated annealing, and genetic algorithms, can be easily implemented, however, none of these algorithms can provide a guarantee of the solution optimality. Deterministic methods, in contrast, are able to provide a rigorous mathematical guarantee of global optimality. The single-tree deterministic algorithms, such as the well-known branch-and-bound (BB) methods [7,18], have been well-studied and intensively extended to a variety of global optimization algorithms, such as Branch-and-Reduce [25], Reduced Space Branch-and-Bound [9], Branch-and-Contract [30], Branch-and-Cut [14] and Branch-and-Sandwich [16]. In general, these techniques are suitable for non-convex MINLP problems of small or medium size. Alternatively, multitree methods are based on iteratively solving a sequence of master problems and slave problems (or subproblems) [8,29]. To handle `non-convex' MINLP problems with certain special features, e.g., bilinear, posynomial, linear fractional, and concave separable, extensions of these well-studied multitree methods can be found in literature [23,24].

The proposed global optimization algorithm is regarded as a multitree method, since it is an iterative algorithm relying on solutions of a sequence of mixed-integer master problems and nonlinear subproblems. The master problem, which formulated as a mixed-integer linear programming (MILP) problem, is a strict relaxation of the MINLP problem formulation. To obtain a relatively tight and computationally efficient master problem, we introduce linear outer approximations and tight, problem specific, upper bounding constraints. The upper bounding subproblem is obtained by fixing all binary variables, which, in this case, results in a subproblem that can be directly computed with a single forward simulation. In this way, iterations cycle between the solution of the master problem and the subproblem, generating a sequence of lower and upper bounds. The global algorithm terminates when the relative optimality gap is below a given tolerance.

The rest of this paper is organized as follows. In Section 2, we briefly review mathematical models for sensor placement problems. Section 3 presents our new problem formulation based on the log-transformation of the original problem formulation from [5]. Section 4 outlines our tailored global solution framework and master problems formulated as mixed-integer linear programming problems. Sections 5 shows numerical results on a real data test problem and Section 6 provides summary and conclusions.

2 Background

In this section, we provide a brief review of the literature on optimal sensor placement. The sensor placement problem can be regarded as a special case of the p-median problem (PMP). In a PMP, we want to locate p facilities to minimize the weighted average distance between the demand nodes and the nearest of the selected facilities [12]. The optimal sensor placement problem assuming perfect sensors is equivalent to a classic PMP, and well-known solution strategies designed for PMPs can be directly implemented, including heuristic and greedy algorithms. However, most of these strategies may fail to guarantee high solution quality. The stochastic programming (SP) approach, on the other hand, provides an alternative way to solve for a PMP. Particularly, the first SP formulation for sensor placement problem in water network systems was proposed by Berry et al. [6]. With the assumption of perfect sensors, the resulting optimization problem is formulated as an MILP problem, which can be solved by general mixed-integer solvers.

Detectors are, however, imperfect and subject to unpredictable failures. In many cases, these imperfections can significantly impact the performance of the entire detector system. To improve the reliability of the entire detection system, therefore, it is necessary to explicitly consider sensor unavailability, i.e., the probability of a false-negative detection. A number of extensions to the original PMPs have been proposed to handle facility unavailabilities. For instance, Snyder and Daskin [26] presented the reliability PMP (RPMP) based on the assumption of uniform unavailabilites. In this approach, the probability products are modeled via the binomial distribution, which leads to an MILP problem. The median problem with unreliable facilities (MPUF) is proposed by Berman et al. [4], where the unvailabilities are assumed to be uniform and the detection levels are limited to a given number. For a comprehensive review of the unavailability considerations into the PMPs please refer to Benavides-Serrano et al [1] and Snyder et al. [27].

In the context of stochastic programming approaches, the first imperfect-sensor model is presented by Berry et al. [5]. This model, though originally proposed to design the contaminant warning systems in water networks, is general and well-suited for any sensor placement problem considering unavailabilities. However, the resulting MINLP problem is very difficult to solve due to strong nonlinearities. To partially address this challenge, previous work has assumed uniform unavailability across all sensors in the network [1]. However, this assumption is not always reasonable since the probability of sensor failure usually depends on the detector type, maintenance condition, and environment. An alternative approach was recently proposed by Benavides-Serrano et al. [3] based on reducing the number of detection levels while maintaining nonuniform unavailabilities. Sensitivity analysis has shown that for small-to-moderate unavailabilities we only need to consider a small number of detection levels. While effective under these assumptions, it is worthwhile to point out that these SP formulations are approximations of the original sensor placement problem. As a result, none of these approaches can provide a rigorous guarantee of solution quality to the original MINLP problem. Moreover, to the best of our knowledge, there exists no solution framework that is designed to solve a general sensor placement problem with nonuniform unavailabilites to global optimality. In this paper, we extend previous problem formulations and present a multitree solution strategy based on tailored relaxations of the MINLP problem.

3 Stochastic Programming Formulations and Solution Approach

The imperfect-sensor SP model, labeled *impSP*, was originally proposed by Berry et al. [5] to design contaminate warning systems for water networks.

$$
\begin{aligned}
\min \quad & \sum_{a \in A} \alpha_a \sum_{i \in L_a} d_{a,i} x_{a,i} \\
s.t. \quad & \sum_{i \in L_a} x_{a,i} = 1 && \forall a \in A \\
& x_{a,i} = (1 - \bar{q}_i) s_i \prod_{j \in L_{a,i}} \left(1 - (1 - \bar{q}_j) s_j\right) && \forall a \in A, i \in L_a \backslash \{D\} \\
& \sum_{i \in L \backslash \{D\}} s_i \leq p \\
& 0 \leq x_{a,i} \leq 1 && \forall a \in A, i \in L_a \\
& s_i \in \{0,1\} && \forall i \in L
\end{aligned}
\qquad (impSP)
$$

The complete list of symbols for this problem formulation are described in Table 1. Here, A represents the set of hazardous scenarios, and L represents the set of all candidate detector locations. The goal is to select a sensor placement that minimizes the expected value of the damage across all the scenarios. The parameter α_a is the probability (or weight) of scenario a, which is obtained from the scenario distribution based on the historical data or computer-aided simulations. Parameter $d_{a,i}$ is the damage coefficient, which, for these studies, is the detection time of scenario a at location i. Typically, and in this study, these damage coefficients are estimated from computational fluid dynamics (CFD) simulations. Further description of this problem formulation can be found in Benavides-Serrano et al [3] and Berry et al. [5].

Table 1: Notation

Sets	
$\boldsymbol{A}$	Set of hazardous scenarios
$\boldsymbol{L}$	Set of candidate detector locations
$\boldsymbol{L_a}$	Set of locations that can detect scenario a
$\boldsymbol{L_{a,i}}$	Set of locations that witness scenario a better (in terms of damage) than i
Parameters	
$\boldsymbol{\alpha_a}$	Probability of scenario a
$\boldsymbol{d_{a,i}}$	Damage coefficient for scenario a if detected by location i
$\boldsymbol{\bar{q}_i}$	Time-averaged unavailability for detector placed at location i
$\boldsymbol{p}$	Maximum number of detectors allowed
Variables	
$\boldsymbol{x_{a,i}}$	Probability that a detector at location i is the first to detect scenario a
$\boldsymbol{\tilde{x}_{a,i}}$, $\boldsymbol{\bar{x}_{a,i}}$	Intermediate variables in our alternate formulation
$\boldsymbol{s_i}$	Binary variable equal to 1 if a detector is placed at location i, and zero otherwise
$\boldsymbol{z_{i,j}}$	Aggregated variable equal to $s_i s_j$ for $i \neq j$

The continuous variable $x_{a,i}$ is the probability that the detector placed at location i will be the first to detect hazardous scenario a. The binary variable s_i is an indicator for a detector placed at location i. If a detector is installed at location i then $s_i = 1$, and otherwise $s_i = 0$. Subset $L_a \subseteq L$ is the set of candidate locations that can provide detection of hazardous scenario a. For a particular scenario, however, it is possible that no candidate location can provide detection, therefore, a dummy location D is also included with a sufficiently large damage coefficient, to account for the impact of an undetected scenario. Subset $L_{a,i}$ is the set of candidate locations that can witness scenario a better (in terms of detection time or another damage metric) than location i. In other words, for $\forall j \in L_{a,i}$ we have $d_{a,j} < d_{a,i}$.

The first constraint in (*impSP*) guarantees that the summation of the probabilities equals 1 for each scenario (recall that a dummy detector is included). For each non-dummy location, the second constraint provides the expression for the probability $x_{a,i}$, where $\bar{q}_i$ is the given time-averaged unavailability of a detector placed at location i. This probability constraint is strongly nonlinear due to the product of the binary variables. Note that, due to the first constraint, the probability of detection by the dummy location, $x_{a,D}$, also provides the probability that all detectors fail to report a hazardous scenario. The third constraint provides an upper bound of the total number of detectors that can be allocated in the system (not including the dummy detector).

3.1 Alternative MINLP Formulation

The original formulation (*impSP*) is strongly nonlinear due to the multiplication of binary variables in the relationship for probability $x_{a,i}$. We propose an alternative formulation, which is mathematically equivalent to the original formulation, based on the log-transformation of the probability equation.

First, we define a new binary variable $z_{i,j}$ as,

$$z_{i,j} \equiv s_i s_j \qquad \forall i,j \in L, i \neq j$$

Note that $z_{i,j}$ indicates if gas detectors are placed at both location i and location j. That is $z_{i,j} = 1$ if and only if both $s_i = 1$ and $s_j = 1$. This logic relationship can be expressed in terms of a set of linear inequalities

$$\begin{aligned} s_i + s_j - 1 &\leq z_{i,j} && \forall i,j \in L, i \neq j \\ z_{i,j} &\leq s_i && \forall i,j \in L, i \neq j \\ z_{i,j} &\leq s_j && \forall i,j \in L, i \neq j \end{aligned} \tag{1}$$

Fortunately, given the fact that s_i is a binary variable, imposing these constraints guarantees that $z_{i,j}$ solves to a binary value, and it can be relaxed as a continuous variable within the range of 0 to 1.

The nonlinear probability constraint in the original formulation (*impSP*) can be rewritten as

$$x_{a,i} = (1-\bar{q}_i)s_i \prod_{j \in L_{a,i}} \left(1 - (1-\bar{q}_j)s_j\right)$$

$$= (1-\bar{q}_i)^{s_i} \prod_{j \in L_{a,i}} \bar{q}_j^{z_{i,j}} + s_i - 1$$

Here we introduce a new variable defined as

$$\bar{x}_{a,i} = \ (1-\bar{q}_i)^{s_i} \prod_{j \in L_{a,i}} \bar{q}_j^{z_{i,j}}$$

and the log-transformation of variable $\bar{x}_{a,i}$ is a linear equality constraint

$$\tilde{x}_{a,i} = s_i \ln(1-\bar{q}_i) + \textstyle\sum_{j \in L_{a,i}} z_{i,j} \ln(\bar{q}_j) \qquad \forall a \in A, i \in L_a \backslash \{D\} \tag{2}$$

Therefore, the original nonlinear probability constraints can be replaced by a set of new constraints and variables

$$\begin{aligned} &\bar{x}_{a,i} = \exp\left(\tilde{x}_{a,i}\right) && \forall a \in A, i \in L_a \\ &x_{a,i} = \bar{x}_{a,i} + s_i - 1 && \forall a \in A, i \in L_a \end{aligned} \tag{3}$$

A mathematically equivalent reformulation of the original formulation (*impSP*) is then given as

$$\begin{aligned} \min \quad & \sum_{a \in A} \alpha_a \sum_{i \in L_a} d_{a,i} x_{a,i} \\ s.t. \quad & \sum_{i \in L_a} x_{a,i} = 1 && \forall a \in A \\ & \tilde{x}_{a,i} = s_i \ln(1-\bar{q}_i) + \sum_{j \in L_{a,i}} z_{i,j} \ln(\bar{q}_j) && \forall a \in A, i \in L_a \backslash \{D\} \\ & \bar{x}_{a,i} = \exp\left(\tilde{x}_{a,i}\right) && \forall a \in A, i \in L_a \\ & x_{a,i} = \bar{x}_{a,i} + s_i - 1 && \forall a \in A, i \in L_a \\ & s_i + s_j - 1 \le z_{i,j} && \forall i, j \in L, i \ne j \\ & z_{i,j} \le s_i && \forall i, j \in L, i \ne j \\ & z_{i,j} \le s_j && \forall i, j \in L, i \ne j \\ & \sum_{i \in L \backslash \{D\}} s_i \le p \\ & 0 \le x_{a,i} \le 1 && \forall a \in A, i \in L_a \\ & s_i \in \{0,1\} && \forall i \in L \\ & 0 \le z_{i,j} \le 1 && \forall i, j \in L, i \ne j \end{aligned} \qquad (\textit{impSP-LT})$$

We label this (*impSP-LT*) to indicate that it is an exact log-transformation of the original formulation (*impSP*). This alternative formulation, nevertheless, is still an MINLP problem due to

binary variables and exponential terms. Compared with the original formulation, however, the reformulation is mathematically preferable since its nonlinearity only arises from convex univariate functions. This property facilitates straightforward development of our global solution strategy.

3.2 MINLP Solution Algorithm

Regarded as a multitree method, our global solution framework is an iterative algorithm relying on solving a sequence of lower bounding master problems and upper bounding subproblems. The master problem, formulated as an MILP problem, is a relaxation of the sensor placement problem formulated in (*impSP-LT*). If the master problem is infeasible, the corresponding sensor placement problem is also infeasible and the algorithm terminates. Otherwise, the master problem provides a valid lower bound and a candidate set of values for the discrete decisions (the sensor placement, s_i). The mixed-integer master problem can be refined by several techniques discussed later. A corresponding upper-bounding subproblem is obtained by fixing all binary variables present in the formulation to the values from the solution of the master problem. In this particular formulation, when all binary variables are specified, the resulting upper-bounding subproblem is square and can be computed directly. This subproblem provides a valid upper bound of the sensor placement problem. The algorithm proceeds through a series of major iterations, cycling between the solution of a mixed-integer master problem (for the lower bound) and a forward simulation of the upper-bounding subproblem, yielding a sequence of lower and upper bounds. Finally, the algorithm terminates when the relative optimality gap is below a given tolerance.

This solution approach requires an effective relaxation of (*impSP-LT*) that can be refined to produce tighter and tighter lower bounds. Notice in the alternative formulation (*impSP-LT*), the nonlinearity only arises from the univariate convex function exp $(\tilde{x}_{a,i})$, which could be relaxed using piecewise outer approximation strategies. In particular, the linear under-estimators of the exponential function are given as

$$\bar{x}_{a,i} \geq \exp\left(\tilde{x}^*_{a,i,m}\right)\left(\tilde{x}_{a,i} - \tilde{x}^*_{a,i,m} + 1\right) \qquad m \in M_{a,i}$$

where segment points $\tilde{x}^*_{a,i,m}$ are pre-specified over the feasible domain of $\tilde{x}_{a,i}$ and $M_{a,i}$ denotes the set of indices m. Note the for various $\tilde{x}_{a,i}$, the number and location of the segment points can be different.

It is possible to construct piecewise over-estimators of the function exp $(\tilde{x}_{a,i})$, however, this requires additional binary variables (or SOS2 constraints) to indicate which segment is currently active. Furthermore, the number of binary variables increases as we increase the number of segments during refinement. As a result, the relaxation could become very challenging to solve or even intractable.

3.2.1 MILP Relaxation with Tight Upper Bounding Constraints

To avoid using the piecewise linear over-estimators, we propose instead a tailored approach and introduce a different convex relaxation without these piecewise linear functions. Given the

objective function and positive damage coefficients $d_{a,i}$ the optimization problem tends to push all $x_{a,i}$ to the lowest possible value so that the object function value is minimized. However, the first constraint in formulation (*impSP-LT*) requires that the probabilities for each scenario sum to 1, therefore locations with larger damage coefficients will still be pushed down to their lower bounds, while the locations with small damage coefficients will be pushed to their upper bound. Therefore, the upper bounds of $x_{a,i}$, especially those of the locations with relatively low damage coefficients can have a strong impact on the tightness of the convex relaxation.

Here, we use the concept of detection levels proposed by Benavides-Serrano et al [3]. In particular, if a sensor is at detection level N for a scenario, then for this detector to be the first to detect the scenario, all $N-1$ detectors at better locations (with smaller damage coefficients) must of failed to operate correctly. For instance, if a detector is placed at a location with the smallest damage coefficients compared with the others, then it is at the first detection level, and the value of $x_{a,i} = 1-\bar{q}_i$. For the second detection level, the probability is given by $x_{a,i} = \bar{q}_j(1-\bar{q}_i)$, where j and i are the locations with the smallest and the second smallest damage coefficients for scenario a, respectively. With this knowledge, we can write the upper bound of $x_{a,i}$ up to two detection levels as,

$$\bar{x}_{a,i} \leq (1-\bar{q}_i)\big(s_i + (\bar{q}_j - 1)z_{i,j}\big) \qquad \forall a \in A, i \in L_a, j \in L_{a,i} \tag{4}$$

Note if there is no detector installed at location i, i.e., $s_i = 0$, then $x_{a,i}$ is forced to be 0. If $s_i = 1$ and location i happens to be at the first detection level for scenario a then we have $x_{a,i} \leq 1-\bar{q}_i$. Recall the fact that at the optimal solution for $x_{a,i}$ corresponding to the smallest damage coefficient will be lifted up to its upper bound and we have that $x_{a,i} = 1-\bar{q}_i$. In other words, this upper bound is active and thus the tightest. Similar arguments hold true for higher detection levels, and the upper bounding constraints shown above are the tightest for the first two detection levels and provide valid upper bounds at higher detection levels.

Alternatively, the upper bound proposed above can be derived directly from the nonlinear probability constraints

$$x_{a,i} = (1-\bar{q}_i)s_i \prod_{j \in L_{a,i}} \big(1-(1-\bar{q}_j)s_j\big) \qquad \forall a \in A, i \in L_a$$

If we only consider one location j in set $L_{a,i}$, the equality becomes inequality

$$x_{a,i} \leq (1-\bar{q}_i)\big(s_i + (\bar{q}_j - 1)s_i s_j\big) \qquad \forall a \in A, i \in L_a, j \in L_{a,i}$$

Replacing $s_i s_j$ with $z_{i,j}$ gives the upper bounding constraint (4). Similarly, we can generate upper bounding constraints for higher detection levels. For instance, if we consider two locations j and k from set $L_{a,i}$, and assume location k is also in $L_{a,j}$, the we have inequality constraints

$$x_{a,i} \leq (1-\bar{q}_i)s_i\big(1-(1-\bar{q}_j)s_j\big)(1-(1-\bar{q}_k)s_k) \qquad \forall a \in A, i \in L_a, j \in L_{a,i}, k \in L_{a,j}$$

which leads to tight upper bounding constraint up to 3 detection levels

$$x_{a,i} \le (1-\bar{q}_i)\left(s_i - (1-\bar{q}_j)z_{i,k} - (1-\bar{q}_k)\left(z_{i,k} - (1-\bar{q}_j)z_{i,j,k}\right)\right) \quad \forall a \in A, i \in L_a, j \in L_{a,i}, k \in L_{a,j}.$$

where we introduce continuous variable

$$z_{i,j,k} \equiv s_i s_j s_k \qquad \forall i \in L_a, j \in L_{a,i}, k \in L_{a,j}$$

and the corresponding logic constraints are

$$\begin{aligned}
& s_i + s_j + s_k - 2 \le z_{i,j,k} && \forall i \in L_a, j \in L_{a,i}, k \in L_{a,j} \\
& z_{i,j,k} \le s_i && \forall i \in L_a, j \in L_{a,i}, k \in L_{a,j} \\
& z_{i,j,k} \le s_j && \forall i \in L_a, j \in L_{a,i}, k \in L_{a,j} \\
& z_{i,j,k} \le s_k && \forall i \in L_a, j \in L_{a,i}, k \in L_{a,j}
\end{aligned}$$

Now we impose the upper bounding constraints leading to the relaxation,

$$\begin{aligned}
\min \quad & \sum_{a \in A} \alpha_a \sum_{i \in L_a} d_{a,i} x_{a,i} \\
s.t. \quad & \sum_{i \in L_a} x_{a,i} = 1 && \forall a \in A \\
& \tilde{x}_{a,i} = s_i \ln(1-\bar{q}_i) + \sum_{j \in L_{a,i}} z_{i,j} \ln(\bar{q}_j) && \forall a \in A, i \in L_a \backslash \{D\} \\
& x_{a,i} \le (1-\bar{q}_i)\left(s_i + (\bar{q}_j - 1) z_{i,j}\right) && \forall a \in A, i \in L_a, j \in L_{a,i} \\
& \bar{x}_{a,i} \ge \exp\left(\tilde{x}^*_{a,i,m}\right)\left(\tilde{x}_{a,i} - \tilde{x}^*_{a,i,m} + 1\right) && \forall a \in A, i \in L_a, m \in M_{a,i} \\
& x_{a,i} = \bar{x}_{a,i} + s_i - 1 && \forall a \in A, i \in L_a \\
& s_i + s_j - 1 \le z_{i,j} && \forall i, j \in L, i \ne j \\
& z_{i,j} \le s_i && \forall i, j \in L, i \ne j \\
& z_{i,j} \le s_j && \forall i, j \in L, i \ne j \\
& \sum_{i \in L \backslash \{D\}} s_i \le p \\
& 0 \le x_{a,i} \le 1 && \forall a \in A, i \in L_a \\
& s_i \in \{0,1\} && \forall i \in L \\
& 0 \le z_{i,j} \le 1 && \forall i, j \in L, i \ne j
\end{aligned} \qquad (\textit{impSP-R})$$

For the sake of simplicity, we only impose the upper bounding constraint up to 2 detection levels in formulation (*impSP-R*). There are two ways to further improve the tightness of the relaxation (*impSP-R*). First, we can increase the number of segment points to refine the linear under-estimators. Second, we can impose similar upper bounding constraints for higher detection levels. Note that no additional binary variables are required in generating tighter upper bounding constraints. Theoretically, we can impose these upper bounding constraints to arbitrary detection levels. However, the number of these constraints may increase dramatically and the resulting relaxation problem can soon become prohibitively large. Moreover, the tightness may not be significantly improved since the probability at higher detection level may be negligible. Therefore,

in our tailored global algorithm the upper bounding constraints for higher detection levels are only added for subset of all candidate locations, which are selected based on the current solution of the master problem. The under-estimators are also further refined by adding more segment points based on the solution of the master problem. By doing that, we want to efficiently improve the tightness of the master problem and control the size of the resulting MILP formulation.

4 Numerical Results

In this section, we test our MINLP formulation and global solution approach on a gas detector placement problem with nonuniform unavailabilities. First, we provide a brief introduction on the simulation data used in this paper. Then we present the computational performance of our tailored algorithm in solving the gas detector placement problem.

4.1 Data Set

The data set used here is previously employed by Benavides-Serrano et al. [1,3] and Legg et al. [19,20]. It is based on a real, medium-scale, proprietary offshore facility geometry capturing the full process features, such as equipment, piping, and support structures. Gas dispersion scenario simulations were provided by *GexCon*, computed with *FLACS*, a validated tool for gas dispersion and explosion modeling in the technical safety context. Particularly, this data set consists of 270 hazard scenarios and 994 potential gas detector locations. The damage coefficient is the time between the initiation of a hazardous scenario a and its detection by a gas sensor placed at location i. To capture undetected scenarios, the damage coefficient of the dummy location is set to a value larger than the other damage coefficients. For a complete discussion regarding the data set, the data generation, and the data collection procedure please refer to previous work [2].

4.2 Sensor Placement Results

The convex relaxation (*impSP-R2*) is used as the master problem in our global solution framework. The resulting lower bounding master problem is formulated as a mixed-integer linear programming (MILP) problem. Our tailor global solution framework is implemented in Pyomo, a Python-based optimization modeling language [13]. The MILP master problem is solved to an optimality gap below 0.001%. The relative optimality gap of the global algorithm is set to be 0.01%. The total computational time limit is 36,000 seconds and the outer iteration number limit is 30. The mixed-integer master problems are solved with Gurobi [21] and the forward simulations are directly computed. The computational performance of the optimization approach is shown in Table 2 for different values of the maximum number of sensors p.

Table 2: Computational Performance Results

p	Best Solution	Lower Bound	Gap (%)	CPU Time	Iteration
1	8622.88	8622.88	0	69	1
5	5954.81	5981.49	0	1003	2
10	4354.6	4357.52	0	2306	2
15	3302.06	3303.6	0	2484	2
20	2553.53	2554.22	0	1911	2
25	1894.25	1894.76	0	4128	3
30	1426.55	1426.57	0	4213	3

35	1068.67	1068.12	0.0005	9032	7
40	779.09	778.43	0.0008	7929	4
45	581.14	579.87	0.0022	46636*	2

As the number of detector increases (from 1 to 45), the object function value improves (from 8623 to 581) since more scenarios can be detected faster. As observed in other work, increasing the number of gas detectors has more impact when the number of sensors are relatively small, since more of the scenarios are detected, and the algorithm is focusing on achieving maximum coverage (to avoid the penalty of the dummy location). However, as the number of sensors increases, full coverage is achieved, and the focus is shifted to reducing the expected time to detection alone with additional detectors. Therefore, trade-offs must be made between the number of detectors and the expected detection time across all scenarios.

From a mathematical point of view, our proposed global solution framework is able to solve this sensor placement problem to global optimality. Particularly, when the number of detectors is relatively small (1 to 30), the resulting sensor placement problems are globally solved in under 2 hours. Even for larger problems, however, the solutions times are still many orders of magnitude less than the time required to compute the dispersion scenarios. We also attempted to solve the MINLP problems using BARON (version 16.12.7), a commercial global optimization package [25], and both the original model (impSP) and the reformulated model (impSP-LT) failed to converge to an optimality gap under 0.1% within 10 hours. Note, however, that we only considered the default options of BARON, and tuning solver options may improve the performance of BARON.

5 Summary and Conclusions

Gas detection and mitigation systems play very important roles in modern process safety since they can protect lives and reduce the potential damage caused by combustible and toxic gas leaks. However, the optimal design of a gas detection system is very challenging because of the inherent uncertainty such as gas compositions, leak locations, process conditions, and weather. To address this uncertainty, prescriptive or semi-quantitative approaches have been widely used for decades, however, none of these techniques can provide rigorous proof of the solution quality. To deal with this issue, there is a need to develop rigorous quantitative strategies for gas detector system design. Stochastic programming (SP) provides an appropriate mechanism for solution of these sensor placement problems.

The SP formulations proposed in this paper consider nonuniform failure probabilities. Whereas previous work considered only two backup levels (valid when unavailability values are low), arriving at a mixed-integer quadratic programming (MIQP) problem, in our formulation, all backup detection levels are explicitly taken into account. The resulting sensor placement problem is formulated as a large-scale mixed-integer nonlinear programming (MINLP) problem. To solve this challenging MINLP problem to global optimality, we propose a multitree method which depends on iteratively solving a sequence of lower-bounding master problems and upper-bounding subproblems. The upper-bounding subproblems can be directly computed (they become square once the binaries are fixed). The master problem, however, is a mixed-integer problem that must be formulated as a convex relaxation of the original MINLP problem. To obtain a relatively tight

and computationally efficient master problem, we first propose an equivalent log-transformation of the original MINLP formulation. Though new variables and constraints are introduced, this alternative formulation is mathematically preferable since all its nonlinearity comes from convex univariate terms. Based on this reformulation, we present a strictly convex relaxation by introducing linear outer approximations and tight upper bounding constraints. The resulting relaxation formulated as a mixed-integer linear programming (MILP) problem is used as the lower-bounding master problem. The proposed global solution strategy is tested on a number of real data problems and the encouraging numerical results indicate that this solution framework is computationally feasible for large datasets.

Acknowledgments

The authors would like to thank GexCon for their support in providing dispersion simulation data for this paper. Sandia National Laboratories is a multimission laboratory managed and operated by National Technology and Engineering Solutions of Sandia, LLC, a wholly owned subsidiary of Honeywell International, Inc., for the U.S. Department of Energy's National Nuclear Security Administration under contract DE-NA0003525. The authors would like to thank Purdue Process Safety and Assurance Center (P2SAC) for their continued support of this research. The work of Carl Laird was also supported in part by Sandia National Laboratories' Laboratory Directed Research and Development (LDRD) program.

References

[1] A.J. Benavides-Serrano, S.W. Legg, R Vazquez-Roman, M.S. Mannan, and C.D. Laird. A stochastic programming approach for the optimal placement of gas detectors: Unavailability and voting strategies. *Industrial & Engineering Chemistry Research*, 53(13):5355–5365, 2013.

[2] A.J. Benavides-Serrano, M.S. Mannan, and C.D. Laird. A quantitative assessment on the placement practices of gas detectors in the process industries. *Journal of Loss Prevention in the Process Industries*, 35:339–351, 2015.

[3] A.J. Benavides-Serrano, M.S. Mannan, and C.D. Laird. Optimal placement of gas detectors: A p-median formulation considering dynamic nonuniform unavailabilities. *AIChE Journal*, 2016.

[4] Oded Berman, Dmitry Krass, and Mozart BC Menezes. Facility reliability issues in network p-median problems: Strategic centralization and co-location effects. *Operations Research*, 55(2):332–350, 2007.

[5] J. Berry, R.D. Carr, W.E. Hart, V.J. Leung, C.A. Phillips, and J. Watson. Designing contamination warning systems for municipal water networks using imperfect sensors. *Journal of Water Resources Planning and Management*, 135(4):253–263, 2009.

[6] J.W. Berry, L. Fleischer, W.E. Hart, C.A. Phillips, and J. Watson. Sensor placement in municipal water networks. *Journal of Water Resources Planning and Management*, 131(3): 237–243, 2005.

[7] Robert J. Dakin. A Tree-Search Algorithm for Mixed Integer Programming Problems. *The Computer Journal*, 8(3):250–255, 1965.

[8] Marco A. Duran and Ignacio E. Grossmann. An Outer-Approximation Algorithm for a Class of Mixed-Integer Nonlinear Programs. *Mathematical programming*, 36(3):307–339, 1986.

[9] Thomas GW Epperly and Efstratios N. Pistikopoulos. A reduced Space Branch and Bound Algorithm for Global Optimization. *Journal of Global Optimization*, 11(3):287–311, 1997.
[10] Bjorn Geißler, Alexander Martin, Antonio Morsi, and Lars Schewe. Using piecewise linear functions for solving minlps. In *Mixed Integer Nonlinear Programming*, pages 287–314. Springer, 2012.
[11] Arthur M. Geoffrion. Generalized Benders Decomposition. *Journal of optimization theory and applications*, 10(4):237–260, 1972.
[12] S Louis Hakimi. Optimum distribution of switching centers in a communication network and some related graph theoretic problems. *Operations Research*, 13(3):462–475, 1965.
[13] William E Hart, Carl Laird, Jean-Paul Watson, and David L. Woodruff. *Pyomo–Optimization Modeling in Python*, volume 67. Springer Science & Business Media, 2012
[14] Padmanaban Kesavan and Paul I. Barton. Generalized Branch-and-Cut Framework for Mixed-Integer Nonlinear Optimization Problems. *Computers & Chemical Engineering*, 24 (2):1361–1366, 2000.
[15] Avner Kessler, Avi Ostfeld, and Gideon Sinai. Detecting accidental contaminations in municipal water networks. *Journal of Water Resources Planning and Management*, 124(4): 192–198, 1998.
[16] Polyxeni-Margarita Kleniati and Claire S. Adjiman. Branch-and-Sandwich: A Deterministic Global Optimization Algorithm for Optimistic Bilevel Programming Problems. Part I: Theoretical Development. *Journal of Global Optimization*, pages 1–34, 2014.
[17] Arun Kumar, ML Kansal, Geeta Arora, Avi Ostfeld, and Avner Kessler. Detecting accidental contaminations in municipal water networks. *Journal of Water Resources Planning and Management*, 125(5):308–310, 1999.
[18] Ailsa H. Land and Alison G. Doig. An Automatic Method of Solving Discrete Programming Problems. *Econometrica: Journal of the Econometric Society*, pages 497–520, 1960.
[19] S.W. Legg, A.J. Benavides-Serrano, J.D. Siirola, J. Watson, S.G. Davis, A. Bratteteig, and C.D. Laird. A stochastic programming approach for gas detector placement using cfd-based dispersion simulations. *Computers & Chemical Engineering*, 47:194–201, 2012.
[20] S.W. Legg, C. Wang, A.J. Benavides-Serrano, and C.D. Laird. Optimal gas detector placement under uncertainty considering conditional-value-at-risk. *Journal of Loss Prevention in the Process Industries*, 26(3):410–417, 2013.
[21] Gurobi Optimization and Others. Gurobi optimizer reference manual. *URL: http://www. gurobi. com*, 2012.
[22] Avi Ostfeld and Elad Salomons. Optimal layout of early warning detection stations for water distribution systems security. *Journal of Water Resources Planning and Management*, 130 (5):377–385, 2004.
[23] Ray Porn and Tapio Westerlund. A Cutting Plane Method for Minimizing Pseudo-Convex Functions in the Mixed Integer Case. *Computers & Chemical Engineering*, 24(12):2655–2665, 2000.
[24] Ray Porn, Iiro Harjunkoski, and Tapio Westerlund. Convexification of Different Classes of Non-Convex MINLP Problems. *Computers & chemical engineering*, 23(3):439–448, 1999.
[25] Hong S. Ryoo and Nikolaos V. Sahinidis. A Branch-and-Reduce Approach to Global Optimization. *Journal of Global Optimization*, 8(2):107–138, 1996.

[26] Lawrence V Snyder and Mark S Daskin. Reliability models for facility location: the expected failure cost case. *Transportation Science*, 39(3):400–416, 2005.
[27] Lawrence V Snyder, Zumbul Atan, Peng Peng, Ying Rong, Amanda J Schmitt, and Burcu Sinsoysal. Or/ms models for supply chain disruptions: A review. *IIE Transactions*, pages 1–21, 2015
[28] Juan Pablo Vielma, Shabbir Ahmed, and George Nemhauser. Mixed-integer models for non- separable piecewise-linear optimization: Unifying framework and extensions. *Operations research*, 58(2):303–315, 2010.
[29] Tapio Westerlund and Frank Pettersson. An Extended Cutting Plane Method for Solving Convex MINLP Problems. *Computers & Chemical Engineering*, 19:131–136, 1995.
[30] Juan M. Zamora and Ignacio E. Grossmann. A Branch and Contract Algorithm for Problems with Concave Univariate, Bilinear and Linear Fractional Terms. *Journal of Global Optimization*, 14(3):217–249, 1999.

1.6. Global solution Strategies for Network Constrained Unit Commitment Problem with Nonlinear AC Transmission Models

Global Solution Strategies for the Network-Constrained Unit Commitment Problem with AC Transmission Constraints

Jianfeng Liu, Carl D. Laird, *Member, IEEE,* Joseph K. Scott, *Member, IEEE,*
Jean-Paul Watson, *Member, IEEE* and Anya Castillo, *Member, IEEE*

***Abstract*—We propose a novel global solution algorithm for the network-constrained unit commitment problem that incorporates a nonlinear alternating current (AC) model of the transmission network, which is a nonconvex mixed-integer nonlinear programming (MINLP) problem. Our algorithm is based on the multi-tree global optimization methodology, which iterates between a mixed-integer lower-bounding problem and a nonlinear upper-bounding problem. We exploit the mathematical structure of the unit commitment problem with AC power flow constraints (UC-AC) and leverage second-order cone relaxations, piecewise outer approximations, and optimization-based bounds tightening to guarantee a globally optimal solution at convergence. Numerical results on four benchmark problems illustrate the effectiveness of our algorithm, both in terms of convergence rate and solution quality.**

A. Notation

Sets

$\mathcal{B}$	Set of all buses $\{1, ..., B\}$
$\mathcal{B}_b$	Set of all buses that are connected to bus b
$\mathcal{C}$	Set of all cycles in a cycle basis for the network
$\mathcal{G}$	Set of all generators $\{1, ..., G\}$
$\mathcal{G}_b$	Set of all generators at bus b
$\mathcal{L}$	Set of all branches (transmission lines)
$\mathcal{L}_c$	Set of branches in cycle c
$\mathcal{L}_b^{in}$	Set of all *inbound* branches to bus b
$\mathcal{L}_b^{out}$	Set of all *outbound* branches from bus b
$\mathcal{S}_g$	Set of startup segments of generator g $\{1, ..., S_g\}$
$\mathcal{SC}$	Set of all synchronous condensers $\{1, ..., SC\}$
$\mathcal{SC}_b$	Set of all synchronous condensers at bus b
$\mathcal{T}$	Set of time periods $\{1, ..., T\}$

Parameters

$A_{g,n}$	Coefficients ($n = 0, 1, 2$) of quadratic production cost function of generator g
B_b^{sh}	Shunt susceptance at bus b
B_l	Imag. part of branch l admittance matrix
G_b^{sh}	Shunt conductance at bus b
G_l	Real part of branch l admittance matrix
$K_{g,\tau}^{su}$	Startup cost of generator g
K_g^{sd}	Shutdown cost of generator g
$P_{b,t}^D$	Real power demand at bus b, time t
P_t^R	System reserve requirement at time t
$P_g^{G,min}$	Min. real power output of generator g
$P_g^{G,max}$	Max. real power output of generator g
$Q_{b,t}^D$	Reactive power demand at bus b, time t
$Q_g^{G,min}$	Min. reactive power output of generator g
$Q_g^{G,max}$	Max. reactive power output of generator g
$Q_{sc}^{SC,min}$	Min. output of synchronous condenser sc
$Q_{sc}^{SC,max}$	Max. output of synchronous condenser sc
RD_g	Ramp-down limit of generator g
RU_g	Ramp-up limit of generator g
S_l^{max}	Apparent power limit on branch l
SD_g	Shutdown capability of generator g
SU_g	Startup capability of generator g
$T_{g,\tau}^{su}$	Startup cost function time segment for generator g
T_g^u	Min. uptime of generator g
T_g^d	Min. downtime of generator g
V_b^{min}	Min. voltage magnitude at bus b
V_b^{max}	Max. voltage magnitude at bus b

Variables

$\delta_{g,\tau,t}$	Startup cost segment indicator
$\theta_{l,t}$	Voltage phase angle difference between ends (bus b and bus k) of branch l at time t, $\theta_{b,k,t}$

J. Liu is with the Department of Chemical Engineering, Purdue University, West Lafayette, IN, 47907 USA e-mail: liu1172@purdue.edu.

C.D. Laird is with Davidson School of Chemical Engineering, Purdue University, West Lafayette, IN, 47907 USA and with Sandia National Laboratories, Albuquerque, NM, 87185 USA e-mail: cdlaird@sandia.gov.

J.K. Scott is with the Department of Chemical and Biomolecular Engineering, Clemson University, Clemson, SC 29634 USA e-mail: jks9@clemson.edu.

J.P. Watson is with Sandia National Laboratories, Albuquerque, NM, 87185 USA e-mail: jwatson@sandia.gov.

A. Castillo is with Sandia National Laboratories, Albuquerque, NM, 87185 USA e-mail: arcasti@sandia.gov.

Manuscript received 1/12/18; under review in IEEE TPWRS.

$c_{b,k,t}$	Second-order cone variable
$c^p_{g,t}$	Production cost for generator g at time t
f^p	Total production cost
f^{sd}	Total shutdown cost
f^{su}	Total startup cost
$p^G_{g,t}$	Real power output of generator g at time t
$p^f_{l,t}$	Real power flow *from* branch l, at time t
$p^t_{l,t}$	Real power flow *to* branch l, at time t
$q^G_{g,t}$	Reactive power output of generator g at time t
$q^f_{l,t}$	Reactive power flow *from* branch l, at time t
$q^t_{l,t}$	Reactive power flow *to* branch l, at time t
$q^{SC}_{sc,t}$	Reactive power output of synchronous condenser sc at time t
$r^a_{g,t}$	Real power reserve provided by generator g at time t
$s_{b,k,t}$	Second-order cone variable
$u_{g,t}$	Startup status, equal to 1 if generator g starts up at time t, 0 otherwise
$v_{b,t}$	Voltage magnitude at bus b at time t, $v^2_{b,t} = (v^r_{b,t})^2 + (v^j_{b,t})^2$
$v^j_{b,t}$	Imag. part of voltage phasor at bus b, time t
$v^r_{b,t}$	Real part of voltage phasor at bus b, time t
$w_{g,t}$	Shutdown status, equal to 1 if generator g shuts down at time t, 0 otherwise
$y_{g,t}$	Unit on/off status, equal to 1 if generator g is on-line at time t, 0 otherwise

I. Introduction

RECENTLY the Federal Energy Regulatory Commission (FERC) reported that uplift – out-of-market payments that result when out-of-merit generation costs are incurred to relieve a constraint – can arise due to the inability of independent system operators (ISOs) to fully model the steady-state physics on an alternating current (AC) network [1]. According to a recent National Academies report [2], solving this problem "could significantly improve the modeling and efficient dispatch of resources during the commitment, dispatching, and pricing processes." Recent work on the day-ahead unit commitment problem, which was led by MISO technical staff in [3], attests to the importance and non-trivial complexity of incorporating AC network constraints due to the performance challenges introduced by denser matrices and additional nonlinearities.

Because of these modeling difficulties, current practice is to perform unit commitment using DC approximations (or copper plate) to represent the transmission network. These approximations do not allow rigorous treatment of AC power flow constraints. As a result, certain resources are consistently committed outside of the market to address unforeseen reliability issues; this results in concentrated uplift payments [1]. Such resources are often required for reactive power compensation in order to provide system voltage control that enables more efficient delivery and utilization of real power [4]. Because such reliability requirements are largely unmodeled in day-ahead unit commitment, more cost effective resources are displaced for these out-of-merit commitments. Alternatively, in the real-time market, operators may have to manually commit and dispatch reliability units while also manually re-dispatching or de-committing other resources, e.g., exceptional dispatches in CAISO [5], out-of-merit generation in NYISO [6], and balancing operating reserves in PJM [7].

To address these concerns, this paper focuses on solution of the unit commitment problem with AC power flow constraints (UC-AC). Solving real-world operations and market settlement with alternating current optimal power flow (ACOPF) is not trivial. Due to the scale of real-world power systems, network-constrained unit commitment problems can be extremely large and computationally challenging to solve. Coupling this with nonconvex AC power flow constraints leads to a mixed-integer nonlinear programming (MINLP) problem that is NP-hard [8–10]. If the continuous relaxation of the MINLP is a convex optimization problem, we refer to it as a *convex* MINLP. Otherwise, the problem is referred to as a *nonconvex* MINLP. With this definition, the UC-AC is a nonconvex MINLP. Algorithms exist to address both convex and nonconvex MINLP problems. However, tailored solution strategies are often required to achieve desired computational performance. In this paper, we present the first known global optimization approach that can successfully solve the UC-AC on a set of small- to medium-sized test problems.

Deterministic MINLP algorithms can be classified into single-tree and multi-tree methods. Single-tree deterministic algorithms, i.e., the well-known Branch-and-Bound (BB) methods [11, 12], seek a global optimum by searching a single tree using a systematic enumeration strategy consisting of three primary steps: branching, bounding, and selection. BB-based global optimization strategies have been well-studied and specialized, yielding strategies such as Branch-and-Reduce [13], Reduced Space Branch-and-Bound [14], Branch-and-Contract [15], Branch-and-Cut [16], and Branch-and-Sandwich [17]. These approaches are suitable for general, nonconvex MINLP problems of small or medium size, but become computationally intractable with increasing numbers of discrete variables, e.g., such as those arising in UC-AC.

In contrast, multi-tree methods [18] iteratively solve a sequence of related lower-bounding (master problem) and upper-bounding (subproblem) problems. For con-

vex MINLP problems, many multi-tree solution strategies – including Generalized Benders Decomposition (GBD) [19], Outer Approximation (OA) [20, 21], and Exact Cutting Plane (ECP) methods [22] – are effective, and have been applied to a broad range of MINLPs in various application domains. Extensions exist for nonconvex MINLPs. While many are heuristic, e.g., see [23, 24], Li et al. [25] propose a rigorous, nonconvex GBD (NGBD) method with piecewise convex relaxations that yields a sequence of nondecreasing lower bounds and nonincreasing upper bounds where monotonic convergence of the bounds is guaranteed. Bonami, Kılınç and Linderoth noted that recent advancements in respective mixed-integer linear programming (MILP) and nonlinear programming (NLP) problem classes have unfortunately resulted in "far more modest" improvements in general algorithms for even convex MINLPs [26], illustrating the need for specialized approaches.

The classic OA approach, a multi-tree technique, was originally developed to solve convex MINLPs. This approach solves a sequence of MILP master and convex NLP subproblems and yields a globally optimal solution for a convex MINLP in a finite number of iterations for a given ϵ-tolerance on the optimality gap [20, 21]. The MILP master problem is a relaxation of the original MINLP that provides a provable lower bound on the MINLP along with a candidate integer solution. Fixing the integers in the MINLP yields a convex NLP subproblem that provides a valid upper bound and a candidate solution (for both continuous and integer variables) to the overall MINLP. In this classic approach, the master problem is further refined (i.e., relaxation strengthened) though the addition of linear outer approximations of convex constraints in the MINLP. The algorithm iterates between the master problem and the NLP subproblem, and terminates when the gap between the lower and upper bounds is sufficiently small. Constraints can also be added to the master problem to remove previously visited integer solutions (using so-called *integer cuts*). These methods have been extended to nonconvex problems where global convergence of the MINLP can be achieved as long as global solutions of the NLP subproblems are ensured [27]. Kesavan et al. [28] develop decomposition algorithms for nonconvex MINLP that finds the global solution on finite termination by solving convex underestimators in the BB search. Similar multi-tree solution strategies for nonconvex MINLPs have also been successfully used in various applications [29–31].

Here, we extend our efforts in [32] and propose a multi-tree method based on OA for the UC-AC problem. The master problem is a mixed-integer second-order cone program (MISOCP) constructed using second-order cone (SOC) relaxations of the nonconvex AC transmission constraints [33]. As the algorithm iterates, the master problem is further refined with piecewise outer approximations to strengthen the tightness of the relaxation and the *lower-bound* computation. The algorithm from [32] is used to find a global solution of the nonconvex NLP subproblem in the *upper-bound* computation. Furthermore, we incorporate optimization-based bounds tightening (OBBT) techniques that are valid in both master and subproblem iterations and, because our proposed approach provides global solution of the NLP subproblem, we are able to include *integer cuts* in the master problem that remove previously visited solutions from the feasible space as the algorithm iterates. To the best of our knowledge, this is the first global solution algorithm successfully applied to the UC-AC problem, identifying solutions with quality certificates (optimality gaps) in time-limited environments.

The remainder of this paper is organized as follows. We begin in Section II by discussing relevant work to solving the UC-AC problem. In Section III we introduce the unit commitment formulation with AC transmission constraints (UC-AC). In Section IV we outline the necessary problem relaxations and the global optimization algorithm. In Section V we report numerical results on the range of currently available test systems. We then conclude in Section VI with a summary of our contributions and directions for future work.

II. Related Work

There is a growing body of literature on algorithms [34–47] for the solution of the UC-AC problem. A recent study by Aghaei et al. noted that the UC-AC problem is presently intractable for commercial MINLP solvers, including BARON, SBB, and DICOPT [42]. In this section we review the most relevant works in further detail.

Amjady et al. [46] leverage a Signomial convexification technique with second order approximations of the trignometric functions in the ACOPF constraint set. Without refinement, branching, or additional cuts, relaxations on their own do not provide a guarantee of global optimality to the original MINLP. Other comparable convexification approaches include the formulations by Bai and Wei [39] and Madani et al. [47], where these studies use semidefinite programming (SDP) to relax the ACOPF constraint set and the 0/1 variables. For these studies, when a solution is non-integral in the unit commitment variables, a rounding procedure is applied to determine a feasible, near-optimal solution. Such rounding heuristics are useful but not sufficient to guarantee a global solution. The other aforementioned methods solve the ACOPF subproblem – or network and voltage security subproblems – with local solution methods, and in some cases apply linearization techniques [44, 45, 48].

Approaches that make use of local solutions of the NLP subproblem (e.g., recent GBD examples include [42–45]) are not guaranteed to find global solutions in a finite number of steps. This is because, as indicated in [49], when applying GBD to nonconvex problems, global solution of the NLP subproblem is required to ensure valid cuts.

On the contrary, Sifuentes et al. [38] argued that such suboptimal outcomes due to nonconvexities can be reduced with constraint specifications (e.g., small angle difference constraints). However, more recent work by Wu et al. [50] indicates that such assumptions do not preclude the occurrence of multiple, local optima. As such, Frank et al. [51] develop a nonconvex GBD approach to solve AC-DC distribution system design problems where a global solver is leveraged for the nonconvex subproblems.

In contrast to GBD methods that have been applied to the UC-AC problem to-date, our *lower-bounding* problem incorporates a relaxation and outer-approximation of the full ACOPF constraint set. This master problem can be arbitrarily refined to provide improved integer solutions (although this was not necessary in our test cases). Furthermore, we apply our approach from [32] to determine a global solution of the *upper-bounding* problem, ensuring that the global solution is identified if the gap closes. Moreover, we are guaranteed finite termination by enumeration in the worst case.

III. UC-AC Problem Formulation

We now introduce our UC-AC problem formulation. We first present the core UC model in Section III-A, which is based on the compact three-binary (3BIN) formulation introduced in [52]. We then present the rectangular power-voltage (RPQV) model [53] in Section III-B to represent the steady-state operations of the nonlinear AC transmission network. We integrate these constraint sets to represent the UC-AC problem, resulting in a nonconvex MINLP. A tailored solution technique for this model is proposed in the following section.

A. Unit Commitment Model

We use the term *UC skeleton* when referring to a unit commitment model consisting only of a cost function, operating constraints, and any associated continuous and binary variables with no network representation. We summarize several key components of the *3BIN* formulation here; refer to [52] for further details.

1) Cost Function: The total cost in UC is the sum of three major components – production costs, startup costs, and shutdown costs – as follows:

$$f^p + f^{su} + f^{sd}.$$

We assume that the production cost f^p is a quadratic monotonically non-decreasing function of real power generation; in practice, this is often replaced with a piecewise approximation. Computation of f^p in the quadratic case is accomplished by imposing the constraints

$$A_{g,2}(p^G_{g,t})^2 + A_{g,1}p^G_{g,t} + A_{g,0}y_{g,t} \leq c^p_{g,t} \qquad \forall\, g,\ t \quad (1)$$

$$f^p = \sum\nolimits_{g\in\mathcal{G}} \sum\nolimits_{t\in\mathcal{T}} c^p_{g,t} \quad (2)$$

where $A_{g,2}$, $A_{g,1}$, and $A_{g,0}$ are known cost coefficients in (\$/MW^{2}h), (\$/MWh) and (\$/h) associated with a specific generator g.

To formulate the total startup cost, f^{su}, we first introduce a new binary variable $\delta_{g,\tau,t}$, which indicates the startup type τ of generator g at time period t. In particular, $\delta_{g,\tau,t}$ takes the value of 1 if the generator g starts up at time t and has been previously offline within $[T^{su}_{g,\tau}, T^{su}_{g,\tau+1})$ hours. The logical constraints between $w_{g,t}$, $u_{g,t}$, and $\delta_{g,\tau,t}$ are given as

$$\delta_{g,\tau.t} \leq \sum\nolimits_{t'=t-T^{su}_{g,\tau}}^{t+1-T^{su}_{g,\tau+1}} w_{g,t'} \qquad \forall\, g,\ t,\ \tau \in [1, S_g) \quad (3)$$

$$u_{g,t} = \sum\nolimits_{\tau\in\mathcal{S}_g} \delta_{g,\tau,t} \qquad \forall\, g,\ t \quad (4)$$

where S_g is the number of startup types for generator g, and $u_{g,t}$ and $w_{g,t}$ indicate startup and shutdown of generator g in time t, respectively. Note that $w_{g,t}$ with positive time index t are variables, otherwise $w_{g,t}$ are treated as constants to demonstrate previous system status.

For a thermal unit, the startup cost is assumed to be a monotonically increasing step function with respect to the generator's previous off-line time. The total startup cost is given by

$$f^{su} = \sum\nolimits_{g\in\mathcal{G}} \sum\nolimits_{t\in\mathcal{T}} \sum\nolimits_{\tau\in\mathcal{S}_g} K^{su}_{g,\tau}\delta_{g,\tau,t} \quad (5)$$

where $K^{su}_{g,\tau}$ is the cost of startup type τ for generator g. Given logical constraints (3) and (4), and the monotonically non-decreasing startup cost function, it can be shown that $\delta_{g,\tau,t}$ will always solve to a binary value. In other words, instead of explicitly defining $\delta_{g,\tau,t}$ as a binary, it can be relaxed as a continuous variable within range $[0, 1]$.

The shutdown cost of generator g is assumed to be independent of its previous on-line states, and the total shutdown cost is:

$$f^{sd} = \sum\nolimits_{g\in\mathcal{G}} \sum\nolimits_{t\in\mathcal{T}} K^{sd}_g w_{g,t}. \quad (6)$$

2) Operating Constraints: According to operating restrictions, a thermal unit must stay in one state (either on-line or off-line) for a certain period of time before its state can be changed again. Such time periods vary between different generator types. To enforce this re-

quirement, we have to introduce minimum uptime and downtime constraints

$$\sum_{t'=t-T_g^u+1}^{t} u_{g,t'} \leq y_{g,t} \qquad \forall\, g,\ t \quad (7)$$

$$\sum_{t'=t-T_g^d+1}^{t} w_{g,t'} \leq 1 - y_{g,t} \qquad \forall\, g,\ t \quad (8)$$

where $u_{g,t}$ and $w_{g,t}$ with positive time index t are unknown variables, otherwise they are treated as constants to indicate previous system status. Additional constraints are required to denote the logical correlation between $u_{g,t}$, $w_{g,t}$, and $y_{g,t}$ in

$$y_{g,t} - y_{g,t-1} = u_{g,t} - w_{g,t} \qquad \forall\, g,\ t. \quad (9)$$

Note that these constraints ensure that a generator cannot start up and shut down within the same time period. Given the fact that $y_{g,t}$ is a binary variable, imposing constraints (7), (8) and (9) together guarantees that $u_{g,t}$ and $w_{g,t}$ take binary values only. Consequently, $u_{g,t}$, $w_{g,t}$, and $\delta_{g,\tau,t}$, though initially defined as binaries, can be relaxed as continuous within $[0,1]$, leaving the $y_{g,t}$ as the only binary variables in our *UC skeleton* formulation. The spinning reserve constraint is defined as

$$P_t^R \leq \sum_{g\in\mathcal{G}} r_{g,t} \qquad \forall\, t \quad (10)$$

and determines the extra generating capacity available by generators included in the commitment solution at time t; typically, the spinning reserve is defined as a fraction of the current total power demand. The upper- and lower-bounds of generator output is dependent on its operating state; the real power productions are constrained by $[P_g^{G,min}, P_g^{G,max}]$, the startup and shutdown capabilities SD_g and SU_g, and state indicators $y_{g,t}$, $u_{g,t}$, and $w_{g,t}$ where both real power generation $p_{g,t}$ and spinning reserve $r_{g,t}$ are accounted for in

$$p_{g,t} + r_{g,t} \leq (P_g^{G,max} - P_g^{G,min})y_{g,t} - (P_g^{G,max} - SU_g)u_{g,t} \qquad \forall\, g,\ t \quad (11)$$

$$p_{g,t} + r_{g,t} \leq (P_g^{G,max} - P_g^{G,min})y_{g,t} - (P_g^{G,max} - SD_g)w_{g,t+1} \qquad \forall\, g,\ t \quad (12)$$

when $T_g^u = 1$, and

$$p_{g,t} + r_{g,t} \leq (P_g^{G,max} - P_g^{G,min})y_{g,t} - (P_g^{G,max} - SU_g)u_{g,t} - (P_g^{G,max} - SD_g)w_{g,t+1} \qquad \forall\, g,\ t \quad (13)$$

when $T_g^u \geq 2$. The real power production is also constrained by ramp-up and ramp-down limits, which are given as

$$p_{g,t} + r_{g,t} - p_{g,t-1} \leq RU_g \qquad \forall\, g,\ t \quad (14)$$

$$-p_{g,t} + p_{g,t-1} \leq RD_g \qquad \forall\, g,\ t. \quad (15)$$

Then, the reactive power productions are only constrained by $[Q_g^{G,min}, Q_g^{G,max}]$ and $y_{g,t}$ in

$$Q_g^{G,min} y_{g,t} \leq q_{g,t}^G \leq Q_g^{G,max} y_{g,t} \qquad \forall\, g,\ t. \quad (16)$$

Synchronous condensers are not modeled with startup/shutdown costs and their reactive power output is constrained by $[Q_{sc}^{SC,min}, Q_{sc}^{SC,max}]$

$$Q_{sc}^{SC,min} \leq q_{sc,t}^{SC} \leq Q_{sc}^{SC,max} \qquad \forall\, sc,\ t. \quad (17)$$

B. AC Transmission Network Model

In electric power system analysis, the *RPQV* model is widely-used to represent an AC transmission network; this approach explicitly models real and reactive power flows in terms of complex voltages in the rectangular form. A transmission line is denoted as $l{\equiv}(b,k)$, where b is the index of the bus at the *from* end and k is the index of the bus at the *to* end of branch l. For integration into our *UC skeleton*, the *RPQV* model is given by

$$\sum_{l\in\mathcal{L}_b^{in}} p_{l,t}^t + \sum_{l\in\mathcal{L}_b^{out}} p_{l,t}^f + G_b^{sh} v_{b,t}^2 + P_{b,t}^D - \sum_{g\in\mathcal{G}_b} p_{g,t}^G = 0 \qquad \forall\, b,\ t \quad (18)$$

$$\sum_{l\in\mathcal{L}_b^{in}} q_{l,t}^t + \sum_{l\in\mathcal{L}_b^{out}} q_{l,t}^f - B_b^{sh} v_{b,t}^2 + Q_{b,t}^D - \sum_{g\in\mathcal{G}_b} q_{g,t}^G - \sum_{sc\in\mathcal{SC}_b} q_{sc,t}^{SC} = 0 \qquad \forall\, b,\ t \quad (19)$$

$$p_{l,t}^f = G_l^{ff} v_{b,t}^2 + G_l^{ft}(v_{b,t}^r v_{k,t}^r + v_{b,t}^j v_{k,t}^j) - B_l^{ft}(v_{b,t}^r v_{k,t}^j - v_{b,t}^j v_{k,t}^r) \qquad \forall\, l,\ t \quad (20)$$

$$q_{l,t}^f = -B_l^{ff} v_{b,t}^2 - B_l^{ft}(v_{b,t}^r v_{k,t}^r + v_{b,t}^j v_{k,t}^j) - G_l^{ft}(v_{b,t}^r v_{k,t}^j - v_{b,t}^j v_{k,t}^r) \qquad \forall\, l,\ t \quad (21)$$

$$p_{l,t}^t = G_l^{tt} v_{k,t}^2 + G_l^{tf}(v_{k,t}^r v_{b,t}^r + v_{k,t}^j v_{b,t}^j) - B_l^{tf}(v_{k,t}^r v_{b,t}^j - v_{k,t}^j v_{b,t}^r) \qquad \forall\, l,\ t \quad (22)$$

$$q_{l,t}^t = -B_l^{tt} v_{k,t}^2 - B_l^{tf}(v_{k,t}^r v_{b,t}^r + v_{k,t}^j v_{b,t}^j) - G_l^{tf}(v_{k,t}^r v_{b,t}^j - v_{k,t}^j v_{b,t}^r) \qquad \forall\, l,\ t \quad (23)$$

$$(V_b^{min})^2 \leq v_{b,t}^2 \leq (V_b^{max})^2 \qquad \forall\, b,\ t \quad (24)$$

$$(p_{l,t}^f)^2 + (q_{l,t}^f)^2 \leq (S_l^{max})^2 \qquad \forall\, l,\ t \quad (25)$$

$$(p_{l,t}^t)^2 + (q_{l,t}^t)^2 \leq (S_l^{max})^2 \qquad \forall\, l,\ t \quad (26)$$

where $v_{b,t}^2{\equiv}(v_{b,t}^r)^2 + (v_{b,t}^j)^2$; see [32] for details on computing G_l and B_l branch admittance submatrices. Note that the *RPQV* problem is nonconvex due to bilinear terms and nonconvex quadratics.

C. UC-AC Problem Formulation

The UC-AC is a nonconvex MINLP formulations that combines the UC skeleton with the nonlinear ACOPF

constraints, giving:

$$\begin{aligned} &\min f^p + f^{su} + f^{sd} \\ &\text{s.t.} \\ &(1) - (26) \\ &y_{g,t}, u_{g,t}, w_{g,t} \in \{0,1\} \quad \forall\, g,\ t \end{aligned} \tag{27}$$

In the next section we exploit the special mathematical structure of this problem to solve the problem globally.

IV. UC-AC Global Solution Framework

The UC-AC is a nonconvex MINLP, and our proposed algorithm is a *nested* multi-tree method where both the outer and inner algorithm are based on a nonconvex OA approach that solves a sequence of lower-bounding master problems and upper-bounding subproblems. In this section, we first provide a high-level explanation of the nested multi-tree approach used to solve the UC-AC MINLP problem, followed by a detailed description of the master and NLP subproblems and the algorithm definition. Here, we denote $d{=}[y, u, w]$ to represent the discrete decisions (i.e., generator commitment variables), and x to represent the continuous variables in the UC-AC problem.

A. Overview

Figure 1 shows the multi-tree approach for the UC-AC problem. The algorithm iterates between a master problem and an NLP subproblem, and each pair of such solves comprise a major iteration q for candidate solution denoted as $[d^q, x^q]$. The high-level description of the

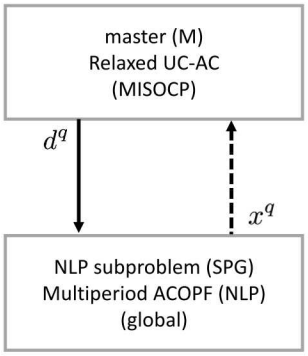

Fig. 1: High-level description of the multi-tree approach for global solution of the UC-AC MINLP problem.

Outer Algorithm is as follows:

The master problem (M) is a relaxation of the UC-AC problem where the AC power flow constraints are relaxed using the SOC representation from [33]. The initial solution of (M) provides a lower bound on the UC-AC problem and a candidate solution for the binary variables (the generator commitments) given by d^q for iteration q. Fixing these variables in the UC-AC MINLP problem yields a nonconvex NLP that represents a multi-period ACOPF problem given by (SPG). This NLP subproblem, if feasible, provides an upper bound, z_U^q, and a candidate solution to the UC-AC, $[d^q, x^q]$. If the gap between the upper and lower bound is sufficiently small, then the solution has been found, i.e., $z^*{=}z_U^q$ for $[d^*, x^*] = [d^q, x^q]$.

To further accelerate exploration of the generator commitments, it is also desirable to add cuts to (M) that remove previously visited solutions d^q from the feasible space. With these *integer cuts* (see Section IV-D1), the solution z_L^q of (M) is not a true lower bound to the original MINLP, and to ensure convergence with this approach, it is required that we find a globally optimal solution to the NLP subproblem (SPG) for each candidate binary solution d^q. Note that, in the limit, this will result in full enumeration, ensuring convergence of the discrete decision space in a finite number of iterations. However, for the applications and test cases presented in this work, only a few outer iterations were required to close the gap.

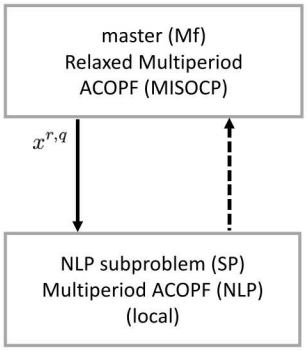

Fig. 2: High-level description of the multi-tree approach for global solution of the NLP subproblem (SPG).

For global solution of the multi-period ACOPF in (SPG) we apply the approach of [32], and for completeness, Figure 2 shows this algorithm. This strategy is also a multi-tree approach, and hence we refer to the overall algorithm as a *nested* multi-tree approach. Recall that the candidate generator commitments d^q are fixed for this problem. Similar to the *Outer Algorithm* in Figure 1, this approach iterates between the master and the NLP subproblem, and each pair of such solves constitutes a minor iteration r on iteration q. The high-level description of the *Inner Algorithm* is as follows:

The master problem (Mf) is a MISOCP relaxation of the problem (SPG) (d^q fixed). Therefore, in (Mf) the only binary variables are those corresponding to

piecewise outer approximations. The master problem (Mf) is solved to find a lower bound for (SPG), and the solution $x^{r,q}$ from (Mf) is used to initialize the NLP subproblem (SP). This NLP subproblem, if feasible provides an upper bound, $z_U^{r,q}$, and a candidate solution $x^{r,q}$. Note that the NLP subproblem (SP) in Figure 2 is the same formulation as (SPG) in Figure 1, however, in this case we only seek a local solution of the NLP subproblem (SP).

Since we do not add integer cuts to the master problem (Mf), it is a true relaxation of (SPG), and closure of the gap between the upper and lower bounds is sufficient to indicate convergence. At each iteration r, the master problem is progressively refined by the addition and/or tightening of piecewise outer approximations, as well as optimization-based bounds tightening (OBBT), as discussed later in Sections IV-D.

Note that for both *Outer* and *Inner Algorithms*, the respective master problems (M) and (Mf) can be further refined with any selection of piecewise outer approximations (see Sections IV-D2 and IV-D3) and with domain reduction techniques, e.g., OBBT (see Section IV-D4).

B. Problem Formulations

This section provides a description of the problem formulations (M), (SPG), (SP), and (Mf) used in the global algorithm. The master problem (M) for the UC-AC problem is based on the SOC relaxation of the power flow equations from [33]. We replace the quadratic and bilinear terms in (27) for all $l{\equiv}(b,k)$ and t with

$$c_{b,b,t} := (v_{b,t}^r)^2 + (v_{b,t}^j)^2$$

$$c_{b,k,t} := v_{b,t}^r v_{k,t}^r + v_{b,t}^j v_{k,t}^j$$

$$s_{b,k,t} := v_{b,t}^r v_{k,t}^j - v_{k,t}^r v_{b,t}^j$$

and introduce a second-order cone relaxation of the condition

$$c_{b,k,t}^2 + s_{b,k,t}^2 = c_{b,b,t} c_{k,k,t} \tag{28}$$

as

$$c_{b,k,t}^2 + s_{b,k,t}^2 \leq c_{b,b,t} c_{k,k,t}. \tag{29}$$

1) Master Problem (M)*:* With the definitions above, the problem formulation for (M) is given as follows:

$$z_L := \min f^p + f^{su} + f^{sd} \tag{M.1}$$

s.t.

$$(1) - (17), (25), (26) \tag{M.2}$$

$$\sum\nolimits_{l \in \mathcal{L}_b^{in}} p_{l,t}^t + \sum\nolimits_{l \in \mathcal{L}_b^{out}} p_{l,t}^f + G_b^{sh} c_{b,b,t} + P_{b,t}^D - \sum\nolimits_{g \in \mathcal{G}_b} p_{g,t}^G = 0 \quad \forall\, b,\ t \tag{M.3}$$

$$\sum\nolimits_{l \in \mathcal{L}_b^{in}} q_{l,t}^t + \sum\nolimits_{l \in \mathcal{L}_b^{out}} q_{l,t}^f - B_b^{sh} c_{b,b,t} + Q_{b,t}^D - \sum\nolimits_{g \in \mathcal{G}_b} q_{g,t}^G - \sum\nolimits_{sc \in \mathcal{SC}_b} q_{sc,t}^{SC} = 0 \quad \forall\, b,\ t \tag{M.4}$$

$$p_{l,t}^f = G_l^{ff} c_{b,b,t} + G_l^{ft} c_{b,k,t} - B_l^{ft} s_{b,k,t} \quad \forall\, l,\ t \tag{M.5}$$

$$q_{l,t}^f = -B_l^{ff} c_{b,b,t} - B_l^{ft} c_{b,k,t} - G_l^{ft} s_{b,k,t} \quad \forall\, l,\ t \tag{M.6}$$

$$p_{l,t}^t = G_l^{tt} c_{k,k,t} + G_l^{tf} c_{k,b,t} - B_l^{tf} s_{k,b,t} \quad \forall\, l,\ t \tag{M.7}$$

$$q_{l,t}^t = -B_l^{tt} c_{k,k,t} - B_l^{tf} c_{k,b,t} - G_l^{tf} s_{k,b,t} \quad \forall\, l,\ t \tag{M.8}$$

$$(V_b^{min})^2 \leq c_{b,b,t} \leq (V_b^{max})^2 \quad \forall\, b,\ t \tag{M.9}$$

$$c_{b,k,t} = c_{k,b,t} \quad \forall\, l,\ t \tag{M.10}$$

$$s_{b,k,t} = -s_{k,b,t} \quad \forall\, l,\ t \tag{M.11}$$

$$c_{b,k,t}^2 + s_{b,k,t}^2 \leq c_{b,b,t} c_{k,k,t} \quad \forall\, l,\ t \tag{M.12}$$

$$y_{g,t}, u_{g,t}, w_{g,t} \in \{0,1\} \quad \forall\, g,\ t \tag{M.13}$$

2) NLP Subproblems (SPG) *and* (SP)*:* The same NLP subproblem is used in both the outer and the inner multi-tree algorithms, however, for (SPG), a global solution is required. The NLP subproblem is formed by fixing the binary variables $d{=}[y,u,w]$ (generator commitments) in the original MINLP formulations for the UC-AC. This produces a multi-period ACOPF formulation. For any iteration j, problem for fixed $d^{(j)}{=}[y^{(j)}, u^{(j)}, w^{(j)}]$ is given as:

$$z_U := \min f^p + f^{su} + f^{sd}$$

s.t.

$$(1) - (26) \tag{SP}$$

where

$$y_{g,t} := y_{g,t}^{(j)}, u_{g,t} := u_{g,t}^{(j)}, w_{g,t} := w_{g,t}^{(j)} \quad \forall\, g,\ t$$

3) Master Problem (Mf)*:* Problem (Mf) is the master problem used in the inner multi-tree approach for obtaining globally optimal solutions to the NLP subproblem (SPG) from the outer problem. It is based on the same SOC relaxation that is used for problem

Algorithm 1 *Outer Algorithm* for UC-AC

1: **Initialization.**
Iteration q=0,
$z_L^* \leftarrow -\infty$. $z_U^* \leftarrow +\infty$. $(d^*, x^*) \leftarrow \emptyset$.
2: **Solve the Master Problem** (M).
Solve problem (M) to compute its objective value z_L^q and binary solution d^q.
(a) If (M) is infeasible, then (d^*, x^*) is the optimal solution (unless $(d^*, x^*) \equiv \emptyset$, then the UC-AC problem is infeasible). Terminate.
(b) If $z_L^* > z_L^q$, then $z_L^* \leftarrow z_L^q$.
3: **Solve for the Upper-Bound.**
Solve the NLP subproblem (SPG) (with fixed d^q) to global optimality using **Algorithm 2**. Let z_U^q and (d^q, x^q) be the optimal objective value and solution.
(a) If feasible and $z_U^* < z_U^q$, then update the candidate solution: $z_U^* \leftarrow z_U^q$ and $(d^*, x^*) \leftarrow (d^q, x^q)$.
4: **Convergence Check**
(a) If gap $(z_U^* - z_L^*)/z_L^* < \epsilon_O$, the optimal solution (d^*, x^*) has been identified. Terminate.
(b) Otherwise add *integer cut* (IC) for d^q to (M). Further refinements possible as in 4(b) of Alg. 2.
5: **Iterate** $q \leftarrow q + 1$. **Go to Step 2**.

(M), however, the generator commitments d=$[y, u, w]$ are fixed. Problem (Mf) for any iteration j with fixed $d^{(j)}$=$[y^{(j)}, u^{(j)}, w^{(j)}]$ is given by:

$$z_{L_{fixed}} := \min f^p + f^{su} + f^{sd}$$

s.t.

$$\text{(M.2)} - \text{(M.12)} \qquad \text{(Mf)}$$

where

$$y_{g,t} := y_{g,t}^{(j)}, u_{g,t} := u_{g,t}^{(j)}, w_{g,t} := w_{g,t}^{(j)} \quad \forall\, g,\ t$$

C. Global Solution Algorithm

In this section, we formally present the *nested* multi-tree algorithm. Algorithm 1 presents the *Outer Algorithm* for the solution of the UC-AC problem, and Algorithm 2 presents the *Inner Algorithm* for global solution of the NLP subproblem from the *Outer Algorithm*. For implementation details on the *integer cuts* (IC), piecewise outer relaxations (UE), (OE), and (CC), and OBBT referred to in the presented algorithms, please see the following section.

D. Algorithm Details

Algorithm 2 *Inner Algorithm* for (SPG)

1: **Initialization.**
For outer iteration q and fixed binary d^q:
Inner iteration $r = 0$.
$z_{L_{fixed}}^* \leftarrow -\infty$. $z_U^q \leftarrow +\infty$. $x^{q,r} \leftarrow \emptyset$.
2: **Solve for the Lower-Bound.**
Solve problem (Mf) (with fixed d^q) to find lower bound $z_{L_{fixed}}^r$ solution $x^{q,r}$.
(a) If (Mf) is infeasible then the subproblem (SPG) is infeasible. Return to **Step 3** in **Algorithm 1**.
(b) If $z_{L_{fixed}}^* > z_{L_{fixed}}^r$, then $z_{L_{fixed}}^* \leftarrow z_{L_{fixed}}^r$.
3: **Solve for the Upper-Bound.**
Solve problem (SP) (initialized from $x^{q,r}$) to compute its objective value $z_{U_{fixed}}^r$ and solution $x_{fixed}^{q,r}$. If $z_U^q < z_{U_{fixed}}^r$, then $z_U^q \leftarrow z_{U_{fixed}}^r$ and $x^q \leftarrow x_{fixed}^{q,r}$.
4: **Convergence Check.**
(a) If $(z_U^q - z_{L_{fixed}}^*)/z_{L_{fixed}}^* < \epsilon_I$ (optimality tolerance), then x^q is optimal. Return z_U^q and x^q to **Step 3** in **Algorithm 1**.
(b) Else perform OBBT on selected variables and add or refine partitions for piecewise outer relaxations (UE), (OE), and (CC).
5: **Iterate** $r \leftarrow r + 1$. **Go to Step 2**.

1) Integer Cuts: At each iteration q of the *Outer Algorithm* we add integer cuts that remove previously visited solutions d^q. These cuts are given by,

$$\sum_{(g,t)\in\mathcal{B}^{(q)}} y_{g,t} - \sum_{(g,t)\in\mathcal{N}^{(q)}} y_{g,t} \leq |\mathcal{B}^{(q)}| - 1 \qquad \text{(IC)}$$

for $q = 1 \ldots Q - 1$ where $\mathcal{B}^{(q)} = \{g, t | y_{g,t}^{(q)} = 1\}$ and $\mathcal{N}^{(q)} = \{g, t | y_{g,t}^{(q)} = 0\}$ This enhancement ensures that distinct solutions are obtained during each major iteration q of our global solution algorithm. As a result, since the solutions to problem (M) are enumerated with these integer cuts, the below refinements (in Sections IV-D2 and IV-D3) can be ignored in Step 4(b) of the *Outer Algorithm*.

2) "Reverse Cone": For any solution of (M) or (Mf), we may have that equation (28) is violated, i.e.,

$$c_{b,b,t}c_{k,k,t} - (c_{b,k,t}^2 + s_{b,k,t}^2) > \varepsilon$$

for any l and t due to the second-order cone relaxation of (28). Therefore, we introduce piecewise relaxations of

$$c_{b,k,t}^2 + s_{b,k,t}^2 \geq c_{b,b,t}c_{k,k,t}, \qquad (33)$$

as necessary in each iteration of the *Inner Algorithm*. To describe these relaxations, we define new variables

$$cs_{b,k,t} := c_{b,k,t}^2 + s_{b,k,t}^2$$

$$cc_{b,k,t} := c_{b,b,t}c_{k,k,t}$$

where we construct piecewise over-estimators for $c^2_{b,k,t} + s^2_{b,k,t}$ and piecewise under-estimators for $c_{b,b,t}c_{k,k,t}$ to obtain an adjustable approximation of (33).

Specifically, as first introduced in [32], we extend the bivariate partitioning scheme in [54]. We denote our partitioning variables as $cs^{i,j}_{b,k,t,}$ and $cc^{i,j}_{b,k,t}$, where $[\underline{c}^i_{b,k,t}, \overline{c}^i_{b,k,t}]$ refers to the i-th interval for $c_{b,k,t} \in [\underline{c}_{b,k,t}, \overline{c}_{b,k,t}]$ and $[\underline{s}^j_{b,k,t}, \overline{s}^j_{b,k,t}]$ refers to the j-th interval for $s_{b,k,t} \in [\underline{s}_{b,k,t}, \overline{s}_{b,k,t}]$.

The piecewise over-estimators for $cs_{b,k,t}$ are

$$cs^{i,j}_{b,k,t} \leq (\underline{c}^i_{b,k,t} + \overline{c}^i_{b,k,t})c^{i,j}_{b,k,t} + (\underline{s}^j_{b,k,t} + \overline{s}^j_{b,k,t})s^{i,j}_{b,k,t}$$
$$-(\underline{c}^i_{b,k,t}\overline{c}^i_{b,k,t})c^{i,j}_{b,k,t} + \underline{s}^j_{b,k,t}\overline{s}^j_{b,k,t})\sigma^{i,j}_{b,k,t} \quad \forall\ (i,j),\ l,\ t$$
$$cs_{b,k,t} = \sum\nolimits_{(i,j)\in\Omega^{cs}_{b,k,t}} cs^{i,j}_{b,k,t} \quad \forall\ l,\ t$$
$$\underline{c}^i_{b,k,t}\sigma^{i,j}_{b,k,t} \leq c^{i,j}_{b,k,t} \leq \overline{c}^i_{b,k,t}\sigma^{i,j}_{b,k,t} \quad \forall\ (i,j),\ l,\ t$$
$$c_{b,k,t} = \sum\nolimits_{(i,j)\in\Omega^{cs}_{b,k}} c^{i,j}_{b,k,t} \quad \forall\ l,\ t$$
$$\underline{s}^j_{b,k,t}\sigma^{i,j}_{b,k,t} \leq s^{i,j}_{b,k,t} \leq \overline{s}^j_{b,k,t}\sigma^{i,j}_{b,k,t} \quad \forall\ (i,j),\ l,\ t \qquad \text{(OE)}$$
$$s_{b,k,t} = \sum\nolimits_{(i,j)\in\Omega^{cs}_{b,k}} s^{i,j}_{b,k,t} \quad \forall\ l,\ t$$
$$\sum\nolimits_{(i,j)\in\Omega^{cs}_{b,k}} \sigma^{i,j}_{b,k,t} = 1 \quad \forall\ l,\ t$$
$$\sigma^{i,j}_{b,k,t} \in \{0,1\} \quad \forall\ (i,j),\ l,\ t$$

where $(i,j) \in \Omega^{cs}_{b,k,t} := [\underline{c}^i_{b,k,t}, \overline{c}^i_{b,k,t}] \times [\underline{s}^j_{b,k,t}, \overline{s}^j_{b,k,t}]$. Then, the piecewise under-estimators for $cc_{b,k,t}$ are

$$cc^{i,j}_{b,k,t} \leq \overline{cc}^{i,j}_{k,k,t}cc^{i,j}_{b,b,t} + \overline{cc}^{i,j}_{b,b,t}cc^{i,j}_{k,k,t}$$
$$-\overline{cc}^{i,j}_{b,b,t}\overline{cc}^{i,j}_{k,k,t}\varphi^{i,j}_{b,k,t} \quad \forall\ (i,j),\ l,\ t$$
$$cc^{i,j}_{b,k,t} \leq \underline{cc}^{i,j}_{k,k,t}cc^{i,j}_{b,b,t} + \underline{cc}^{i,j}_{b,b,t}cc^{i,j}_{k,k,t}$$
$$-\underline{cc}^{i,j}_{b,b,t}\underline{cc}^{i,j}_{k,k,t}\varphi^{i,j}_{b,k,t} \quad \forall\ (i,j),\ l,\ t$$
$$cc_{b,k,t} = \sum\nolimits_{(i,j)\in\Omega^{cc}_{b,k,t}} cc^{i,j}_{b,k,t} \quad \forall\ l,\ t$$
$$\underline{c}^i_{b,b,t}\varphi^{i,j}_{b,k,t} \leq c^{i,j}_{b,b,t} \leq \overline{c}^i_{b,b,t}\varphi^{i,j}_{b,k,t} \quad \forall\ (i,j),\ l,\ t \qquad \text{(UE)}$$
$$c_{b,b,t} = \sum\nolimits_{(i,j)\in\Omega^{cc}_{b,k,t}} c^{i,j}_{b,b,t} \quad \forall\ l,\ t$$
$$\underline{c}^i_{k,k,t}\varphi^{i,j}_{b,k,t} \leq c^{i,j}_{k,k,t} \leq \overline{c}^i_{k,k,t}\varphi^{i,j}_{b,k,t} \quad \forall\ (i,j),\ l,\ t$$
$$c_{k,k,t} = \sum\nolimits_{(i,j)\in\Omega^{cc}_{b,k,t}} c^{i,j}_{k,k,t} \quad \forall\ l,\ t$$
$$\sum\nolimits_{(i,j)\in\Omega^{cc}_{b,k,t}} \varphi^{i,j}_{b,k,t} = 1 \quad \forall\ l,\ t$$
$$\varphi^{i,j}_{b,k,t} \in \{0,1\} \quad \forall\ (i,j),\ l,\ t$$

where $(i,j) \in \Omega^{cc}_{b,k,t} := [\underline{c}^i_{b,b,t}, \overline{c}^i_{b,b,t}] \times [\underline{c}^j_{k,k,t}, \overline{c}^j_{k,k,t}]$. Note that unique $c^{i,j}_{b,b,t}$ and $c^{i,j}_{k,k,t}$ variables must be introduced for every line l where the under-estimators are constructed.

3) Cycle Constraints: In the second order cone relaxations used in (M) and (Mf), Kirchhoff's voltage law (KVL) is no longer guaranteed to be satisfied, but can be enforced through the *cycle constraints*,

$$\sum\nolimits_{(b,k)\in\mathcal{L}_c} \theta_{b,k,t} = 0 \qquad (36)$$

for all t and

$$\theta_{b,k,t} = -\arctan(s_{b,k,t}/c_{b,k,t}) \qquad (37)$$

for all l and t. As the *Inner Algorithm* iterates, these constraints are gradually enforced as needed in subproblem (Mf) by addition and refinement of piecewise outer approximations. We construct the respective piecewise under- and over-estimators for each $\theta_{b,k,t} = -\arctan(s_{b,k,t}/c_{b,k,t})$ term, where

$$\theta^{i,j}_{b,k,t} \geq \alpha^{i,j}_n s^{i,j}_{b,k,t} + \beta^{UE}_n c^{i,j}_{b,k,t} + \gamma^{UE}_n \quad \forall n,\ (i,j),\ l,\ t$$
$$\theta^{i,j}_{b,k,t} \leq \alpha^{i,j}_n s^{i,j}_{b,k,t} + \beta^{OE}_n c^{i,j}_{b,k,t} + \gamma^{OE}_n \quad \forall n,\ (i,j),\ l,\ t$$
$$\theta_{b,k,t} = \sum\nolimits_{(i,j)\in\Omega^{cs}_{b,k}} \theta^{i,j}_{b,k,t} \qquad \text{(CC)}$$
$$\sum\nolimits_{(b,k)\in\mathcal{L}_c} \theta_{b,k,t} = 0$$

where $n \in \{1,2\}$ and the parameters α, β, and γ are based on the planes constructed in [55]; please see [32] for implementation details.

4) Optimization-Based Bounds Tightening: The optimization-based bounds tightening (OBBT) is only computed for the second-order cone variables $c_{b,k,t}$ and $s_{b,k,t}$ to perform domain reduction on the initial lower-bounding subproblem (Mf). This approach results in two optimization routines per variable, i.e.,

$$\underline{c}_{b,k,t} \leftarrow \max\left(\underline{c}_{b,k,t}, \min\{c_{b,k,t} | c(\mathsf{Mf}), z^0_U \leq z^*_U\}\right)$$
$$\overline{c}_{b,k,t} \leftarrow \min\left(\overline{c}_{b,k,t}, \max\{c_{b,k,t} | c(\mathsf{Mf}), z^0_U \leq z^*_U\}\right)$$
$$\underline{s}_{b,k,t} \leftarrow \max\left(\underline{s}_{b,k,t}, \min\{s_{b,k,t} | c(\mathsf{Mf}), z^0_U \leq z^*_U\}\right)$$
$$\overline{s}_{b,k,t} \leftarrow \min\left(\overline{s}_{b,k,t}, \max\{s_{b,k,t} | c(\mathsf{Mf}), z^0_U \leq z^*_U\}\right)$$

for all l and t where $c(\mathsf{Mf})$ denotes the constraint set of (Mf). This procedure is computed selectively for $c_{b,k,t}$ and $s_{b,k,t}$ corresponding to large violations in second-order cone constraints (28).

V. Numerical Results

We now test our global UC-AC solution algorithm on four benchmark problems: a 6-bus test system (`6-bus`) with 3 generators [37], two 24-bus test systems – `RTS-79` [56] and `RTS-96` – each with 33 generators [57], and a modified IEEE 118-bus test system (`IEEE-118mod`) with 54 generators [37]. The scheduling horizon solution for all test cases is 24 hours at hourly time resolution, but we solve for 48 hours (by stacking the same 24-hour demand profile) to address end of time horizon impacts. Our global solution algorithm is implemented in *Pyomo*, a Python-based open-source optimization modeling language [58]. All computational experiments are conducted on a 64-bit server with 24 CPUs (Intel(R) Xeon(R) CPU E5-2697 v2 @ 2.70GHz) and 256 GB of RAM. All SOCP and MISOCP subproblems are solved using Gurobi 6.5.2 [59] limited to 24 threads. All NLP subproblems are solved with Ipopt 3.12.6 [60] using HSL's MA27 linear solver [61].

While having a tight and compact formulation is one path toward obtaining improved performance in global solution frameworks, convergence speed is also a function of other characteristics of the underlying numerical problem that impact computational difficulty, including formulation size and degeneracy / symmetry in the solution space. Typically, there is a large subset of solutions that are within an ϵ-tolerance of an optimal-cost schedule. To balance computational burden and solution quality, we initially set the Gurobi MILP gap to 0.1%. Then, if the optimality gap of our global solution algorithm does not show improvement within N iterations, we tighten the MILP gap by a factor of 10.

In all of our computational experiments, we set N=5 with a total wall clock time limit of $14400s$ and a major iteration limit q=30. The optimality tolerance for both our global solution algorithm and its nested multi-tree algorithm are set to 0.1%. Note that in contrast to research on global solution of MILP models, in which accepted optimality tolerances are typically $1 \cdot 10^{-4}$, standards for global solution of MINLP models are typically within 1% – due to the relative increase in computational difficulty.

A. Computational Performance

Computational results for our global UC-AC solution algorithm on the 4 benchmark problems are reported in Table I. The second column reports the best obtained upper bound, which corresponds to the *best known solution* to the UC-AC problem. The third column reports the best obtained lower bound, which corresponds to the solution of the problem defined in (M). The relative optimality gap is shown in the fourth column, followed by the total wall clock time and the number of major iterations. All problems are solved to within a 0.5% global optimality gap under the wall clock time limit. For `IEEE-118mod`, we obtained a 0.34% optimality gap after the first iteration (in approximately $8400s$), which remains unchanged before the time limit is reached in major iteration k=2 with a 0.11% MIP gap for the lower-bounding problem.

Table II additionally reports `IEEE-118mod` results for our global UC-AC algorithm compared to results obtained with version 16.12.7 of the commercially available general MINLP solver BARON [62, 63], and heuristic UC-AC methods as reported in [48] and in [36]. BARON was unable to solve any of the UC-AC problems within a time limit of 10 hours using the default solver parameters, CLP/CBC for the LP/MILP subproblems, and IPOPT and FILTERSD for the NLP subproblems. It is possible that better performance could be obtained with BARON by leveraging commercial subproblem solvers and additional tuning.

Our global UC-AC upper bound solution is 0.92% less costly than the heuristic OA [48] solution and 1.84% less costly than the heuristic GBD [36] solution. We expect for the improvement attained by solving the UC-AC problem globally to increase with the size of the network and generator set. Even a percentage improvement in operating efficiency leads to a monetary savings of billions annually [53].

B. Globally Optimal Unit Commitment Schedules

In addition to the differences in optimal objective value, we also want to compare the commitment schedules obtained with global and local algorithms. The globally optimal generator commitment schedules for our test cases are reported in Table III, IV, and V. Due to symmetry (e.g., co-location of identical generating units at a given bus), there can be multiple global solutions with the same objective value (here, we have not included alternate solutions). Comparing these commitment schedules with those from the local results in [48], we observe that they are the same for the `6-Bus` case, but differ for `RTS-79` (where a slightly improved solution is found) and `IEEE-118mod` (where a significantly improved solution is found).

VI. Conclusions

Solving the UC-AC problem is fundamental to obtaining real-world operations and market settlements that fully incorporate the impact of alternating current network physics. We have introduced, to the best of our knowledge, the first globally optimal approach to solving this practically critical and computationally difficult problem

TABLE I: Numerical results for our global UC-AC solution algorithm

Case	Upper Bound ($)	Lower Bound ($)	Optimality Gap (%)	Wall Clock Time (s)	Iteration (k)
6-bus	101,763	101,740	0.02%	8.5	2
RTS-79	895,040	894,392	0.07%	1394	6
RTS-96	886,362	885,707	0.07%	321.0	1
IEEE-118mod	835,926	833,057	0.34%	14400†	2

† MIP gap of 0.11% for the master problem at the time limit.

TABLE II: Comparative results with alternative UC-AC approaches

Case	Upper Bound ($)			
	Our Global UC-AC	BARON UC-AC	*Castillo et al.* UC-AC [48]	*Fu et al.* UC-AC [36]
IEEE-118mod	835,926	n/a	843,591	851,274

TABLE III: Commitments for the 6-Bus System

Bus	Gen	Commitment (h)
B1	G1	1-24
B2	G2	1, 12-21
B6	G3	10-22

TABLE IV: Commitments for the 24-Bus Systems

Bus	Gen	Commitment (h)	
		RTS-79	RTS-96
B1	G1, G2	Ø	Ø
B1	G3, G4	8-23	8-23
B2	G5, G6	10	Ø
B2	G7	8-24	8-24
B2	G8	8-23	8-23
B7	G9	1-23	1-23
B7	G10	9-24	10-24
B7	G11	10-18	Ø
B13	G12	11-22	1-18
B13	G13	Ø	11-22
B13	G14	Ø	Ø
B14	G15	1-24	1-24
B15	G16-G18	10-15	Ø
B15	G19, G20	10-13	Ø
B15	G21	9-24	9-24
B16	G22	1-24	1-24
B18	G23	1-24	1-24
B21	G24	1-24	1-24
B22	G25-G30	1-24	1-24
B23	G31-G33	1-24	1-24

TABLE V: Commitments for the IEEE-118mod System

Gen	Commitment (h)	Gen	Commitment (h)
G1	Ø	G28	1-24
G2	Ø	G29	1-24
G3	Ø	G30	1-24
G4	1-10, 24	G31	Ø
G5	1-24	G32	Ø
G6	Ø	G33	Ø
G7	11-22	G34	7-24
G8	Ø	G35	1-24
G9	Ø	G36	1-24
G10	1-2, 12-24	G37	8-23
G11	1-24	G38	Ø
G12	Ø	G39	Ø
G13	Ø	G40	1-10, 22-24
G14	10-22	G41	Ø
G15	Ø	G42	Ø
G16	9-16	G43	1-24
G17	Ø	G44	Ø
G18	Ø	G45	1-24
G19	Ø	G46	Ø
G20	1-24	G47	Ø
G21	8-24	G48	Ø
G22	Ø	G49	Ø
G23	Ø	G50	Ø
G24	9-23	G51	9-13
G25	Ø	G52	14-23
G26	Ø	G53	7-24
G27	1-2, 13-24	G54	9-23

Although our obtained run times are still longer than those required for operations, our proposed approach can be used to quantify the (near-) global optimality of "off-line" solutions, as well as test and validate other algorithmic approaches including the heuristics and local solution techniques referenced in Section II.

A considerable fraction of the computational time associated with our algorithm is in the global solution of the subproblems. Efficient global solution of ACOPF subproblems is an ongoing focus in the literature [64, 65] and furthermore can be leveraged to produce valid cuts in the master problem. Optimization results on larger data sets will require further development that potentially leverages a variety of advancements in relaxation refinements, MISOCP solvers, cut generation, and decomposition techniques. For example, other future directions for research include incorporating symmetry-breaking methods, and decomposition and parallelization techniques to improve the efficiency of determining lower bounds. Improvements to the mixed-integer refinement problem in the nested algorithm include adaptive, non-uniform partitioning schemes. Security (e.g., N-1) considerations and parameter uncertainties do not alter the core UC-AC problem that needs to be solved, but does increase the dimensionality of the problem; such dimensionality increase is addressable through the aforementioned advancements, which are extensions left for future work.

ACKNOWLEDGMENTS

Sandia National Laboratories is a multimission laboratory managed and operated by National Technology & Engineering Solutions of Sandia, LLC, a wholly owned subsidiary of Honeywell International Inc., for the U.S. Department of Energy's National Nuclear Security Administration under contract DE-NA0003525. *Disclaimer:* This paper describes objective technical results and analysis. Any subjective views or opinions that might be expressed in the paper do not necessarily represent the views of the U.S. Department of Energy or the United States Government. The work of Jianfeng Liu, Jean-Paul Watson, and Carl Laird was supported in part by the U.S. Department of Energy, Office of Science, Office of Advanced Scientific Computing Research, Applied Mathematics program under contract number KJ0401000 through the project "Multifaceted Mathematics for Complex Energy Systems". The work of Anya Castillo, Jean-Paul Watson, and Carl Laird was supported in part by Sandia National Laboratories' Laboratory Directed Research and Development (LDRD) program.

REFERENCES

[1] W. Sauer, "Uplift in RTO and ISO markets," Federal Energy Regulatory Commission, Tech. Rep., 2014.

[2] National Academies of Sciences, Engineering, and Medicine, *Analytic Research Foundations for the Next-Generation Electric Grid*. The National Academies Press, 2016.

[3] Y. Chen, A. Casto, F. Wang, Q. Wang, X. Wang, and J. Wan, "Improving large scale day-ahead security constrained unit commitment performance," *IEEE Transactions on Power Systems*, vol. 31, no. 6, pp. 4732–4743, 2016.

[4] M. Ilic, S. Cvijic, J. H. Lang, and J. Tong, "Operating beyond today's PV curves: Challenges and potential benefits," in *Proc. of the IEEE PES General Meeting*, 2015.

[5] *CAISO eTariff, § 34.11.*

[6] *NYISO Manual 12 Transmission and Dispatching Operations, § 5.7.4.*

[7] *Intra-PJM Tariff, OATT, attach. K, § 3.2.3.*

[8] A. Verma, "Power grid security analysis: An optimization approach," Ph.D. dissertation, Columbia University, 2009.

[9] K. Lehmann, A. Grastien, and P. V. Hentenryck, "AC-feasibility on tree networks is NP-hard," *IEEE Trans. on Power Syst.*, no. 99, pp. 1–4, 2015.

[10] C. Tseng, "On power system generation unit commitment problems." Ph.D. dissertation, Department of Industry Engineering and Operations Research, University of California at Berkeley, 1996.

[11] A. H. Land and A. G. Doig, "An automatic method of solving discrete programming problems," *Econometrica*, pp. 497–520, 1960.

[12] R. J. Dakin, "A tree-search algorithm for mixed integer programming problems," *The Computer Journal*, vol. 8, no. 3, pp. 250–255, 1965.

[13] H. S. Ryoo and N. V. Sahinidis, "A branch-and-reduce approach to global optimization," *J. Global Optim*, vol. 8, no. 2, pp. 107–138, 1996.

[14] T. G. Epperly and E. N. Pistikopoulos, "A reduced space branch and bound algorithm for global optimization," *J. Global Optim*, vol. 11, no. 3, pp. 287–311, 1997.

[15] J. M. Zamora and I. E. Grossmann, "A branch and contract algorithm for problems with concave univariate, bilinear and linear fractional terms," *J. Global Optim*, vol. 14, no. 3, pp. 217–249, 1999.

[16] P. Kesavan and P. I. Barton, "Generalized branch-and-cut framework for mixed-integer nonlinear optimization problems," *Comput Chem Eng.*, vol. 24, no. 2, pp. 1361–1366, 2000.

[17] P.-M. Kleniati and C. S. Adjiman, "Branch-and-

sandwich: A deterministic global optimization algorithm for optimistic bilevel programming problems. part i: Theoretical development," *J. Global Optim*, pp. 1–34, 2014.

[18] P. Belotti, C. Kirches, S. Leyffer, J. Linderoth, J. Luedtke, and A. Mahajan, "Mixed-integer nonlinear optimization," *Acta Numerica*, vol. 22, pp. 1–131, 2013.

[19] A. M. Geoffrion, "Generalized Benders decomposition," *J. Optim Theory Appl*, vol. 10, no. 4, pp. 237–260, 1972.

[20] M. A. Duran and I. E. Grossmann, "An outer-approximation algorithm for a class of mixed-integer nonlinear programs," *Math. Prog.*, vol. 36, no. 3, pp. 307–339, 1986.

[21] R. Fletcher and S. Leyffer, "Solving mixed integer nonlinear programs by outer approximation," *Math. Prog.*, vol. 66, pp. 327–349, 1994.

[22] T. Westerlund and F. Pettersson, "An extended cutting plane method for solving convex MINLP problems," *Comput Chem Eng.*, vol. 19, pp. 131–136, 1995.

[23] R. Pörn, I. Harjunkoski, and T. Westerlund, "Convexification of different classes of non-convex MINLP problems," *Comput Chem Eng.*, vol. 23, no. 3, pp. 439–448, 1999.

[24] R. Pörn and T. Westerlund, "A cutting plane method for minimizing pseudo-convex functions in the mixed integer case," *Comput Chem Eng.*, vol. 24, no. 12, pp. 2655–2665, 2000.

[25] X. Li, Y. Chen, and P. Barton, "Nonconvex generalized benders decomposition with piecewise convex relaxations for global optimization of integrated process design and operation problems," *Industrial & Engineering Chemistry Research*, vol. 51, pp. 7287–7299, 2004.

[26] P. Bonami, M. Kılınç, and J. Linderoth, "Algorithms and software for convex mixed integer nonlinear programs," in *Mixed Integer Nonlinear Programming*. New York: Springer, 2012, pp. 1–39.

[27] M.L.Bergamini, P. Aguirre, and P. Grossmann, "Logic-based outer approximation for globally optimal synthesis of process networks," *Computers and Chemical Engineering*, vol. 29, pp. 1914–1933, 2005.

[28] P. Kesavan, R. Allgor, E. Gatzke, and P. Barton, "Outer approximation algorithms for separable nonconvex mixed-integer nonlinear programs," *Math. Program.*, vol. A, no. 100, pp. 517–535, 2004.

[29] M. L. Bergamini, P. Aguirre, and I. Grossmann, "Logic-based outer approximation for globally optimal synthesis of process networks," *Computers & chemical engineering*, vol. 29, no. 9, pp. 1914–1933, 2005.

[30] M. L. Bergamini, N. J. Scenna, and P. A. Aguirre, "Global optimal structures of heat exchanger networks by piecewise relaxation," *Industrial & engineering chemistry research*, vol. 46, no. 6, pp. 1752–1763, 2007.

[31] R. Karuppiah, K. C. Furman, and I. E. Grossmann, "Global optimization for scheduling refinery crude oil operations," *Computers & Chemical Engineering*, vol. 32, no. 11, pp. 2745–2766, 2008.

[32] Liu, Jianfeng and Bynum, Michael and Castillo, Anya and Watson, Jean-Paul and Laird, Carl D., "A multitree approach for global solution of acopf problems using piecewise outer approximations," *Computers & Chemical Engineering*, 2017.

[33] Jabr, Rabih A., "A conic quadratic format for the load flow equations of meshed networks," *IEEE Trans. on Power Syst.*, vol. 22, no. 4, pp. 2285–2286, 2007.

[34] H. Ma and M. Shahidehpour, "Unit commitment with transmission security and voltage constraints," *IEEE Trans. Power Syst.*, vol. 14, no. 2, pp. 757–764, 1999.

[35] C. Murillo-Sanchez and R. J. Thomas, "Thermal unit commitment with nonlinear power flow constraints," in *IEEE Power & Energy Society Winter Meeting*, 1999, pp. 484–489.

[36] Y. Fu, M. Shahidehpour, and Z. Li, "Security-constrained unit commitment with AC constraints," *IEEE Trans. on Power Syst.*, vol. 20, no. 3, pp. 1538–1550, 2005.

[37] ——, "AC contingency dispatch based on security-constrained unit commitment," *IEEE Trans. on Power Syst.*, vol. 21, no. 2, pp. 897–908, 2006.

[38] W. S. Sifuentes and A. Vargas, "Hydrothermal scheduling using benders decomposition: Accelerating techniques," *IEEE Trans. on Power Syst.*, vol. 22, no. 3, pp. 1351–1359, 2007.

[39] A. Bai and H. Wei, "Semi-definite programming-based method for security-constrained unit commitment with operational and optimal power flow constraints," *IET Generation, Transmission & Distribution*, vol. 3, no. 2, pp. 182–197, 2009.

[40] N. Amjady and M. R. Ansari, "Hydrothermal unit commitment with ac constraints by a new solution method based on benders decomposition," *Energy Conversion and Management*, vol. 65, pp. 57–65, 2013.

[41] M. R. Ansari, N. Amjady, and B. Vatani, "Stochastic security-constrained hydrothermal unit commitment considering uncertainty of load forecast, inflows to reservoirs and unavailability of units by a new hybrid decomposition strategy," *IET Genera-*

tion, Transmission & Distribution, vol. 8, no. 12, pp. 1900–1915, 2014.

[42] J. Aghaei, A. Nikoobakht, P. Siano, M. Nayeripour, A. Heidari, and M. Mardaneh, "Exploring the reliability effects on the short term AC security-constrained unit commitment: A stochastic evaluation," *Energy*, vol. 114, no. 1, pp. 1016–1032, 2016.

[43] A. Nasri, S. J. Kazempour, A. J. Conejo, and M. Ghandhari, "Network-constrained AC unit commitment under uncertainty: A benders' decomposition approach," *IEEE Trans. on Power Syst.*, vol. 31, no. 1, pp. 412–422, 2016.

[44] M. Nick, O. Alizadeh-Mousavi, R. Cherkaoui, and M. Paolone, "Security constrained unity commitment with dynamic thermal line rating," *IEEE Transactions on Power Systems*, vol. 31, no. 3, pp. 2014–2025, 2016.

[45] A. Nikoobakht, M. Mardaneh, J. Aghaei, V. Guerrero-Mestre, and J. Contreras, "Flexible power system operation accommodating uncertain wind power generation using transmission topology control: an improved linearised AC SCUC model," *IET Generation, Transmission & Distribution*, vol. 11, no. 1, pp. 142–153, 2016.

[46] N. Amjady, S. Dehghan, A. Attarha, and A. J. Conejo, "Adaptive robust network-constrained ac unit commitment," *IEEE Transactions on Power Systems*, vol. 32, no. 1, pp. 672–683, 2017.

[47] R. Madani, A. Atamt'urk, and A. Davoudi, "A scalable semidefinite relaxation approach to grid scheduling," *arXiv preprint arXiv:1707.03541*, 2017.

[48] A Castillo et al., "The unit commitment problem with AC optimal power flow constraints," *IEEE Trans. on Power Syst.*, vol. 31, no. 6, pp. 4853–4866, 2016.

[49] N. Sahinidis and I. E. Grossmann, "Convergence properties of generalized benders decomposition," *Computers chem. Engng.*, vol. 15, no. 7, pp. 481–491, 1991.

[50] D. Wu, D. K. Molzahn, B. C. Lesieutre, and K. Dvijotham, "A deterministic method to identify multiple local extrema for the ac optimal power flow problem," *IEEE Transactions on Power Systems*, vol. 33, no. 1, pp. 654–668, 2018.

[51] S. M. Frank and S. Rebennack, "Optimal design of mixed ac–dc distribution systems for commercial buildings: A nonconvex generalized benders decomposition approach," *European Journal of Operational Research*, vol. 242, no. 3, pp. 710–729, 2015.

[52] G. Morales-España, J. M. Latorre, and A. Ramos, "Tight and compact MILP formulation of start-up and shut-down ramping in unit commitment," *IEEE Trans. on Power Syst.*, vol. 28, no. 2, pp. 1288–1296, 2013.

[53] M. B. Cain, R. P. O'Neill, and A. Castillo, "Optimal power flow papers: Paper 1. History of optimal power flow and formulations," Federal Energy Regulatory Commission, Tech. Rep., 2013.

[54] M. M. Hasan and I. A. Karimi, "Piecewise linear relaxation of bilinear programs using bivariate partitioning," *AIChE journal*, vol. 56, no. 7, pp. 1880–1893, 2010.

[55] B. Kocuk, S. S. Dey, and X. A. Sun, "Strong SOCP relaxations for the optimal power flow problem," *Oper. Res*, vol. 64, no. 6, pp. 1177–1196, 2016.

[56] P. M. Subcommittee, "IEEE reliability test system," *IEEE Trans. Power App. Syst.*, vol. PAS-98, no. 6, pp. 2047–2054, Nov 1979.

[57] P. Wong et al., "The IEEE reliability test system-1996. a report prepared by the reliability test system task force of the application of probability methods subcommittee," *IEEE Trans. on Power Syst.*, vol. 14, no. 3, pp. 1010–1020, Aug 1999.

[58] W. E. Hart et al., *Pyomo–Optimization Modeling in Python*, 2nd ed. Springer Science & Business Media, 2017, vol. 67.

[59] Gurobi Optimization, Inc., "Gurobi optimizer reference manual," 2016. [Online]. Available: http://www.gurobi.com

[60] A. Wächter and L. T. Biegler, "On the implementation of an interior-point filter line-search algorithm for large-scale nonlinear programming," *Math. prog.*, vol. 106, no. 1, pp. 25–57, 2006.

[61] HSL, "A collection of fortran codes for large scale scientific computation http://www.hsl.rl.ac.uk/," 2013.

[62] N. V. Sahinidis, "BARON: A General Purpose Global Optimization Software Package," *Journal of Global Optimization*, vol. 8, no. 2, pp. 201–205, 1996.

[63] M. Tawarmalani and N. V. Sahinidis, "A polyhedral branch-and-cut approach to global optimization," *Mathematical Programming*, vol. 2, no. 103, pp. 225–249, 2005.

[64] M. Bynum, A. Castillo, J.-P. Watson, and C. Laird, "Tightening mccormick relaxations toward global solution of the acopf problem," *Optimization Online preprint:2018/04/6572.pdf*, 2018.

[65] M. Lu, H. Nagarajan, R. Bent, S. D. Eksioglu, and S. J. Mason, "Tight piecewise convex relaxations for global optimization of optimal power flow," *arXiv preprint arXiv:1803.04633v1*, 2018.

Jianfeng Liu received a B.S. degree in Control Science and Engineering from Zhejiang University, Hangzhou, China, in 2011, a M.S. degree in Chemical Engineering from Carnegie Mellon University, Pittsburgh, PA, in 2012, and a Ph.D. degree in Chemical Engineering from Purdue University, West Lafayette, IN, in 2017. His research focuses on development and application of advanced solution strategies for large-scale, complex optimization problems. He is currently working at Amazon, Seattle, as an Operations Research Scientist.

Carl D. Laird (M'15) received the B.S. degree from the University of Alberta and the Ph.D. degree from Carnegie Mellon University in 2006, both in Chemical Engineering. He is a Principal Member of Technical Staff in the Center for Computing Research at Sandia National Laboratories in Albuquerque, New Mexico, and he has an Associate Professor appointment with the Davidson School of Chemical Engineering, Purdue University in West Lafayette, Indiana. He is the recipient of several research and teaching awards, including the prestigious Wilkinson Prize for his work on IPOPT, a National Science Foundation Faculty Early Development (CAREER) Award, and the Montague Center for Teaching Excellence Award.

Joseph K. Scott is an Assistant Professor in the Department of Chemical and Biomolecular Engineering at Clemson University. He received his B.S. (2006) in Chemical Engineering from Wayne State University, and his M.S. (2008) and Ph.D. (2012) in Chemical Engineering from MIT. His honors include the 2012 Best Paper Award from the Journal of Global Optimization, the 2016 W. David Smith, Jr. Award from the Computing and Systems Technology Division of the AIChE, the 2014-2016 Automatica Paper Prize from the International Federation of Automatic Control, and the 2016 Air Force Young Investigator Research Program Award. His research interests include dynamical systems, optimization theory, simulation and optimization of chemical processes, advanced process control, and fault diagnosis.

Jean-Paul Watson (M'10) holds B.S., M.S., and Ph.D. degrees in Computer Science. He is a Distinguished Member of Technical Staff in the Data Science and Cyber Analytics Department at Sandia National Laboratories in Livermore, California. He leads a number of research efforts related to stochastic optimization, ranging from fundamental algorithm research and development, to applications including power grid operations and planning.

Anya Castillo (M'11) holds a B.S. in Electrical and Computer Engineering with a Minor in Computer Science from Carnegie Mellon University, a M.S. from the Technology and Policy Program at the Massachusetts Institute of Technology, and a Ph.D. in Environmental Engineering from Johns Hopkins University. Currently, she is a Senior Member of Technical Staff in the Data Science and Applications Department at Sandia National Laboratories in Albuquerque, New Mexico. Her current project work spans both transmission and distribution systems to assess the integration of technologies, markets, and regulation that will meet ongoing challenges and support future grid requirements.

2. DISTRIBUTION

Email—Internal

Name	Org.	Sandia Email Address
Technical Library	01177	libref@sandia.gov

Sandia National Laboratories is a multimission laboratory managed and operated by National Technology & Engineering Solutions of Sandia LLC, a wholly owned subsidiary of Honeywell International Inc. for the U.S. Department of Energy's National Nuclear Security Administration under contract DE-NA0003525.